# ***DESCRIPTION OF THE SUBROUTINES USED***

# ***TO COMPUTE GROUND BRDF***

## ***SUBROUTINE HAPKALBE***

**Function**: To calculate the spherical albedo using the BRDF computed by *Hapke*'s (1981) model.

**Description**: The target spherical albedo s is equal to the flux reflected by the target divided by the incoming flux from an isotropic source. It is defined as:

$$s = \frac{\int_0^{\pi/2} a(\theta_s)\cos(\theta_s)\sin(\theta_s)d\theta_s}{\int_0^{\pi/2} \cos(\theta_s)\sin(\theta_s)d\theta_s}$$

where $a(\theta_s)$ is the directional albedo for a parallel solar beam, given by

$$a(\theta_s) = \frac{\int_0^{2\pi}\int_0^{\pi/2} \rho(\theta_s, \theta_v, \phi = \phi_s - \phi_v)\cos(\theta_v)\sin(\theta_v)d\theta_v d\phi}{\int_0^{2\pi}\int_0^{\pi/2} \cos(\theta_v)\sin(\theta_v)d\theta_v d\phi}$$

with the bidirectional reflectance $\rho(\theta_s, \theta_v, \phi)$ generated by the user's inputs (see HAPRBRDF).

## ***SUBROUTINE IAPIALBE***

**Function**: Same as HAPKALBE but for a BRDF from the subroutine IAPIBRDF.

## ***SUBROUTINE MINNALBE***

**Function**: Same as HAPKALBE but for a BRDF from the subroutine MINNBRDF.

## ***SUBROUTINE OCEALBE (and GLITALBE)***

**Function**: Same as HAPKALBE but for a BRDF from the subroutine OCEABRDF.

## ***SUBROUTINE RAHMALBE***

**Function**: Same as HAPKALBE but for a BRDF from the subroutine RAHMBRDF.

## ***SUBROUTINE ROUJALBE***

**Function**: Same as HAPKALBE but for a BRDF from the subroutine ROUJBRDF.

## ***SUBROUTINE VERSALBE***

**Function**: Same as HAPKALBE but for a BRDF from the subroutine VERSBRDF.

## ***SUBROUTINE WALTALBE***

**Function**: Same as HAPKALBE but for a BRDF from the subroutine WALTBRDF.

## ***SUBROUTINE BRDFGRID***

**Function:** To generate a BRDF following the user's inputs.

**Description:** The user enters the value of ρ for the Sun at a given sun zenith angle $\theta_s$ for the view zenith angle $\theta_v$ ranging from 0° to 80° by steps of 10° and equal to 85°, and for the view azimuth angle $\phi_v$ ranging from 0° to 360° by steps of 30°. The user does the same for the Sun which would be at $\theta_v$. In addition, the spherical albedo of the surface and observed reflectance in the selected geometry $\rho(\theta_s, \theta_v, \phi_s, \phi_v)$ need to be specified.

**Parameters:**

**1.** for $\theta_s$ the user has to enter $\rho(\theta_v, \phi_v)$:

ρ(0°,0°), ρ(10°,0°), ... ρ(80°,0°), ρ(85°,0°)
ρ(0°,30°), ρ(10°,30°), ... ρ(80°,30°), ρ(85°,30°)
...
ρ(0°,360°), ρ(10°,360°), ... ρ(80°,360°), ρ(85°,360°)

**2.** for $\theta_s=\theta_v$ the user has to enter $\rho(\theta_v, \phi_v)$:

ρ(0°,0°), ρ(10°,0°), ... ρ(80°,0°), ρ(85°,0°)
ρ(0°,30°), ρ(10°,30°), ... ρ(80°,30°), ρ(85°,30°)
...
ρ(0°,360°), ρ(10°,360°), ... ρ(80°,360°), ρ(85°,360°)

**3.** the spherical albedo of the surface

**4.** the observed reflectance in the selected geometry $\rho(\theta_s, \theta_v, \phi_s, \phi_v)$

## ***SUBROUTINE HAPKBRDF***

**Function:** To generate a BRDF following *Hapke*'s (1981) model.

**Description (from *Pinty & Verstraete,* 1991):** From the fundamental principles of radiative transfer theory, *Hapke* (1981) derived an analytical equation for the bidirectional reflectance function of a medium composed of dimensionless particles. The singly scattered radiance is derived exactly, whereas the multiply scattered radiance is evaluated from a two-stream approximation, assuming that the scatterers making up the surface are isotropic. The bidirectional reflectance ρ of a surface illuminated by the sun from a direction $(\theta_s, \phi_s)$, observed from a direction $(\theta_v, \phi_v)$, and normalized with respect to the reflectance of a perfectly reflecting Lambertian surface under the same condition is given by

$$\rho(\theta_s, \phi_s, \theta_v, \phi_v) = \frac{\omega}{4} \frac{1}{\mu_s + \mu_v} \{[1 + B(g)]P(g) + H(\mu_s)H(\mu_v) - 1\},$$

where

ω is the average single scattering albedo of medium particles,

$\mu_s = \cos(\theta_s)$ and $\mu_v = \cos(\theta_v)$,

g is the phase angle between the incoming and outgoing rays, defined as

$$\cos(g) = \cos(\theta_s)\cos(\theta_v) + \sin(\theta_s)\sin(\theta_v)\cos(\phi_s - \phi_v),$$

B(g) is a backscattering function that accounts for the hot spot effect:

$$B(g) = \frac{S(0)}{\omega P(0)[1 + (1/h)\tan(g/2)]},$$

with the amplitude and width of the hot spot S(0) and h,

P(g) is the average phase function of medium particles, computed here by the *Heyney and Greenstein*'s function:

$$P(g) = \frac{1 - \Theta^2}{1 + \Theta^2 + 2\Theta\cos(g)}$$

with the asymmetry factor Θ ranging from -1 (backward scattering) to +1 (forward scattering), and H(μ) is a function to account for multiple scattering:

$$H(\mu) = \frac{1 + 2\mu}{1 + 2(1 - \omega)^{1/2}\mu}.$$

**Parameters:**

ω, Θ, S(0), h.

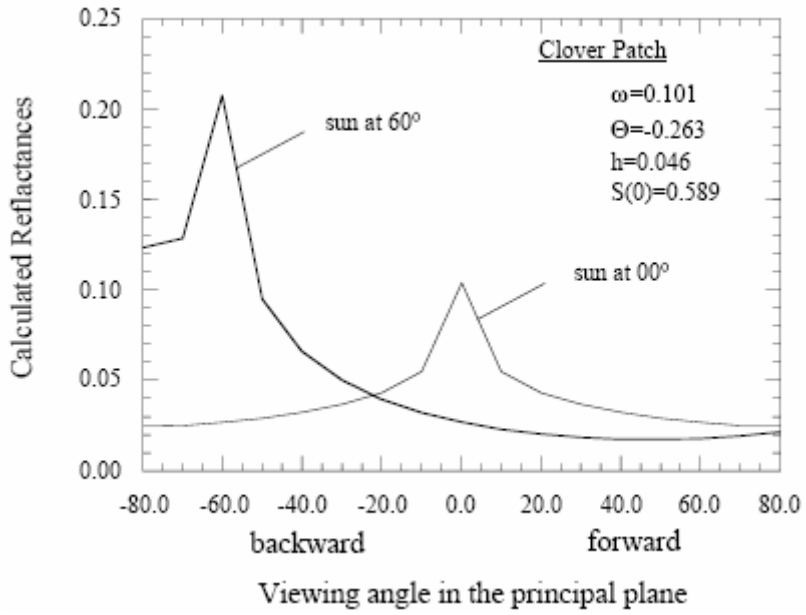


**References:**

B. Hapke, Bidirectional reflectance spectroscopy: 1. Theory, *Journal of Geophysical Research*, 86, 3039-3054, 1981.

B. Hapke, Bidirectional reflectance spectroscopy: 4. The extinction coefficient and the opposition effect, *Icarus*, 67, 264-280, 1986.

B. Pinty and M. Verstraete, Extracting information on surface properties from bidirectional reflectance measurements, *Journal of Geophysical Research,* 96, 2865-2874, 1991.

## ***SUBROUTINE IAPIBRDF***

**Function**: To generate a BRDF following *Iaquinta and Pinty*'s (1994) model.

**Description (from Iaquinta & Pinty, 1994)**: The model presents an improvement of the original model developed by *Verstraete et al.* (1990), in order to account for the effects due to an underlying soil below a vegetation canopy. The singly scattered component is solved exactly using an analytical hot-spot description. The multiply scattered component is approximated on the basis of a Discrete Ordinates method reduced to a one-angle problem.

The reflectance field is split into three main components: unscattered (0), singly scattered (1) and multiply scattered (M) by leaf elements:

$$\rho^{tot}(\Omega_0,\Omega) = \rho^0(\Omega_0,\Omega) + \rho^1(\Omega_0,\Omega) + \rho^M(\Omega_0), \quad (1)$$

where the vegetation canopy is illuminated by direct solar radiation from the direction $\Omega_0(\mu_0 = \cos(\theta_0),\phi_0))$, and observed from the direction $\Omega(\mu = \cos(\theta),\phi))$.

• The uncollided radiation $\rho^0(\Omega_0,\Omega)$ (first order reflectance from the soil) can be written as

$$\rho^0(\Omega_0,\Omega) = R_s T_0(L_T) T(L_T), \quad (2)$$

where $R_s$ is the soil albedo, $G(\Omega)$ is the *Ross-Nilson* G-function, L ($0<L<L_T$) is the leaf area index, $T_0(L)$ is the transmission of direct solar radiation through canopy layers above the level L:

$$T_0(L) = \exp\left(-\frac{G(\Omega_0)}{|\mu_0|}L\right), \quad (3)$$

and T(L) is the transmission of scattered radiation:

$$T(L) = \exp\left(-\frac{G(\Omega_0)V_2(\Omega_0,\Omega,L)}{\mu \quad V(\Omega,L)}L\right), \quad (4)$$

where

$$\begin{aligned} \frac{V_2(\Omega_0,\Omega,L)}{V(\Omega,L)} &\cong \left(1-\frac{4}{3\pi}\right)\frac{L}{L_i}, \quad \text{if } L < L_i \\ \frac{V_2(\Omega_0,\Omega,L)}{V(\Omega,L)} &= 1-\frac{4}{3\pi}\frac{L}{L_i}, \quad \text{if } L \geq L_i \end{aligned} \quad (5)$$

with

$$L_i = \frac{2r\Lambda}{\sqrt{\tan^2(\theta_0) + \tan^2(\theta) - 2\tan(\theta_0)\tan(\theta)\cos(\phi_0 - \phi)}}. \quad (6)$$

Here $\Lambda$ denotes the leaf area density [$m^2m^{-3}$] and r [m] is the radius of sun-flecks on an illuminated leaf.

• The single scattering by canopy elements $\rho^1(\Omega_0,\Omega)$ is given by

$$\rho^1(\Omega_0,\Omega) = \frac{\Gamma(\Omega_0 \to \Omega)}{|\mu_0|\mu} \int_0^{L_T} T_0(L)T(L)dL, \quad (7)$$

where

$\Gamma(\Omega_0 \to \Omega)$ is the area scattering phase function (bi-Lambertian).

• Using a canopy transport equation reduced to a one-angle problem and assuming isotropic scattering, the multiply scattered radiation exiting at the top of canopy is given by

$$\rho^M(\Omega_0) = \frac{1}{|\mu_0|} \int_0^1 I^M(0,\mu')\mu' d\mu', \quad (8)$$

where $I^M$ is the intensity of photons which have been scattered twice or more times in the canopy.

The $G(\Omega)$ function is the leaf area projected to the direction $\Omega$ by a unit leaf area:

$$G(\Omega) = \frac{1}{2\pi} \int_{2\pi+} g_L(\Omega_L) |\Omega_L \cdot \Omega| d\Omega_L, \quad (9)$$

where $g_L(\Omega_L)$ is the probability density of the distribution of leaf normals with respect to the upward hemisphere (its computation depends on the input parameter ild).

The area scattering phase function $\Gamma(\Omega_0 \to \Omega)$ is given by

$$\frac{1}{\pi}\Gamma(\Omega' \to \Omega) = \frac{1}{2\pi} \int_{2\pi+} g_L(\Omega_L) |\Omega' \cdot \Omega_L| f(\Omega' \to \Omega, \Omega_L) d\Omega_L, \quad (10)$$

where $f(\Omega' \to \Omega, \Omega_L)$ is the leaf scattering distribution function. Here it is assumed that the leaves follow a bi-Lambertian scattering model, and $f(\Omega' \to \Omega, \Omega_L)$ is defined as

$$f(\Omega' \to \Omega, \Omega_L) = \begin{cases} \frac{r_L |\Omega \cdot \Omega_L|}{\pi}, & \text{if } (\Omega \cdot \Omega_L)(\Omega' \cdot \Omega_L) < 0 \\ \frac{t_L |\Omega \cdot \Omega_L|}{\pi}, & \text{if } (\Omega \cdot \Omega_L)(\Omega' \cdot \Omega_L) > 0 \end{cases}, \quad (11)$$

with $r_L$ and $t_L$ are the leaf reflection and transmission coefficients.

**Parameters:**

**1** - ild, ihs

**2** - $L_T$, 2rΛ

**3** - $r_L$, $t_L$, $R_S$

where ild is the leaf angle distribution (1=planophile, 2=erectophile, 3=plagiophile, 4=extremophile, and 5=uniform), ihs is a hot spot descriptor (0=no hot-spot, 1=hot spot), $L_T$ the leaf area index in [1.0, 15.0], 2rΛ is a hot-spot parameter in [0.0 (no hot-spot), 2.0], $r_L$ is the leaf reflection coefficient in [0.0, 0.99], $t_L$ is the leaf transmission coefficient in [0.0, 0.99], and $R_S$ is the soil albedo in [0.0, 0.99].

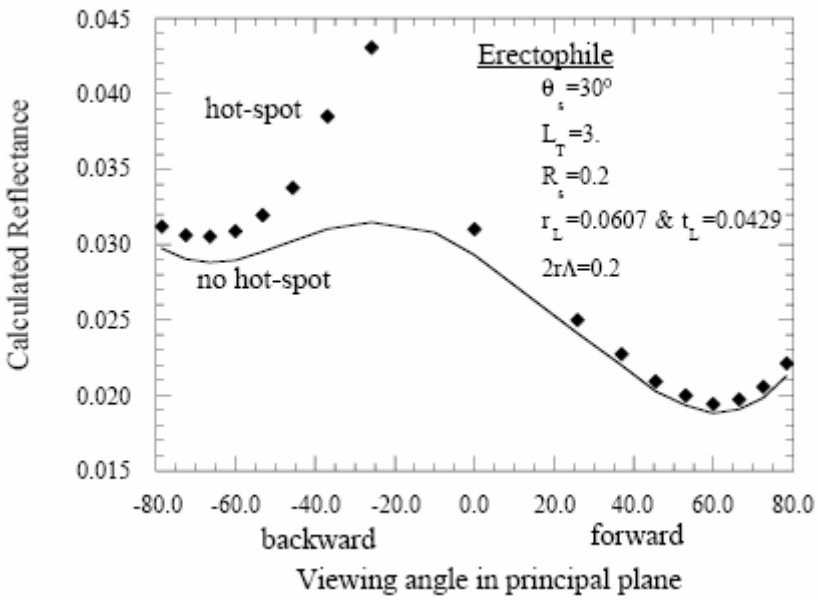


**References:**

J. Iaquinta, and B. Pinty, Adaptation of a bidirectional reflectance model including the hot-spot to an optically thin canopy, *Proceedings of the VI International Colloquium: Physical measurements and signatures in remote sensing*, Val d'Isère, France, 683-690, 1994.

M. Verstraete, B. Pinty, and R.E. Dickinson, A physical model of the bidirectional reflectance of vegetation canopies: 1. Theory, *Journal of Geophysical Research*, 95, 11755-11765, 1990.

## ***SUBROUTINE MINNBRDF***

**Function**: To generate a BRDF following *Minnaert*'s (1941) model.

**Description**: Using the optical reciprocity principle, *Minnaert* (1941) defined a simple model to compute the BRDF. The reflectance is written as

$$\rho(\theta_s,\theta_v,\phi) = \rho_0 \frac{k+1}{2}(\cos(\theta_v)\cos(\theta_s))^{k-1}$$

where $\rho_0$ is the albedo of a given surface and k is the surface parameter. For k=1, the BRDF corresponds to an ideal Lambertian surface; k=0 corresponds to the minimum reflectance at nadir and k=2 to the maximum reflectance at nadir.

**Parameters:**

k, $\rho_0$

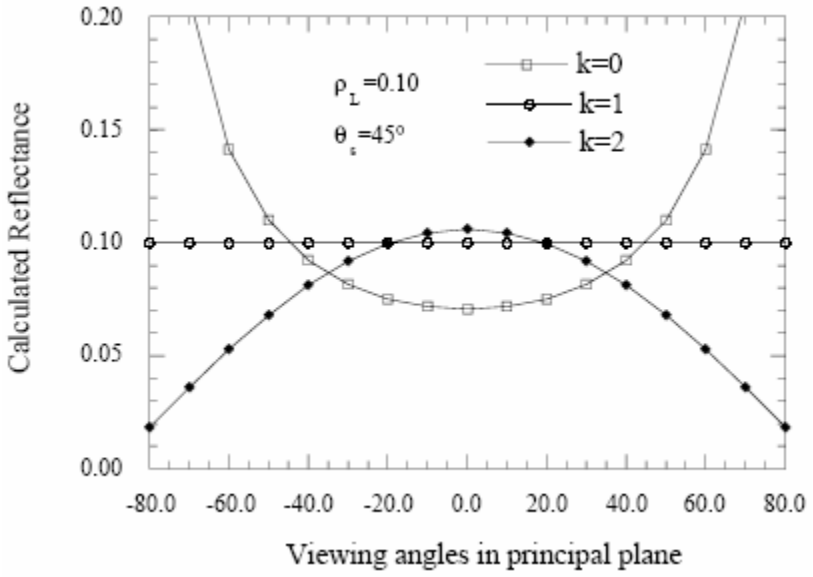


**Reference**

M. Minnaert, The reciprocity principle in lunar photometry, *The Astrophysical Journal*, 93, 403 410, 1941.

## ***SUBROUTINE OCEABRDF (and OCEATOOLS)***

**Function**: To compute the BRDF of an ocean surface by taking into account the influence of whitecaps, sun glint and pigment concentration.

**Description**: In the solar spectral range, the reflectance of an ocean surface $\rho_{os}(\lambda)$ can be assumed for a given set of geometrical condition $\theta_s$, $\theta_v$ and $\phi$ ($=\varphi_s-\varphi_v$) as the sum of three components dependent on the wavelength $\lambda$ (*Koepke*, 1984):

$$\rho_{os}(\theta_s,\theta_v,\phi,\lambda) = \rho_{wc}(\lambda) + \{1-W\}\cdot\rho_{gl}(\theta_s,\theta_v,\phi,\lambda) + \{1-\rho_{wc}(\lambda)\}\cdot\rho_{sw}(\theta_s,\theta_v,\phi,\lambda),$$

where

- $\rho_{wc}(\lambda)$ is the reflectance due to whitecaps,
- $\rho_{gl}(\lambda)$ is the specular reflectance at the ocean surface,
- $\rho_{sw}(\lambda)$ is the scattered reflectance emerging from sea water, and
- W is the relative area covered with whitecaps, which can be expressed from the wind speed ws (*Monahan & O'Muircheartaigh*, 1980) as $W=2.9510^{-6}ws^{3.52}$ for water temperatures greater than 14°C.

*1 - Reflectance of whitecaps $\rho_{wc}(\lambda)$*

According to *Koepke* (1984), "the optical influence of whitecaps is given by the product of the area of each individual whitecap W and its corresponding reflectance $\rho_f(\lambda)$. However, the area of an individual whitecap increases with its age, while its reflectance decreases. Since whitecaps of different ages are taken into consideration in the W values, the combination of W with $\rho_f(\lambda)$ gives $\rho_{wc}(\lambda)$ values that are too high". Thus *Koepke* defines, instead of $\rho_f(\lambda)$, an effective reflectance of ocean foam patches $\rho_{ef}(\lambda)$ and calculates $\rho_{wc}(\lambda)$ as

$$\rho_{wc}(\lambda) = W\cdot\rho_{ef}(\lambda) = W\cdot f_{ef}\cdot\rho_f(\lambda),$$

where $f_{ef}$ is the efficiency factor slightly dependent on the wind speed but independent of the wavelength ($f_{ef}= 0.4\pm 0.2$).

Figure 1 shows the reflectance of whitecaps as a function of the wind speed in the visible spectral range; in this range the effective reflectance $\rho_{ef}(\lambda)$ is a constant value (22 ± 11)%.

*2 - Reflectance of the sun glint $\rho_{gl}(\lambda)$ (**SUBROUTINE SUNGLINT**)*

*Cox & Munk* (1954, 1955) made measurements of the sun glitter from aerial photographs. They defined a many-faceted model surface whose wave-slopes vary according to isotropic and anisotropic Gaussian distributions with respect to the surface wind.

Lets consider the system of coordinates (P;X,Y,Z) where P is the observed point, Z is the altitude, PY is pointed at the sun direction and PX at the direction perpendicular to the sun plane. In this system, the surface slope is defined by its two components $Z_x$ and $Z_y$,

$$Z_x = \frac{\partial Z}{\partial X} = \sin(\alpha)\tan(\beta) \qquad \text{and} \qquad Z_y = \frac{\partial Z}{\partial Y} = \cos(\alpha)\tan(\beta),$$

where $\alpha$ is the azimuth of the ascent (clockwise from the sun) and $\beta$ is the tilt. Using spherical trigonometry, $Z_x$ and $Z_y$ can be related to the incident and reflected directions ($\pi/2 \geq \theta_s$ and $\theta_v \geq 0$) as

$$Z_x = \frac{-\sin(\theta_v)\sin(\varphi_s - \varphi_v)}{\cos(\theta_s) + \cos(\theta_v)} \qquad \text{and} \qquad Z_y = \frac{\sin(\theta_s) + \sin(\theta_v)\cos(\varphi_s - \varphi_v)}{\cos(\theta_s) + \cos(\theta_v)}.$$

For the case of an anisotropic distribution of slope components (dependent on the wind direction), lets consider new principal axes (P;X',Y',Z'=Z) defined by a rotation of $\chi$ from the sun (P;X,Y,Z) system with PY' parallel to the wind direction (related clockwise from the North by $\varphi_w$, then $\chi = \varphi_s - \varphi_w$) The slope components are now expressed as

$$Z_X' = \cos(\chi)\cdot Z_X + \sin(\chi)\cdot Z_y \qquad \text{and} \qquad Z_y' = -\sin(\chi)\cdot Z_X + \text{con}(\chi)\cdot Z_y,$$

and the slope distribution is expressed by a *Gram-Charlier* series as

$$P(Z_x', Z_y') = \frac{1}{2\pi\sigma'_x\,\sigma'_y}\exp\left(-\frac{\xi^2+\eta^2}{2}\right)\left\{1 - \frac{1}{2}C_{21}(\xi^2-1) - \frac{1}{6}C_{03}(\eta^3-\eta)\right.$$
$$\left. + \frac{1}{24}C_{40}(\xi^4 - 6\xi^2 + 3) + \frac{1}{4}C_{22}(\xi^2-1)(\eta^2-1) + \frac{1}{24}C_{04}(\eta^4 - 6\eta^2 + 3)\right\},$$

where

$\xi = Z_x'/\sigma_x'$ and $\eta = Z_y'/\sigma_y'$,

$\sigma_x'$ and $\sigma_y'$ are the rms values of $Z_x'$ and $Z_y'$, the skewness coefficients $C_{21}$ and $C_{03}$, and the peakedness coefficients $C_{40}$, $C_{22}$ and $C_{04}$ are defined by *Cox & Munk* (1954, 1955) for a clean (uncontaminated) surface as

$$(\sigma_x')^2 = 0.003 + 0.00192\text{ws} \pm 0.002, \quad (\sigma_y')^2 = 0.00316\text{ws} \pm 0.004,$$

$$C_{21} = 0.01 - 0.0086\text{ws} \pm 0.03\ , \qquad C_{03} = 0.04 - 0.033\text{ws} \pm 0.12,$$

$$C_{40} = 0.\ 40 \pm 0.23\ ,\ C_{22} = 0.12 \pm 0.06,\ \text{and}\ C_{04} = 0.23 \pm 0.\ 41.$$

Thus, the directional reflectance is written as

$$\rho_{gl}(\theta_s, \theta_v, \varphi_s, \varphi_v) = \frac{\pi P(Z'_x, Z'_y) R(n, \theta_s, \theta_v, \varphi_s, \varphi_v)}{4\cos(\theta_s)\cos(\theta_v)\cos^4(\beta)},$$

where $R(n, \theta_s, \theta_v, \varphi_s, \varphi_v)$ is *Fresnel*'s reflection coefficient (n is the complex refractive index of sea water), defined below.

Figure 2 shows computations of $\rho_{gl}$ for the wind speed of 5 and 15m/s, $\chi$ equal to 0, 90, 180, and 270°, solar zenith angle of 30°, and wavelength of 0.550μm.

*3 - Fresnel's reflection coefficient (**SUBROUTINE FRESNEL** and **INDWAT**)*

The reflection coefficient $R(n, \theta_s, \theta_v, \varphi_s, \varphi_v)$ is computed (*Born & Wolf*, 1975) involving the absorption of water ( $n = n - in_i$ ) as

$$R(n, \theta_s, \theta_v, \varphi_s, \varphi_v) = \frac{1}{2} \frac{\left[(n_r^2 - n_i^2)\cos(\theta_i) - u\right]^2 + \left[2n_r n_i \cos(\theta_i) + v\right]^2}{\left[(n_r^2 - n_i^2)\cos(\theta_i) + u\right]^2 + \left[2n_r n_i \cos(\theta_i) - v\right]^2}$$

with

$$u^2 = \frac{1}{2}\left\{ n_r^2 - n_i^2 - \sin^2(\theta_i) \mid + \sqrt{\left[n_r^2 - n_i^2 - \sin^2(\theta_i)\right]^2 + 4n_r^2 n_i^2} \right\},$$

$$v^2 = \frac{1}{2}\left\{ - \mid n_r^2 - n_i^2 - \sin^2(\theta_i) \mid + \sqrt{\left[n_r^2 - n_i^2 - \sin^2(\theta_i)\right]^2 + 4n_r^2 n_i^2} \right\},$$

$$\cos(\theta_i) = \sqrt{\frac{1}{2}\left[1 + \cos(\theta_s)\cos(\theta_v) + \sin(\theta_s)\sin(\theta_v)\sin(\varphi_s - \varphi_v)\right]}, \text{ and}$$

$$\sin(\theta_i) = \sqrt{\frac{1}{2}\left[1 - \cos(\theta_s)\cos(\theta_v) + \sin(\theta_s)\sin(\theta_v)\sin(\varphi_s - \varphi_v)\right]}.$$

In 6S, the complex index of refraction of sea water (we assume that the outside medium is vacuum) is deduced from the complex index of refraction of pure water, specified by *Hale & Querry* (1973). By default, we assume a typical sea water (salinity=34.3ppt, chlorinity=19ppt) as reported by *Sverdrup* (1942, p.173). *McLellan* (1965, p.129) reported that the index of refraction increased as a function of chlorinity. For the chlorinity of 19.0 ppt, the increase was found to

have a value of +0.006 and be linear with the salt concentration $C_{sal}$ (see also *Friedman*, 1969). For the extinction coefficient, *Friedman* (1969) reported that no correction was required between 1.5 and 9 μm.

Thus, in 6S we apply the correction $\delta n_r$ of +0.006 on the index of refraction of pure water and no correction $\delta n_i$ for the extinction coefficient. The user is able to enter his/her own salt concentration. In this case, a linear interpolation is assumed to correct the index of refraction of pure water, so that $\delta n_r = 0$ for $C_{sal}$ = 0ppt and $\delta n_r$ =+0.006 for $C_{sal}$ =34.3ppt.

*4 - Reflectance emerging from sea water $\rho_{sw}(\lambda)$ (**SUBROUTINE MORCASIWAT** for $R_w$)*

The reflectance emerging from sea water (also called the remote sensing reflectance of sea water) $\rho_{sw}(\theta_s, \theta_v, \phi, \lambda)$ is the reflectance observed just above the sea surface (level $0^+$).This reflectance can be related to the reflectance $R_w$, which is the ratio of upwelling to downwelling radiance just below the sea surface (level $0^-$) If we assume that the ocean is a Lambertian reflector, $\rho_{sw}(\theta_s, \theta_v, \phi, \lambda)$ can be expressed as

$$\rho_{sw}(\theta_s, \theta_v, \phi, \lambda) = \frac{1}{n^2} \frac{R_w(\lambda) \cdot t_d(\theta_s) \cdot t_u(\theta_v)}{1 - a \cdot R_w(\lambda)},$$

where

• $t_d$ is the transmittance for downwelling radiance, calculated using the Fresnel reflectance coefficient $R_{a-w}(\theta_s, \theta_d, \phi)$ for the air-water interface as

$$t_d(\theta_s) = 1 - \int_0^{2\pi} \int_0^{\pi/2} R_{a-w}(\theta_s, \theta_d^a, \phi) \cdot \cos(\theta_d^a) \cdot \sin(\theta_d^a) \cdot d\theta_d^a \cdot d\phi .$$

The angle $\theta_d$ represents (see Fig. 3) the zenith angle of a reflected solar beam according to the wave-slopes distribution (*Cox & Munk*'s model, see below).

• $t_u$ is the transmittance for upwelling radiance, calculated using the Fresnel reflectance coefficient $R_{a-w}(\theta_s, \theta_u, \phi)$ for the water-air interface as

$$t_u(\theta_v) = 1 - \int_0^{2\pi} \int_0^{\pi/2} R_{w-a}(\theta_v, \theta_u^w, \phi) \cdot \cos(\theta_u^w) \cdot \sin(\theta_u^w) \cdot d\theta_u^w \cdot d\phi .$$

The angle $\theta_u^w$ represents (see Fig. 3) the zenith angle of an upwelling beam in the water, according to *Fresnel & Snell*'s law ($n_{air}\sin(\theta_{air}) = n_{sea}\sin(\theta_{sea})$) and the wave-slopes distribution.

• a is defined by

$$a = 1 - \int_0^{\pi/2} t_u(\theta_v) \cdot \cos(\theta_v) \cdot \sin(\theta_v) \cdot d\theta_v .$$

In order to minimize computations, we adopted a constant value of a=0.485. Theoretically, the value of a depends on the wind speed and water index of refraction. Practically, this value varies very little with wind speed (see Table 2 of *Austin*, 1974), and the index of refraction of water is almost constant in the wavelength range from 0.4μm to 0.7μm and assumed to be equal to 1.341.

As described above, the irradiance reflectance $R_w(\lambda)$ is the ratio of the upwelling spectral irradiance $E_u(\lambda)$ to the downwelling irradiance $E_d(\lambda)$ just below the surface. This ratio is particularly dependent on the inherent optical properties of sea water: the total absorption coefficient $a(\lambda)$ [$m^{-1}$] and the total backscattering coefficient $b_b(\lambda)$ [$m^{-1}$]. For example, *Morel & Prieur* (1977) showed that within a good approximation (when $a(\lambda)<<1$) it could be expressed as

$$R_w(\lambda) = 0.33 \frac{b_b(\lambda)}{a(\lambda)} .$$

According to *Morel* (1988), "in many situations phytoplanktons and their derivative, and detrital products (mainly particulate, but also dissolved) play a predominant role in determining the optical properties of oceanic waters. These waters are classified as "case I" waters and are opposed to "case II" waters for which sediments, or dissolved yellow substance, make an important or dominant contribution to the optical properties". Here we use the so-called "case I waters" (defined in the range from 0.4 to 0.7 μm) which roughly correspond to cases I, IA, IB, II, and III of *Jerlov*'s chart of optical water type (*Jerlov*, 1951, 1976). For the so-called "case I waters", *Morel* splits the total backscattering coefficient into 2 components:

$$b_b(\lambda) = \frac{1}{2} b_w(\lambda) + \tilde{b}_b(\lambda) \cdot b ,$$

where

• $b_w(\lambda)$ is the molecular scattering coefficient of water (Fig. 4), and

• $\tilde{b}_b(\lambda)$ is the ratio backscattering/scattering coefficient of pigments, related to the pigment concentration C (Chl a + Pheo a) [$mg \cdot m^{-3}$] and the wavelength [μm] as

$$\tilde{b}_b(\lambda) = 0.002 + 0.02(0.5 - 0.25 \log_{10} C) \frac{0.550}{\lambda} ,$$

and

• b is the scattering coefficient of pigments, calculated as

$$b = 0.3 C^{0.62} .$$

For *Morel*'s "case I waters", the total absorption coefficient is written as

$$a(\lambda) = u(\lambda) \cdot K_d(\lambda),$$

where

• $u(\lambda)$ is the wavelength-dependent function computed as

$$u(\lambda) = 0.90 \frac{1 - R_w(\lambda)}{1 + 2.25\, R_w(\lambda)},$$

and

• $K_d(\lambda)$ is the total diffuse attenuation coefficient for downwelling irradiance, given by

$$K_d(\lambda) = K_w(\lambda) + \chi_c(\lambda) C^{e(\lambda)},$$

where $K_w(\lambda)$ is the diffuse attenuation coefficient for pure oceanic water, $\chi_c(\lambda)$ and $e(\lambda)$ are tabular values. Figure 5 illustrates computations of $K_d(\lambda)$ for several pigment concentrations.

Also, according to the *Morel*'s "case I waters" model, the computation of the reflectance $R_w(\lambda)$ is only dependent on the pigment concentration C. Figure 6 shows the computed reflectance $R_w$ in the range of 0.4 to 0.7 μm for different concentrations C.

If the only information you have is the water type following *Jerlov*'s chart, you can use the approximate C values given by *Morel* (1988):

| | | | | | |
|---|---|---|---|---|---|
| 0-0.01 | 0.05 | 0.1 | 0.5 | 1.5-2 | $mg \cdot m^{-3}$ |
| I | IA | IB | II | III | |

**Parameters:**

ws, $\varphi_w$, $C_{sal}$, C

where

ws is the wind speed [m/s],

$\varphi_w$ is the direction of the wind (clockwise from the North),

$C_{sal}$ is the salt concentration [ppt] (if $C_{sal}<0$ then $C_{sal}$=34.3ppt by default), and

C is the pigment concentration ((Chl a + Pheo a) in $mg \cdot m^{-3}$).

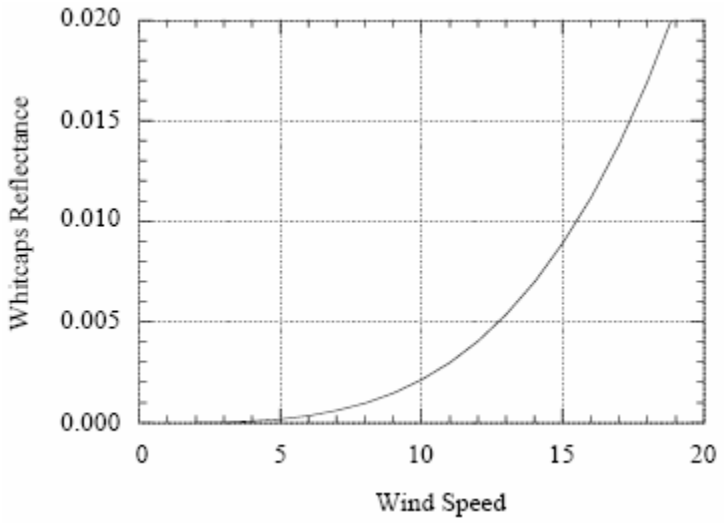


**Fig. 1.** Whitecaps reflectance as defined by *Koepke* (1984) in the visible spectral range.

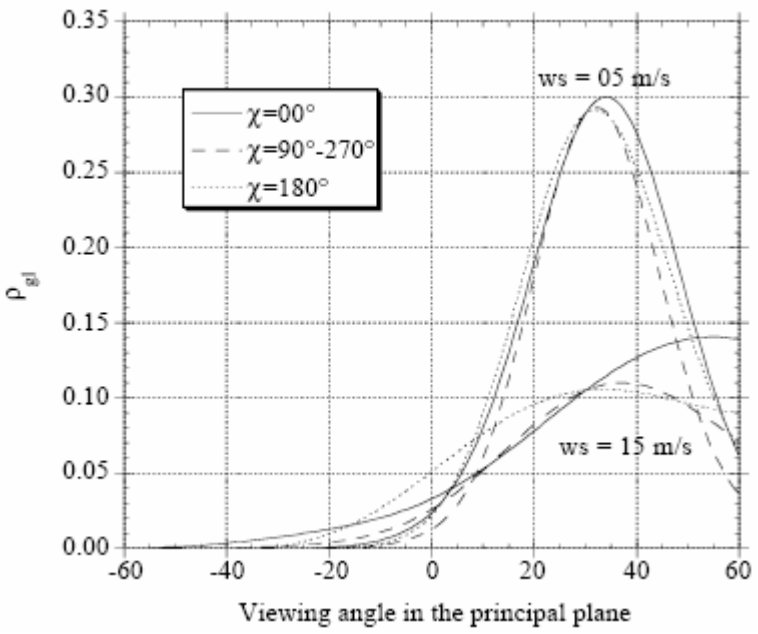


**Fig. 2.** Reflectance of the sunglint in the principal plane for a wind speed of 5 and 15 m/s and for several $\chi = \varphi_s - \varphi_w$. The solar zenith angle is 30° and the wavelength is 0.550 µm.

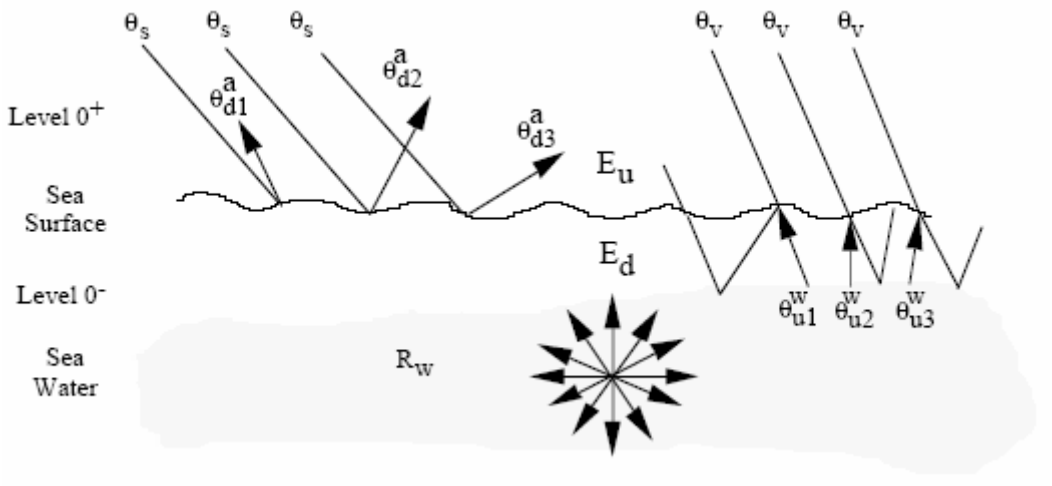


**Fig. 3.** Reflectance emerging from sea water.

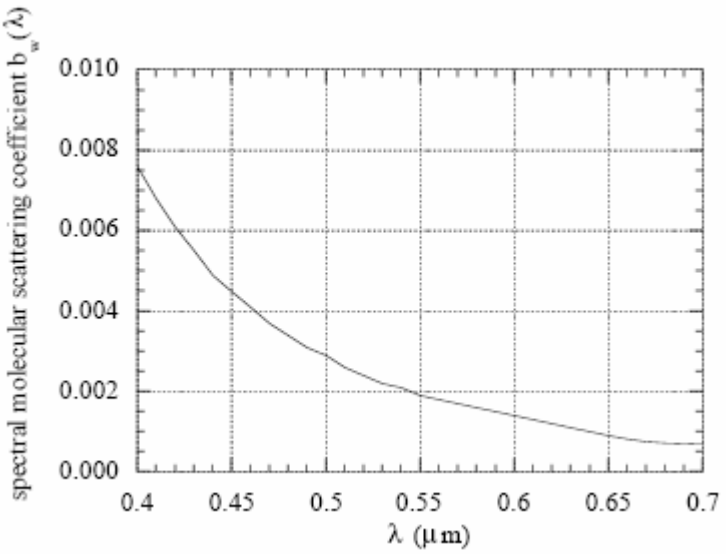


**Fig. 4.** Spectral molecular scattering coefficients ($m^{-1}$).

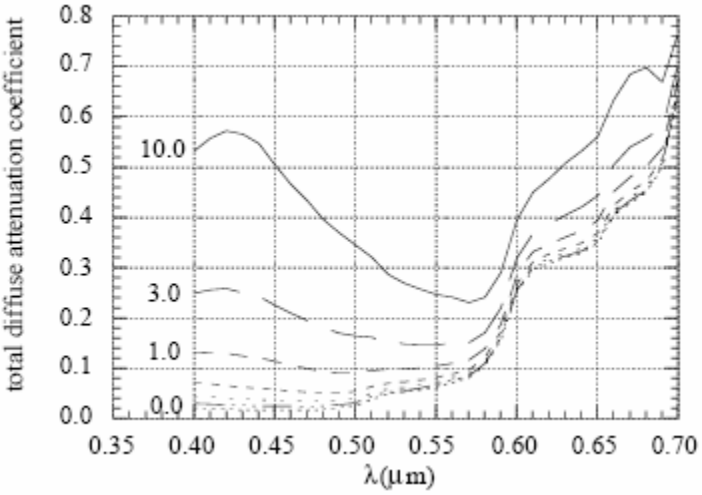


**Fig. 5.** Diffuse attenuation coefficients [$m^{-1}$] as modeled in *Morel*'s "case I waters" for several pigment concentrations (0.0, 0.03, 0.1, 0.3, 1.0, 3.0, and 10.0 $mg \cdot m^{-3}$).

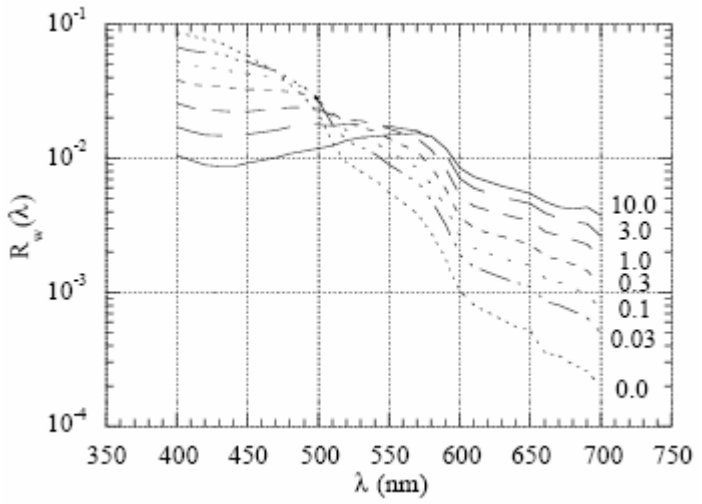


**Fig. 6.** Spectral irradiance reflectances as defined by *Morel'*s "case I waters" model for several pigment concentrations (0.0, 0.03, 0.1, 0.3, 1.0, 3.0, and 10.0 $mg \cdot m^{-3}$).

**References:**

R.W. Austin, and T.J. Petzold, Spectral dependence of the diffuse attenuation coefficient of light in ocean water, *Optical Engineering*, 25, 471-479, 1986.

M. Born, and E. Wolf, Principles of Optics - fifth edition, Pergamon Press, New-York, 1975.

C. Cox, and W. Munk, Statistics of the sea surface derived from sun glitter, *Journal of Marine Research*, 13, 198-227, 1954.

C. Cox, and W. Munk, Measurement of the roughness of the sea surface from photographs of the sun's glitter, *Journal of the Optical Society of America*, 44, 838-850, 1954.

C. Cox, and W. Munk, Some problems in optical oceanography, *Journal of Marine Research*, 14, 63-78, 1955.

D. Friedman, Infrared characteristics of ocean water (1.5-15μm), *Applied Optics*, 8(10), 2073-2078, 1969.

G.M. Hale, and M.R. Querry, Optical constants of water in the 200 nm to 200 μm wavelength region, *Applied Optics*, 12(3), 555-563, 1973.

N.G. Jerlov, Optical studies of ocean water, *Reports of the Swedish Deep-Sea Expedition*, 1947-1948, 3, 1-19, 1951.

N.G. Jerlov, Marine Optics, *Elsevier Oceanography Series*, 14, 231, Elsevier, Amsterdam, 1976.

P. Koepke, Effective Reflectance of Oceanic Whitecaps, *Applied Optics*, 23(11), 1816-1824, 1984.

H.J. McLellan, *Elements of physical oceanography*, Pergamon Press, Inc., New-York, 1965.

E.C. Monahan, and I. O'Muircheartaigh, Optimal power-law description of oceanic whitecap dependence on wind speed, *Journal of Physical Oceanography*, 10(12), 2094–2099, 1980.

A. Morel, Optical modeling of the upper ocean in relation to its biogenous matter content (case I waters), *Journal of Geophysical Research*, 93(C9), 10749-10768, 1988.

A. Morel, and L. Prieur, Analysis of variations in ocean color, *Limnology and Oceanography*, 22(4), 709-722, 1977.

H. V. Sverdrup, M.W. Johnson, and R.H. Fleming, *The ocean*, Prentice-Hall, Inc., Englewood Cliffs, N.J., 1942.

## ***SUBROUTINE RAHMBRDF***

**Function**: To generate a BRDF following *Rahman et al.*'s model.

**Description (from *Raman et al.*, 1993)**: It's a semiempirical model for arbitrary natural surfaces in visible and near-infrared spectra on the basis of 3 parameters. The reflectance $\rho_s$ of a surface illuminated from a direction $(\theta_s, \phi_s)$ and observed from a direction $(\theta_v, \phi_v)$ is calculated as

$$\rho_s(\theta_s, \phi_s, \theta_v, \phi_v) = \rho_0 \frac{\cos^{k-1}\theta_s \cos^{k-1}\theta_v}{(\cos\theta_s + \cos\theta_v)^{1-k}} F(g)[1 + R(G)],$$

where

$\rho_0$ is the arbitrary parameter characterizing the intensity of the reflectance of the surface cover,

k is the structural parameter indicating the level of anisotropy of the surface,

F(g) is the modified *Henyey & Greenstein*'s function defined as

$$F(g) = \frac{1 - \Theta^2}{[1 + \Theta^2 - 2\Theta\cos(\pi - g)]^{1.5}},$$

with the phase angle g given by

$$\cos g = \cos\theta_s \cos\theta_v + \sin\theta_s \sin\theta_v \cos(\phi_s - \phi_v)$$

and the asymmetry factor $\Theta$ controlling the relative amount of forward ($0 \le \Theta \le +1$) and backward ($0 \le \Theta \le -1$) scattering,

and R(g) is the function accounting for the hot spot effect, defined as

$$R(G) = \frac{1 - \rho_0}{1 + G},$$

with the geometric factor G given by

$$G = [\tan^2\theta_s + \tan^2\theta_v - 2\tan\theta_s \tan\theta_v \cos(\phi_s - \phi_v)]^{1/2}.$$

**Parameters:**

$\rho_0$, $\Theta$, k

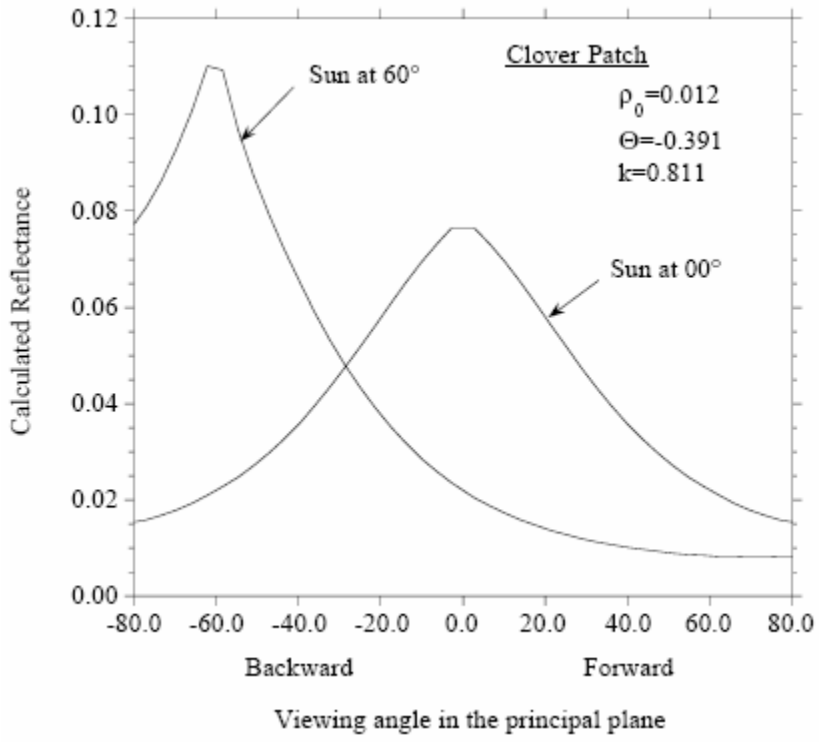


**References:**

H. Rahman, B. Pinty, and M.M. Verstraete, Coupled surface-atmosphere reflectance (CSAR) model. 1. Model description and inversion on synthetic data, *Journal of Geophysical Research*, 98(D11), 20791-20801, 1993.

H. Rahman, B. Pinty, and M.M. Verstraete, Coupled surface-atmosphere reflectance (CSAR) model. 2. Semiempirical surface model usable with NOAA Advanced Very High Resolution Radiometer Data, *Journal of Geophysical Research*, 98, 20791-20801, 1993.

## ***SUBROUTINE ROUJBRDF***

**Function**: To generate a BRDF following *Roujean et al.*'s (1992) model.

**Description (from *Roujean et al.*, 1992)**: The model follows a semi-empirical approach and is designed to be applicable to heterogeneous surfaces. The observed surface bidirectional reflectance is assumed to be the sum of two main processes operating at a local scale:

- diffuse reflection, which takes into account the geometrical structure of opaque reflectors (protrusions) placed on a flat horizontal surface and shadowing effects, and
- volume scattering by a collection of dispersed facets, which simulates the volume scattering properties of canopies and bare soils.

Following this assumption, the bidirectional reflectance $\rho(\theta_s, \theta_v, \phi)$ can be expressed as:

$$\rho(\theta_s, \theta_v, \phi) = \alpha\rho_{geom} + (1-\alpha)\rho_{vol},$$

where α is an empirical coefficient which characterizes the relative weight of the geometric and volume components in the final bidirectional signature.

Then, the bidirectional reflectance can be written as

$$\rho(\theta_s, \theta_v, \phi) = k_0 + k_1 f_1(\theta_s, \theta_v, \phi) + k_2 f_2(\theta_s, \theta_v, \phi),$$

where

- $\phi = |\phi_s - \phi_v|$
- $k_0$, $k_1$ and $k_2$ are related to basic macroscopic properties of the surface:

$$k_0 = \rho_0[\alpha + (1-\alpha)e^{-bF}] + \frac{r}{3}(1-e^{-bF})(1-\alpha),$$

$$k_1 = \frac{hl}{S}\rho_0\alpha, \text{ and}$$

$$k_2 = r(1-e^{-bF})(1-\alpha),$$

with $\rho_0$, the background and protrusion reflectance,
h, the average height of surface protrusions,
l, the average length of surface protrusions,
S, the horizontal surface associated with each protrusion,
r, the facet reflectance, and
F, the facet area index.

• $f_1$ and $f_2$ are simple analytic functions of the solar and view angles:

$$f_1(\theta_s,\theta_v,\phi)=\frac{1}{2\pi}\{(\pi-\phi)\cos(\phi)+\sin(\phi)\}\,tg(\theta_s)tg(\theta_v)$$
$$-\frac{1}{\pi}\left\{tg(\theta_s)+tg(\theta_v)+\sqrt{tg^2(\theta_s)+tg^2(\theta_v)-2tg(\theta_s)tg(\theta_v)\cos(\phi)}\right\}, \text{ and}$$

$$f_2(\theta_s,\theta_v,\phi)=\frac{4}{3\pi}\frac{1}{\cos(\theta_s)+\cos(\theta_v)}\left\{(\frac{\pi}{2}-\xi)\cos(\xi)+\sin(\xi)\right\}-\frac{1}{3}$$

with the phase angle $\xi$ defined as

$$\cos(\xi)=\cos(\theta_s)\cos(\theta_v)+\sin(\theta_s)\sin(\theta_v)\cos(\phi).$$

**Parameters:**

$k_0$, $k_1$, $k_2$

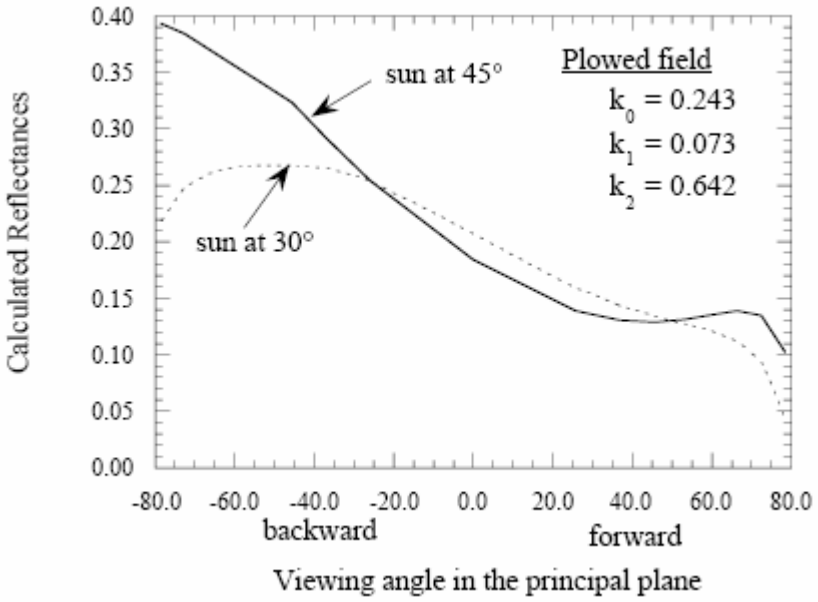


**References:**

J.L. Roujean, M. Leroy, and P.Y. Deschamps, A bidirectional reflectance model of the Earth surface for the correction of remote sensing data, *Journal of Geophysical Research*, 97, 20455-20468, 1992.

## ***SUBROUTINE VERSBRDF***

**Function**: To generate a BRDF following *Verstraete et al.*'s (1990) model.

**Description (from *Pinty & Verstraete*, 1991)**: Using the basic framework previously suggested by *Hapke* (1981) (see HAPKBRDF), *Verstraete et al.* (1990) have developed a model for predicting the bidirectional reflectance exiting from a simple vegetation canopy. They concentrate on the case of a fully covered, homogeneous and semi-infinite canopy made of leaves only. With the same notations as for *Hapke*'s model, the parametric version of the derived model (see *Pinty et al.*, 1990) is as follows:

$$\rho(\theta_s,\phi_s,\theta_v,\phi_v)=\frac{\omega}{4}\frac{\kappa_s}{\kappa_v\mu_s+\kappa_s\mu_v}\left\{[1+P_v(G)]P(g)+H(\kappa_s/\mu_s)H(\kappa_v/\mu_v)-1\right\},$$

where

• $\omega$ is average single-scattering albedo of particles making up the surface

• $\mu_s=\cos(\theta_s)$ and $\mu_v=\cos(\theta_v)$

• $\kappa_s$ and $\kappa_v$ describe the leaf orientation distribution for the illumination and view angles, respectively. There are 3 possible options (see below, line1-opt3)

- $\kappa_s$ and $\kappa_v$ are entered by the user;
- $\kappa$ is obtained from *Goudriaan*'s (1977) parameterization;

$$\kappa_x = \Psi_1 + \Psi_2\,\mu_x$$

with $\Psi_1 = 0.5 - 0.6333\,\chi_l - 0.33\,\chi_l^2$ and $\Psi_2 = 0.877\,(1 - 2\,\Psi_1)$;

- $\kappa$ is obtained from *Dickinson et al.*'s (1990) correction to *Goudriaan*'s (1977) parameterization

$$\kappa_x = \Psi_1 + \Psi_2\,\mu_x$$

with $\Psi_1 = 0.5 - 0.489\,\chi_l - 0.11\,\chi_l^2$ and $\Psi_2 = 1 - 2\,\Psi_1$.

where $\chi_l$ is the leaf angle distribution function of the canopy, which varies from -0.4 for an erectophile canopy to +0.6 for a planophile canopy. The equal probability for all leaf orientations is given by $\chi_l = 0$.

• $P_v(G)$ is the function that accounts for the joint transmission of incoming and outgoing radiation and, thereby, also for the hot spot phenomenon:

$$P_v(\theta_s,\phi_s,\theta_v,\phi_v) = \frac{1}{1+V_p(\theta_s,\phi_s,\theta_v,\phi_v)}$$

with the function $V_p(\theta_s,\phi_s,\theta_v,\phi_v)$ defined by

$$V_p(\theta_s,\phi_s,\theta_v,\phi_v) = 4(1-\frac{4}{3\pi})\frac{\mu_v}{2r\Lambda\kappa_v}\sqrt{\tan^2(\theta_s)+\tan^2(\theta_v)-2\tan(\theta_s)\tan(\theta_v)\cos(\phi_s-\phi_v)}\,,$$

where r is the radius of Sun flecks on the inclined scatterers [m] and $\Lambda$ is the scatterer area density of the canopy [$m^2m^{-3}$].

• P(g) is the average phase function of particles. There are 3 options to compute P(g) (see below, line1-opt4):

-the case of an isotropic phase function

$$P(g) = 1;$$

- the empirical function introduced by *Henyey & Greenstein* (1941)

$$P(g) = \frac{1-\Theta^2}{1+\Theta^2+2\Theta\cos(g)};$$

- the phase function approximated by a Legendre polynomial function

$$P(g) = 1+\Theta\cos(g)+L_2\frac{3\cos^2(g)-1}{2},$$

where $\Theta$ is the asymmetry factor ranging from -1 (backward scattering) to +1, g is the phase angle between the incoming and outgoing rays defined as

$$\cos(g) = \cos(\theta_s)\cos(\theta_v)+\sin(\theta_s)\sin(\theta_v)\cos(\phi_s-\phi_v),$$

and $L_2$ is the second coefficient of the Legendre polynomial.

• H(x) is a function to account for multiple scattering (see below, line1-opt5):

- for single scattering

$$H(x) = 0;$$

- for multiple scattering

$$H(x) = \frac{1+2x}{1+2(1-\omega)^{1/2}x}.$$

**There are three lines of input parameters:**

line 1- choice of options: opt3, opt4, opt5

line 2- structural parameters: str1, str2, str3, str4

line 3- optical parameters: optics1, optics2, optics3

line 1:

opt 3 - 0 for the user's values of $\kappa$

1 for *Goudriaan*'s parameterization of $\kappa$

2 for *Dickinson et al.*'s correction to *Goudriaan*'s parameterization of $\kappa$

opt 4 - 0 for the isotropic phase function

1 for *Heyney & Greenstein*'s phase function

2 for the Legendre polynomial phase function

opt 5 - 0 for single scattering only

1 for *Dickinson et al.*'s parameterization of multiple scattering

line 2:

str1 - leaf area density [$m^2m^{-3}$]

str2 - radius of sun flecks on the scatterer [m]

str3 - leaf orientation parameter

if opt3=0, then str3=$\kappa_s$

if opt3=1 or 2, then str3=$\chi_l$

str4 - leaf orientation parameter (continued)

if opt3=0, then str4=$\kappa_v$

if opt3=1 or 2, then str4 is not used

line 3:

optics 1 - single scattering albedo, value between 0.0 and 1.0

optics 2 - phase function parameter

if opt4=0, then this input is not used

if opt4=1, then the asymmetry factor, value between -1.0 and 1.0

if opt4=2, then the first coefficient of the Legendre polynomial

optics 3 - second coefficient of the Legendre polynomial (if opt4=2)

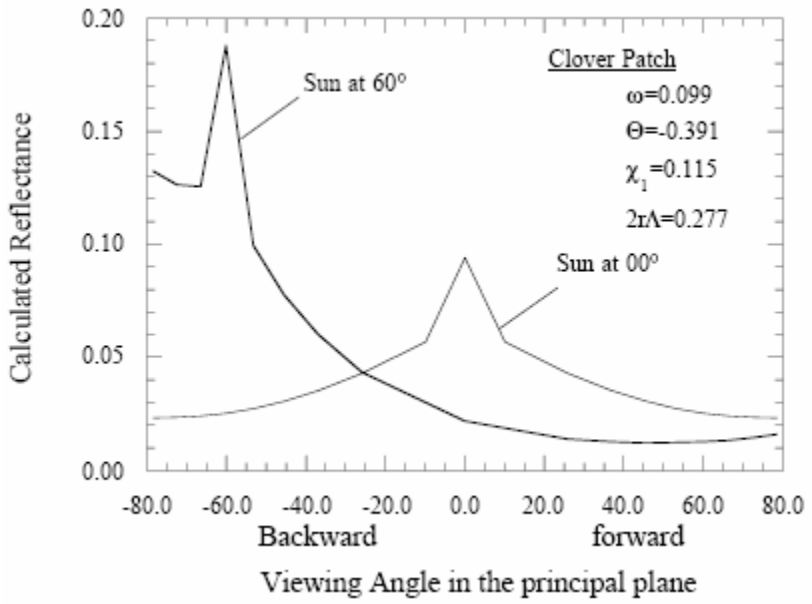


**References:**

R.E. Dickinson, B. Pinty, and M. Verstraete, Relating surface albedos in gcm to remotely sensed data, *Agricultural and Forest Meteorology*, 52, 109-131, 1990.

J. Goudriaan, Crop micrometeorology: a simulation study (Wageningen: Wageningen Centre for Agricultural Publishing and Documentation), 1977.

L.G. Henyey and J.L. Greenstein, Diffuse radiation in the galaxy. *Astrophysical Journal*, 93**,** 70, 1941.

B. Pinty, M. Verstraete, and R.E. Dickinson, A physical model of the bidirectional reflectance of vegetation canopies. 1. Inversion and validation, *Journal of Geophysical Research*, 95, 11767-11775, 1990.

B. Pinty, and M. Verstraete, Extracting information on surface properties from bidirectional reflectance measurements, *Journal of Geophysical Research*, 96, 2865-2874, 1991.

M. Verstraete, B. Pinty, and R.E. Dickinson, A physical model of the bidirectional reflectance of vegetation canopies. 1. Theory, *Journal of Geophysical Research*, 95, 11755-11765, 1990.

## ***SUBROUTINE WALTBRDF***

**Function**: To generate a BRDF following *Walthall et al.*'s (1985) model.

**Description (from *Walthall et al.*, 1985)**: Using a deterministic model, *Walthall et al.* (1985) have simulated different canopy reflectance distributions. The 2-D contours of these distributions appeared to be similar to the shape of the Pascal limacon. Using the simple limacon equation, *Walthall et al.* checked other equation forms trying to fit the 3-D reflectance surface directly. They found satisfactory results with the following equation:

$$\rho(\theta_s, \theta_v, \phi_s, \phi_v) = a\ \theta_v^{\ 2} + b\ \theta_v \cos(\phi_v - \phi_s) + c$$

where ρ is the reflectance at given view zenith $\theta_v$ and view azimuth $\phi_v$ angles, and a, b, and c are coefficients derived using a linear least-squares fitting procedure.

The model has to be slightly modified to match the reciprocity principle. The reflectance is written:

$$\rho(\theta_s, \theta_v, \phi_s, \phi_v) = a\ \theta_s^{\ 2}\theta_v^{\ 2} + a'(\theta_s^{\ 2} + \theta_v^{\ 2}) + b\ \theta_s\ \theta_v \cos(\phi_v - \phi_s) + c\ .$$

**Parameters:**

a, a', b, c

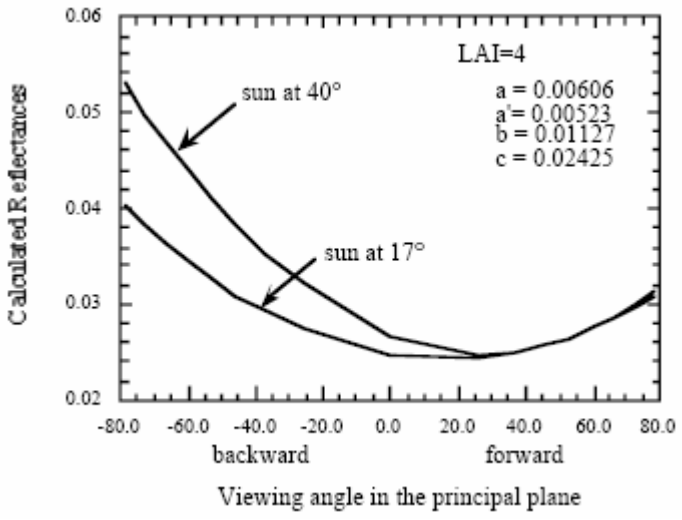


**Reference:**

C.L. Walthall, J.M. Norman, J.M. Welles, G. Campbell, and B.L. Blad, Simple equation to approximate the bidirectional reflectance from vegetative canopies and bare soil surfaces, *Applied Optics*, 24(3), 383-387, 1985.

## ***SUBROUTINE AKBRDF***

**Function**: To generate a BRDF following *Kuusk*'s (1994) model.

**Description (from *Kuusk*, 1994, 1995):** The single scattering radiance of a canopy layer with the height H is

$$I_c^1 = \frac{F_0\mu_0}{\pi\mu\mu_0}\int_0^H u_L(z)\,\Gamma(r_0,r)\,p(z,r_0,r)\,dz \qquad (1)$$

where $F_0\mu_0/\pi$ is the intensity of the incident direct flux on a horizontal surface, $u_L$ is the leaf area density, $\Gamma(r_0,r)$ is the phase function of single scattering, $p(z,r_0,r)$ is the bidirectional gap probability inside a canopy at the level z in directions $r_0(\theta_0,\phi_0)$ and $r(\theta,\phi)$, and $\mu_0$ and $\mu$ are the respective cosines.

The phase function $\Gamma=\Gamma_D+\Gamma_{SP}$ and bidirectional gap probability $p(z,r_0,r) = p(r_0)p(r)C_{HS}(r_0,r)$ are functions of the leaf angle distribution $g_L(\theta_L)$. Here $\Gamma_D$ is the phase function of diffuse scattering of lambertian leaves (see Eq. (10) of subroutine IAPIBRDF), and $\Gamma_{SP}$ is the phase function of Fresnel reflection on the leaf surface. The phase function of specular reflection is corrected for the leaf hair and surface roughness (*Nilson & Kuusk*, 1989). The hot spot factor

$$C_{HS}(H,\alpha) = \exp\left\{\sqrt{\frac{G_L^{(1)}\,G_L^{(2)}}{\mu_1\mu_2}}\;\frac{L_H s_L}{\Delta(r_1,r_2)}\left[1-\exp\left(-\frac{\Delta(r_1,r_2)}{s_L}\right)\right]\right\} \qquad (2)$$

considers for the finite leaf size $s_L$. Here $\Delta(r_1,r_2)=\sqrt{1/\mu_1^2+1/\mu_2^2-2\cos\alpha/(\mu_1\mu_2)}$ is the geometry factor, and $\pi$-$\alpha$ is the scattering angle.

The function $G_L(r)$ is given by Eq. (9) of subroutine IAPIBRDF. For the cases of a spherical orientation of leaves and fixed angle of leaves, exact analytical expressions for the phase function $\Gamma$ and G-function were obtained by *T. Nilson* (see *Ross*, 1981). In case of an elliptical leaf angle distribution :

$$g_L(\theta_L) = B_g\Big/\sqrt{1-\varepsilon^2\cos^2(\theta_L-\theta_m)}\,, \qquad (3)$$

the analytical approximations for the G-function and phase function $\Gamma$ were obtained by *Kuusk* (1995). Here the eccentricity $\varepsilon$ and modal inclination $\theta_m$ are the LAD parameters, $B_g$ is a normalizing factor.

Single scattering from soil is given by

$$I^{I}_{soil} = \rho_{soil}(r_0, r)\ \rho(H, r_0, r) \quad (4)$$

where $\rho_{soil}(r_0,r)$ is the bidirectional reflectance of soil. The parabolic approximation of *Walthall et al.* (1985) is applied for the BRDF of soil $\rho_{soil}(r_0,r)$.

Multiple scattering of radiation on foliage and soil is defined by *Schwarzschild*'s approximation (*Nilson & Kuusk*, 1989).

The wavelength-dependent optical parameters of the CR model are calculated with *Jacquemoud & Baret* PROSPECT model (1990) for leaves, and with *Price*'s (1990) base functions (1990) for soil.

Figure 1 shows the comparison of the measured and calculated BRDF for a barley canopy, and in Fig. 2 the nadir reflectance spectrum of a corn canopy is compared to that measured by *Ranson et al.* (1984).

As all double integrals for directional functions are calculated analytically, the model works very fast.

**Parameters:**

line 1: structural parameters ($u_L$, $\varepsilon$, $\theta_m$, $s_L$)

line 2: optical parameters ($c_{AB}$, $c_W$, N, $c_n$, $s_1$)

$u_L$ – LAI

$\varepsilon$, $\theta_m$ – LAD parameters

$s_L$ – relative leaf size

$c_{AB}$ – chlorophyll content, $\mu g/cm^2$

$c_W$ – leaf water equivalent thickness, cm

N – the effective number of elementary layers inside a leaf

$c_n$ – the ratio of refractive indices of the leaf surface wax and internal material

$s_1$ – the weight of the 1st Price function for the soil reflectance

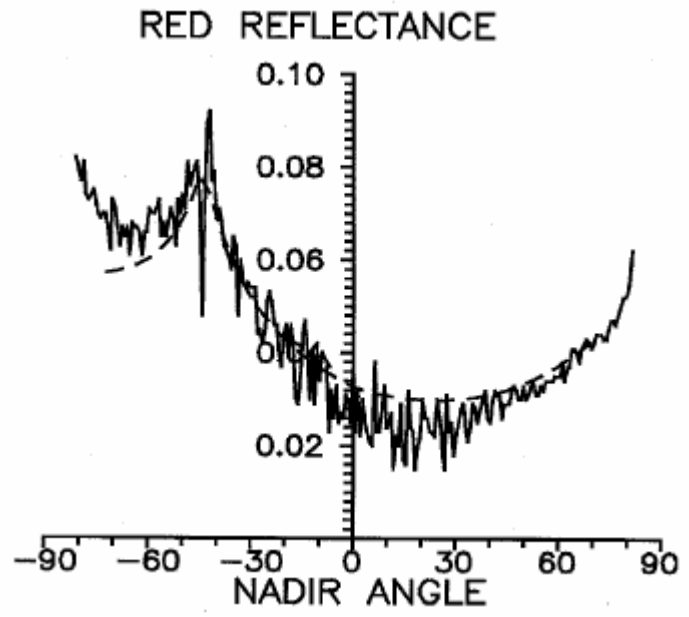


**Fig. 1.** The calculated BRDF vs. the measured one for a barley canopy.

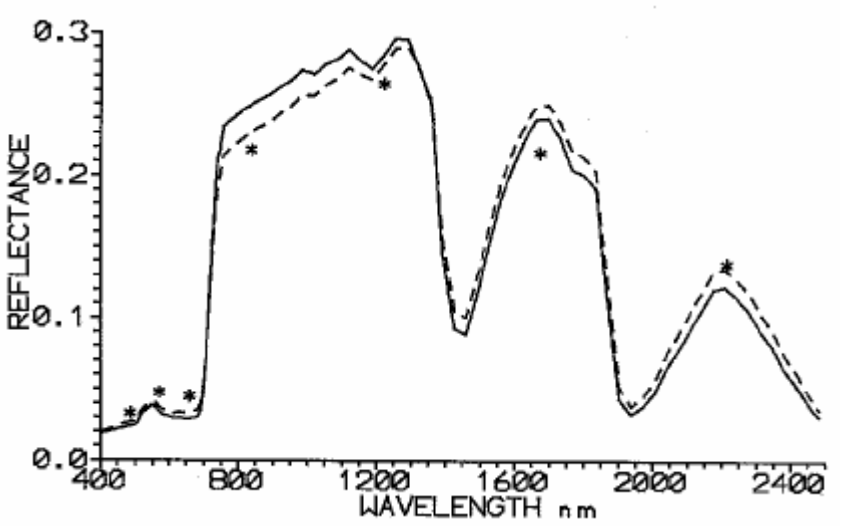


**Fig. 2.** The calculated nadir reflectance spectrum vs. the measured one for a corn canopy.

**References:**

A. Kuusk, A multispectral canopy reflectance model, *Remote Sensing of Environment*, 50, 75-82, 1994.

A. Kuusk, A computer-efficient plant canopy reflectance model, *Computers & Geosciences*, 22(2), 149-163, 1996.

S. Jacquemoud and F. Baret, Prospect, a model of leaf optical properties spectra, *Remote Sensing*

*of Environment*, 34, 75-91, 1990

T. Nilson and A. Kuusk, A reflectance model for the homogeneous plant canopy and its inversion, *Remote Sensing of Environment*, 27, 157-167, 1989.

J.C. Price, On the information content of soil reflectance spectra, *Remote Sensing of Environment*, 33, 113-121, 1990.

J. Ross, The radiation regime and architecture of plant stands, W. Junk, The Hague, 391 p., 1981.

C.L. Walthall, J.M. Norman, M.J. Welles, G. Campbell, and B.L. Blad, Simple equation to approximate the bidirectional reflectance from vegetative canopies and bare soil surfaces, *Applied Optics*, 24(3), 383-387, 1985.

## ***SUBROUTINE AKLABE***

**Function**: To calculate the spherical albedo using the BRDF computed by *Kuusk*'s (1994) model.

**Description:** This subroutine is based on the same physical principles as the other 6SV subroutines used for spherical albedo calculations; the only difference is in the programming method. AKALBE is a part of the "Multispectral Canopy Reflectance Model" package which was written by A. Kuusk himself in 1994 and directly incorporated into 6S soon afterwards.

**References:**

A. Kuusk, A multispectral canopy reflectance model, *Remote Sensing of Environment*, 50, 75-82, 1994.

A. Kuusk, A computer-efficient plant canopy reflectance model, *Computers & Geosciences*, 22(2), 149-163, 1996.

## ***SUBROUTINE MODISBRDF***

**Function**: To generate a BRDF following the reciprocal RossThick-LiSparse model.

**Description:** This is a linear kernel-driven model which calculates the land surface BRDF as a sum of three theoretically constructed kernels representing basic scattering types: isotropic, volumetric and geometric-optical (*Wanner et al.*, 1995), i.e.,

$$\rho_\lambda(\theta_s,\theta_v,\phi) = p_1 + p_2 K_{RT}(\theta_s,\theta_v,\phi) + p_3 K_{LS}(\theta_s,\theta_v,\phi),$$

Here

• $\theta_s$, $\theta_v$, and $\phi$ are the solar zenith, view zenith, and relative azimuth angles, respectively;

• $p_1$, $p_2$ and $p_3$ are coefficients of the kernels, equal to the reflectances for three basic scattering types;

• $K_{RT}$ is the RossThick kernel which represents scattering from a dense canopy layer of small leaf scatterers with a uniform leaf angle distribution, a Lambertian background, and equal values of transmittance and reflectance based on a single-scattering approximation of radiative transfer theory (*Ross,* 1981*; Roujeau et al.*, 1992; *Lucht et al.*, 2000):

$$K_{RT} = \left[(\pi/2-\xi)\cos\xi + \sin\xi\right] / \left[\cos\theta_s + \cos\theta_v\right] - \pi/4,$$

where $\xi$ is the phase angle calculated as

$$\cos\xi = \cos\theta_s \cos\theta_v + \sin\theta_s \sin\theta_v \cos\phi;$$

• $K_{LS}$ is the LiSparse kernel which represents scattering from a sparse ensemble of 3-D surface objects casting shadows on a Lambertian background (*Li & Strahler*, 1992):

$$K_{LS} = O(\theta_s,\theta_v,\phi) - \sec\theta_s' - \sec\theta_v' + \tfrac{1}{2}(1+\cos\xi')\sec\theta_s'\sec\theta_v',$$

where $O(\theta_s,\theta_v,\phi)$ is the overlap area between the view and solar shadows, calculated as

$$O = \frac{1}{\pi}(t - \sin t\cos t)(\sec\theta_s' + \sec\theta_v'),$$

with

$$\cos t = \frac{h}{b}\frac{\sqrt{D^2 + (\tan\theta_s'\tan\theta_v'\sin\phi)^2}}{\sec\theta_s' + \sec\theta_v'},$$

$$D = \sqrt{\tan^2\theta_s' + \tan^2\theta_v' - 2\tan\theta_s'\tan\theta_v'\cos\phi},$$

$$\cos\xi' = \cos\theta_s'\cos\theta_v' + \sin\theta_s'\sin\theta_v'\cos\phi,$$

$\theta_s^{'} = \tan^{-1}\left(\frac{b}{r}\tan\theta_s\right)$, and $\theta_v^{'} = \tan^{-1}\left(\frac{b}{r}\tan\theta_v\right)$.

The ratios h/b and b/r are the dimensionless crown relative height and shape parameters which should be preselected. The MODIS products assume h/b=2 and b/r=1, i.e., the spherical crowns are separated from the ground by half their diameter (*Lucht et al.*, 2000).

**References:**

W. Wanner, X. Li and A.H. Strahler, On the derivation of kernels for kernel-driven models of bidirectional reflectance, *Journal of Geophysical Research*, 100(D10), 21077–21090, 1995.

J.K. Ross, The radiation regime and architecture of plant stands, Dr. W. Junk, Norwell, MA, 392 p., 1981.

J.L. Roujean, M. Leroy, and P.Y. Deschamps, A bidirectional reflectance model of the Earth's surface for the correction of remote sensing data, *Journal of Geophysical Research,* 97(D18), 20455–20468, 1992.

X. Li and A.H. Strahler, Geometric-optical bidirectional reflectance modeling of the discrete crown vegetation canopy: effect of crown shape and mutual shadowing, *IEEE Transactions on Geoscience and Remote Sensing,* 30(2), 276-292, 1992.

W. Lucht, C.B. Schaaf, and A.H. Strahler, An algorithm for the retrieval of albedo from space using semiempirical BRDF models, *IEEE Transactions on Geoscience and Remote Sensing,* 38(2), 977-998, 2000.

## ***SUBROUTINE MODISALBE***

**Function**: To calculate the spherical albedo using the BRDF values computed by the MODISBRDF subroutine.

**Description:** The spherical albedo s is calculated as

$$s = p_1 + p_2 \cdot 0.189184 - p_3 \cdot 1.377622,$$

where $p_1$, $p_2$ and $p_3$ are coefficients of the kernels, representing the reflectances of the isotropic, radiative transfer-type volumetric, and geometric-optical surface (see subroutine MODISBRDF).

# ***DESCRIPTION OF THE SUBROUTINES USED***

# ***TO UPDATE THE ATMOSPHERIC PROFILE***

# ***(AIRPLANE OR ELEVATED TARGET SIMULATIONS)***

## ***SUBROUTINE PRESPLANE***

**Function**: Update the atmospheric profile ($P(z),T(z),H_2O(z),O_3(z)$) if the observer is on-board an aircraft.

**Description**: Given the altitude or pressure at the aircraft level as an input, the first task is to compute the altitude (if the pressure has been entered) or pressure (if the altitude has been entered) at the plane level. Then, a new atmospheric profile is created ($P_p,T_p,H_2O_p,O_{3p}$), for which the last level is located at the plane altitude. This profile is used in the gaseous absorption computation (subroutine ABSTRA) for the path from target to sensor (upward transmission). The ozone and water vapor integrated content of the "plane" atmospheric profile are also outputs of this subroutine. The last output is the proportion of molecules below the plane level, which is used in scattering computations (subroutines OSPOL and ISO).

## ***SUBROUTINE PRESSURE***

**Function**: Update the atmospheric profile (P(z),T(z),$H_2O$(z),$O_3$(z)) if the target is not at the sea level.

**Description**: Given the altitude of the target in km as an input, we transform the original atmospheric profile (pressure, temperature, water vapor, ozone) so that the first level of the new profile is the one at the target altitude. We also compute the new integrated content of water vapor and ozone, which is used as an output in computations when the user chooses to enter a specific amount of $H_2O$ and $O_3$.

# ***DESCRIPTION OF THE SUBROUTINES USED TO READ THE DATA***

## ***SUBROUTINE SOLIRR***

**Function**: To read the solar irradiance (in $Wm^{-2}\mu m^{-1}$) from 250 nm to 4000 nm by steps of 2.5 nm. The total solar irradiance is put equal to 1372 $Wm^{-2}$. Between 250 and 4000 nm we have 1358 $Wm^{-2}$.

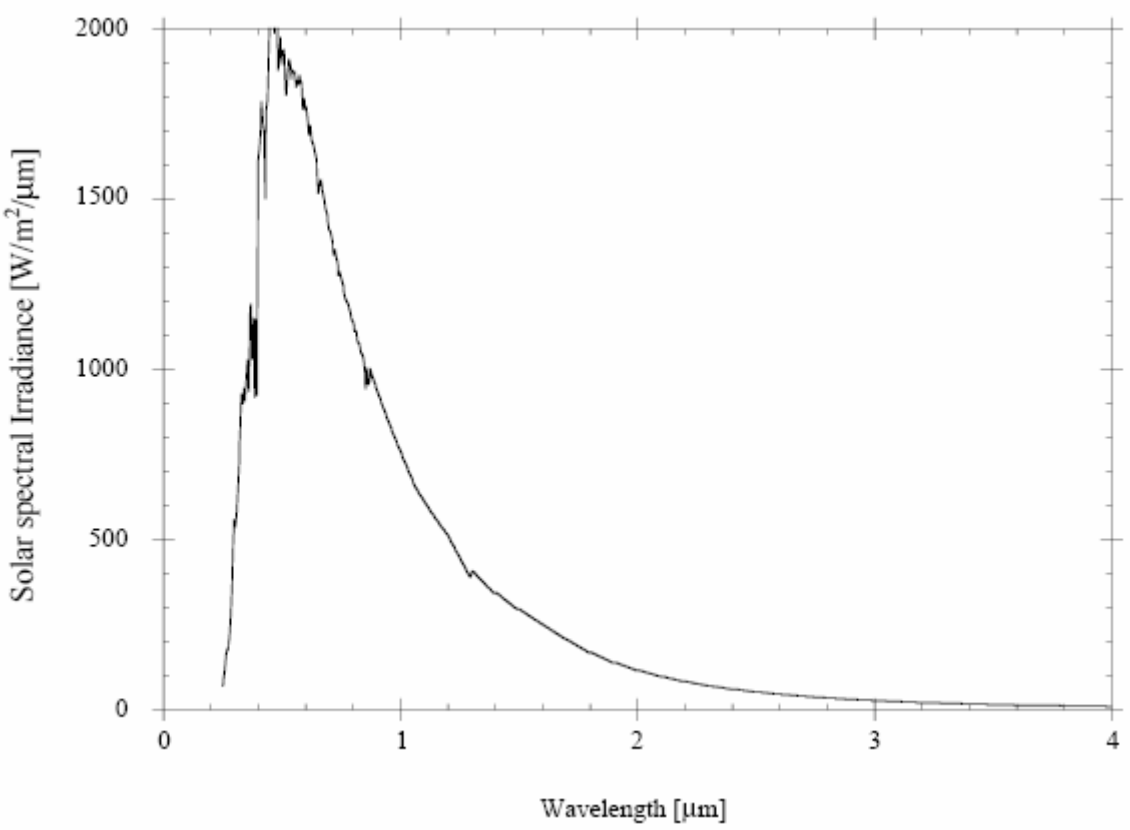


**Reference:**

H. Neckel, and D. Labs, The solar radiation between 3300 and 12500, *Solar Physics*, 90, 205-258, 1984.

## ***SUBROUTINE VARSOL***

**Function**: To take into account the variation of the solar constant as a function of the Julian day.

**Description**: We apply a simple multiplicative factor $D_S$ to the solar constant $C_S$. $D_S$ is written as

$$D_S = \frac{1}{(1 - e\cos M)^2}$$

with

$$M = 0.9856\,(J - 4)\frac{\pi}{180}$$

where e = 0.01673 and J is the Julian day.

**Reference**:

G.W. Paltridge, and C.M.R. Platt, Radiative processes in meteorology and climatology, Elsevier Publishing, New-York, 1977.

## ***SUBROUTINE AATSR***

**Function**: To read the four spectral bands (red and near infrared) of the Advanced Along-Track Scanning Radiometer (AATSR) onboard the European Space Agency satellite ENVISAT. (extreme wavelengths and spectral response of the filter function).

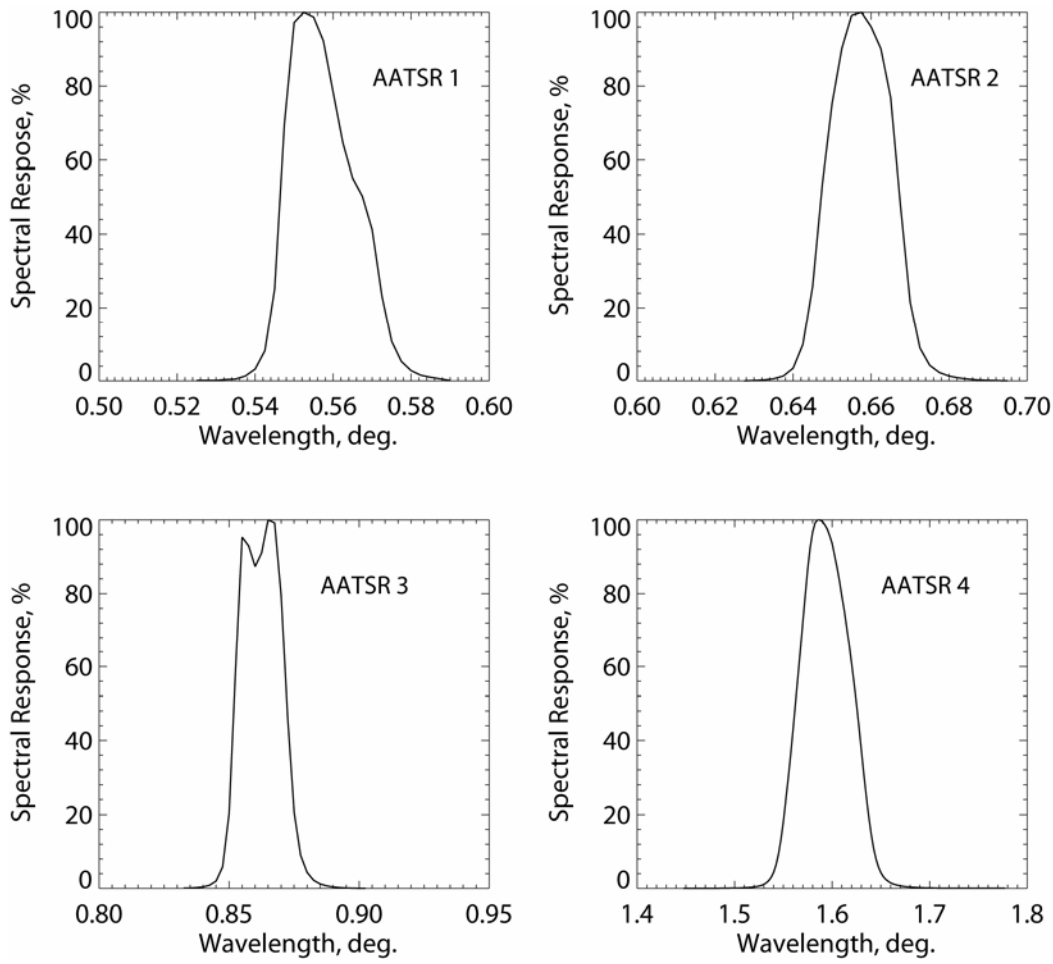


**References:**

W.M.F. Grey, P.R.J. North, O.S. Los, and R.M. Mitchell, Aerosol optical depth and land surface reflectance from multi-angle AATSR measurements: global validation and inter-sensor comparisons, *IEEE Transactions on Geoscience and Remote Sensing*, 44(8), 2184-2197, 2006.

A.G. O'Carroll, J.G. Watts, L.A. Horrocks, R.W. Saunders, and N.A. Rayner, Validation of the AATSR Meteo product Sea Surface Temperature, *Journal of Atmospheric and Oceanic Technology*, 23(5), 711-726, 2006.

**Links:**

http://envisat.esa.int/instruments/aatsr/

http://www.atsr.rl.ac.uk/documentation/index.shtml

http://www.leos.le.ac.uk/aatsr/

## ***SUBROUTINE ALI***

**Function**: To read the nine visible to infrared spectral bands of ALI (Advanced Land Imager) onboard the EO-1 satellite (extreme wavelengths and spectral response of the filter function).

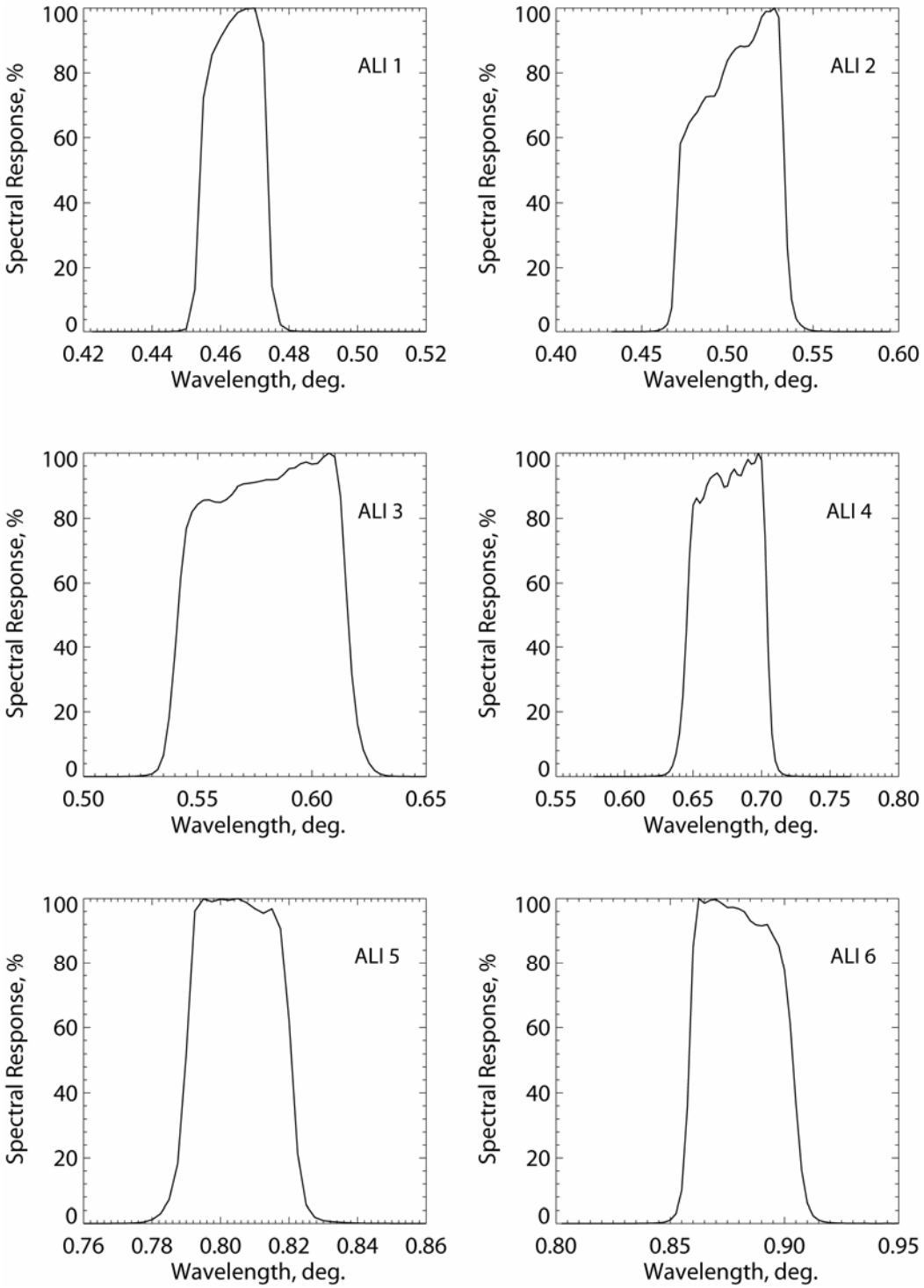

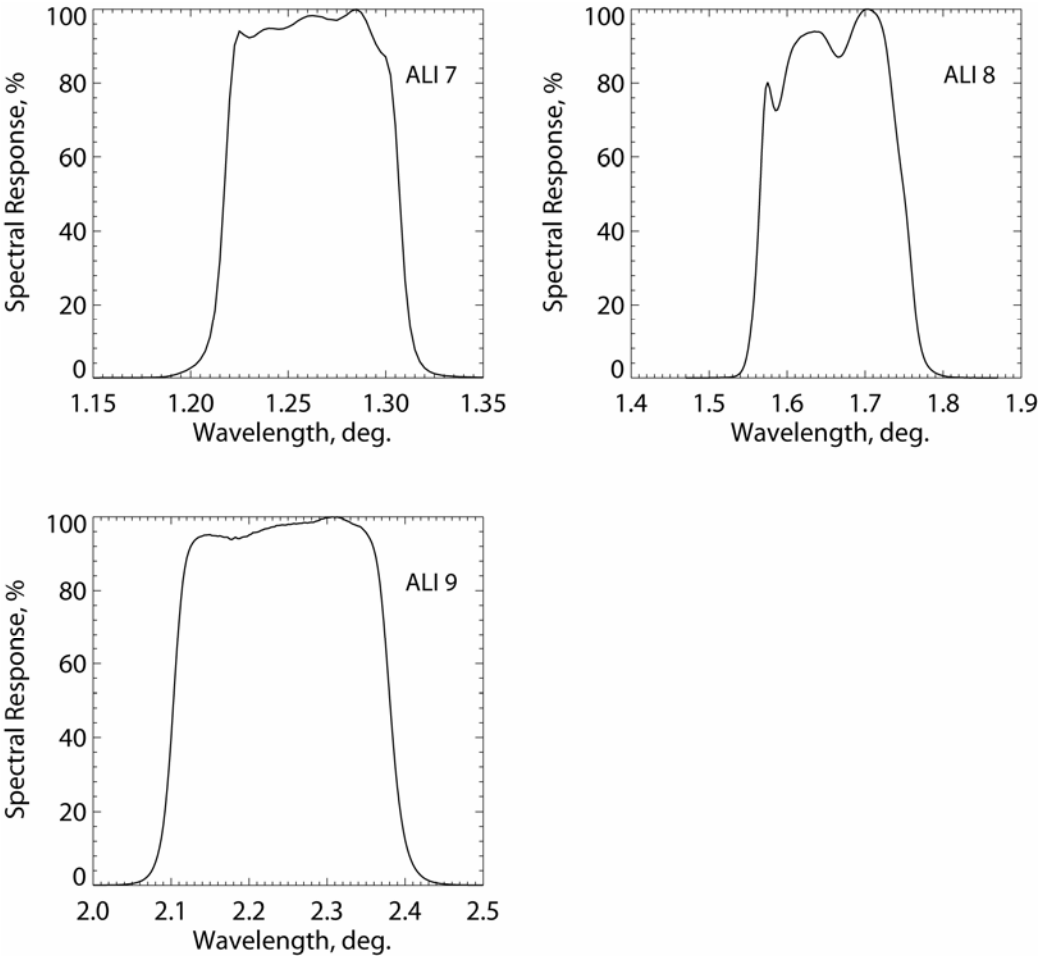


**References:**

R. Bryant, M.S. Moran, S.A. McElroy, C. Holifield, K.J. Thome, T. Miura, and S. F. Biggar, Data continuity of Earth Observing 1 (EO-1) Advanced Land Imager (ALI) and Landsat TM and ETM+, *IEEE Transactions on Geoscience and Remote Sensing*, 41(6), part 1, 1204-1214, 2003.

J.C. Storey, M.J. Choate, and D.J. Meyer, A geometric performance assessment of the EO-1 Advanced Land Imager, *IEEE Transactions on Geoscience and Remote Sensing*, 42(3), 602-607, 2004.

**Link:**

http://eo1.usgs.gov/ali.php

## ***SUBROUTINE ASTER***

**Function**: To read the fourteen visible to thermal infrared spectral bands of ASTER (Advanced Spaceborne Thermal Emission and Reflection radiometer) onboard Terra (extreme wavelengths and spectral response of the filter function).

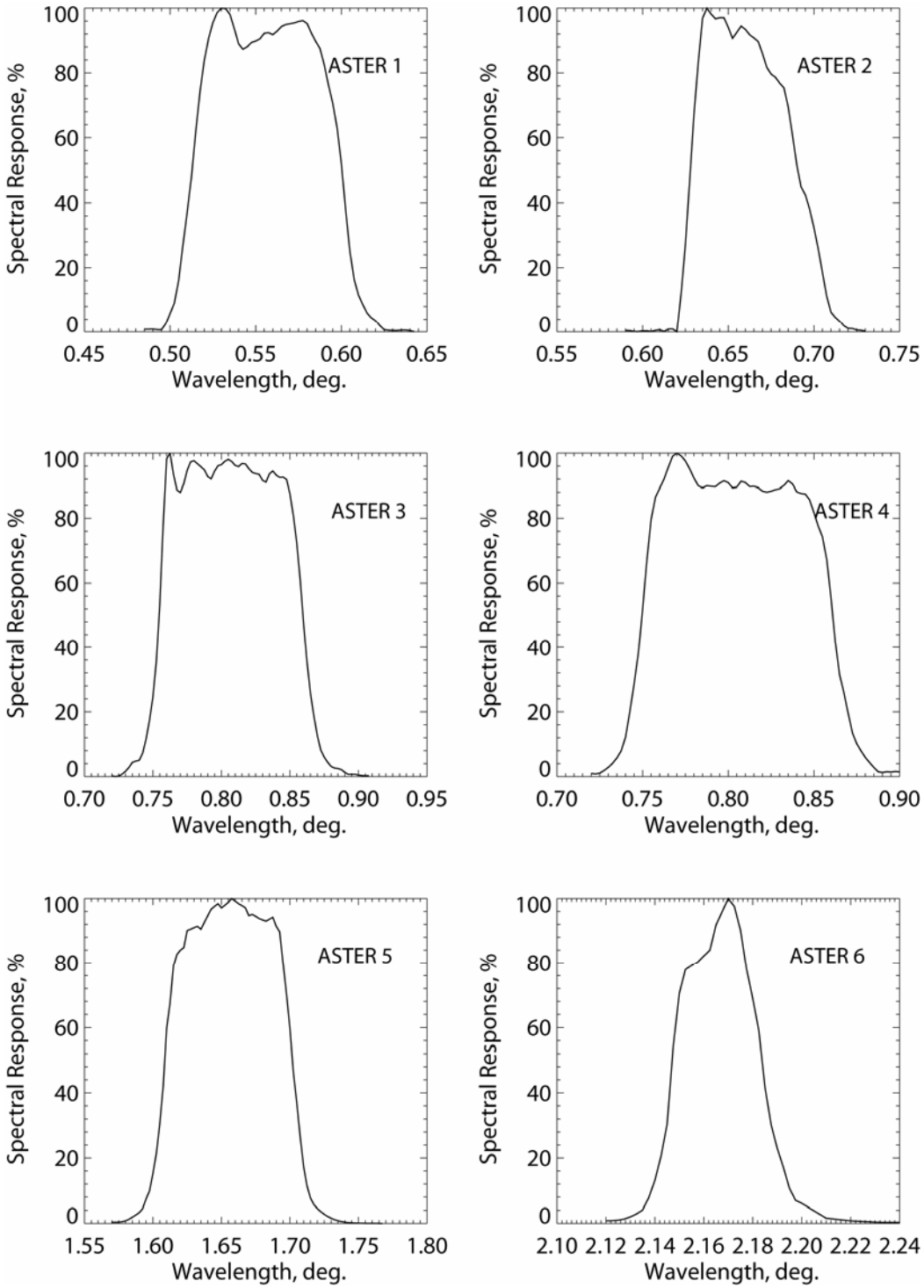

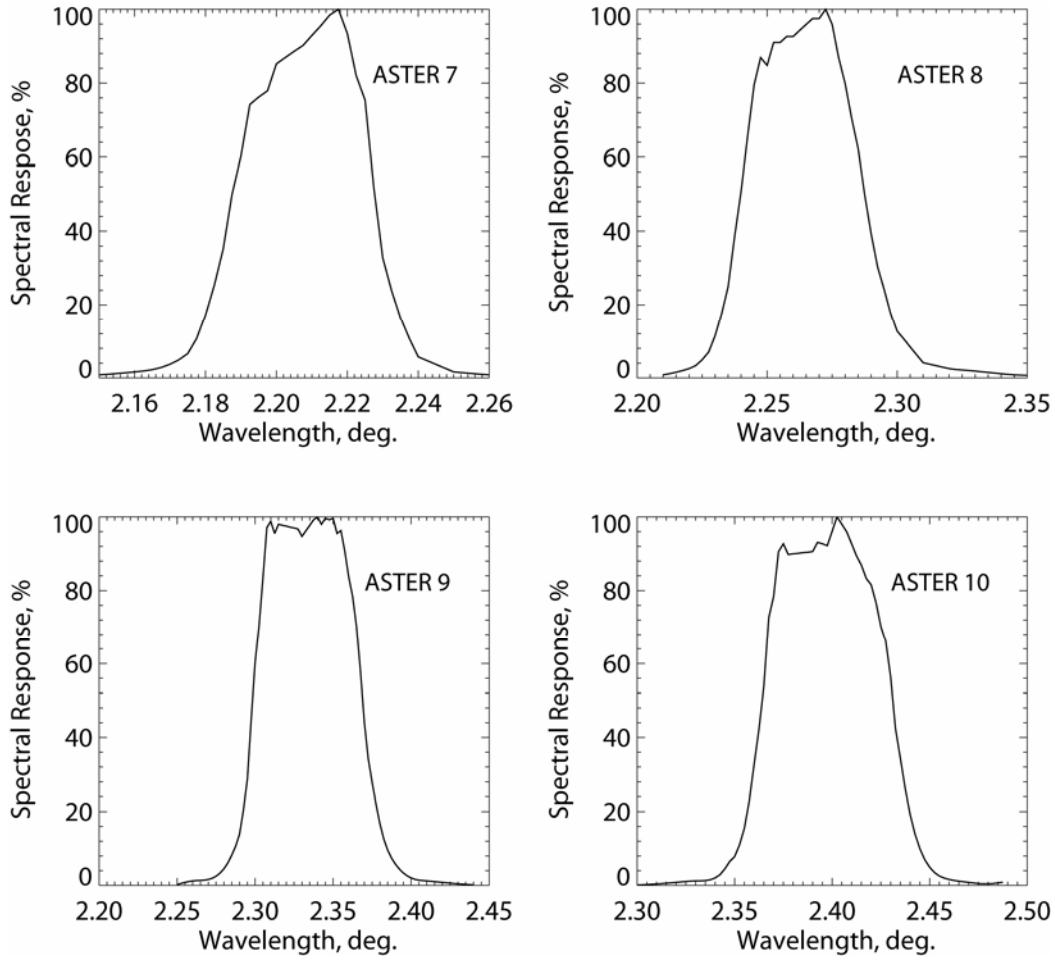


**References:**

M. Abrams, The Advanced Spaceborne Thermal Emission and Reflection Radiometer (ASTER): data products for the high spatial resolution imager on NASA's Terra platform, *International Journal of Remote Sensing*, 21(5), 847-859, 2000.

Y. Yamaguchi, A.B. Kahle, H. Tsu, T. Kawakami, and M. Pniel, Overview of Advanced Spaceborne Thermal Emission and Reflection Radiometer (ASTER), *IEEE Transactions on Geoscience and Remote Sensing*, 36(4), 1062-1071, 1998.

**Link:**

http://asterweb.jpl.nasa.gov/

## ***SUBROUTINE AVHRR***

**Function**: To read the two spectral bands (red and near infrared) of the Advanced Very High Resolution Radiometer (AVHRR) onboard NOAA 6, 7, 8, 9, 10, 11, 12 and 14 (extreme wavelengths and spectral response of the filter function).

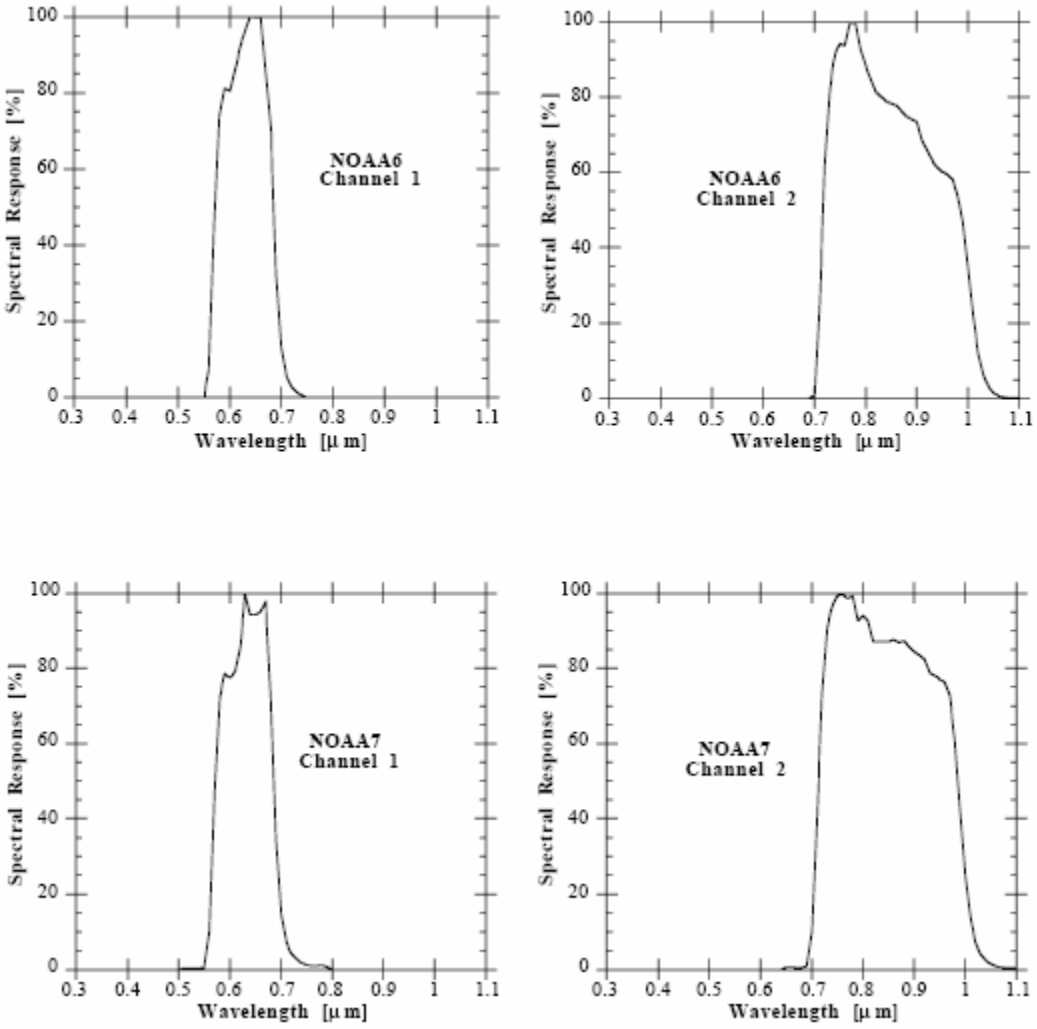

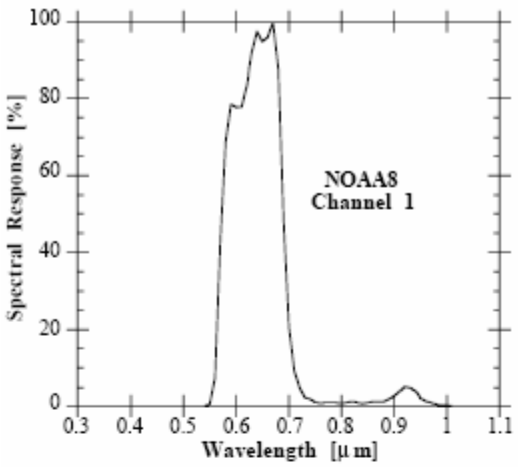
NOAA8
Channel 1
Spectral Response [%]
Wavelength [µm]

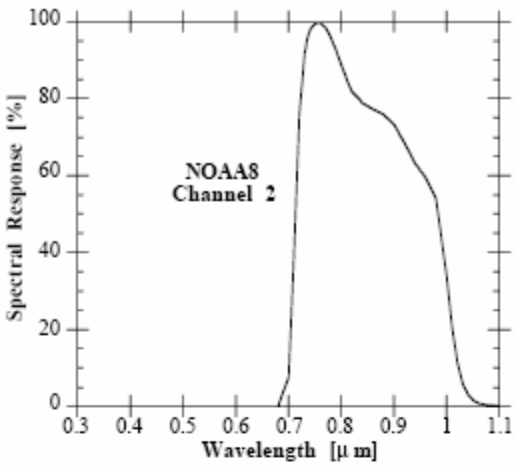
NOAA8
Channel 2
Spectral Response [%]
Wavelength [µm]

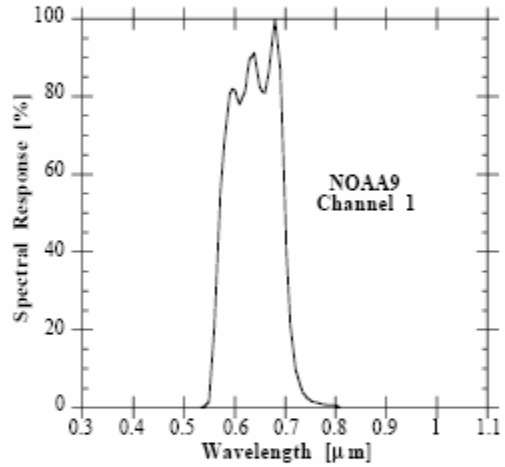
NOAA9
Channel 1
Spectral Response [%]
Wavelength [µm]

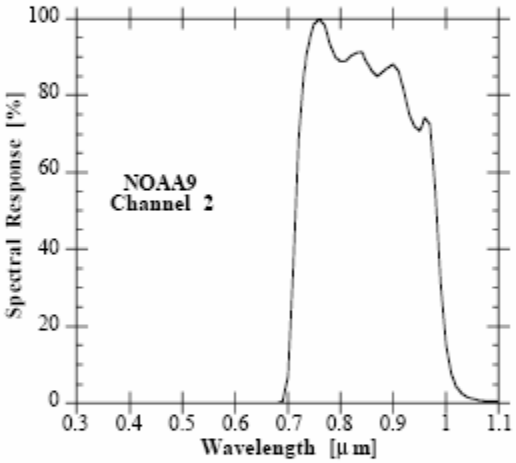
NOAA9
Channel 2
Spectral Response [%]
Wavelength [µm]

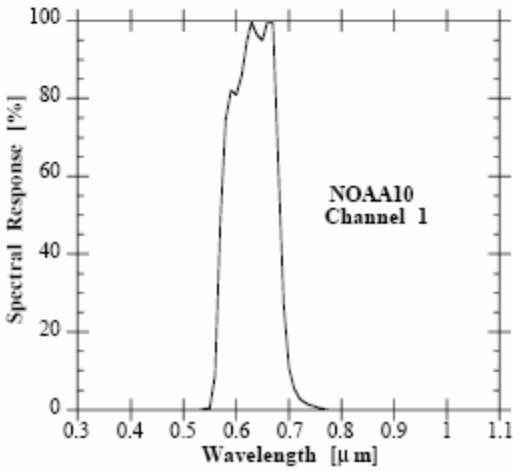
NOAA10
Channel 1
Spectral Response [%]
Wavelength [µm]

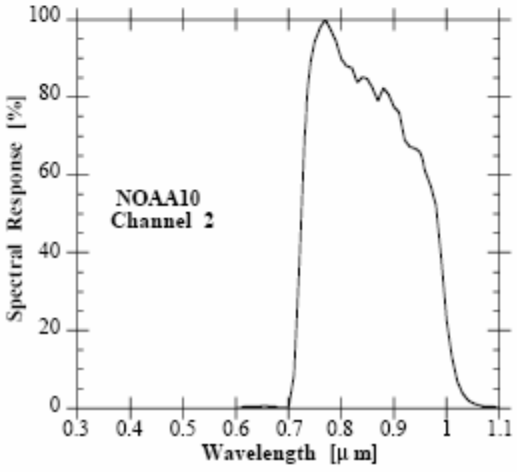
NOAA10
Channel 2
Spectral Response [%]
Wavelength [µm]

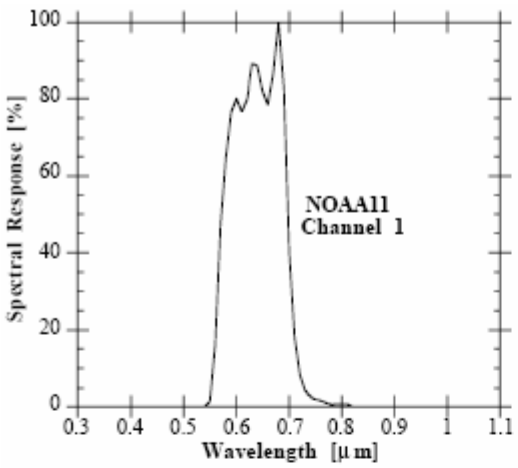
Spectral Response [%]
NOAA11
Channel 1
Wavelength [µm]

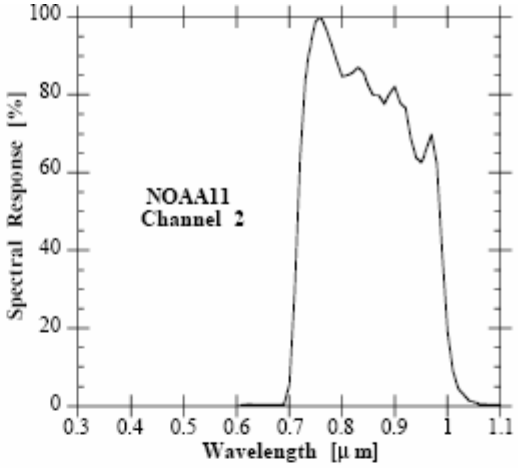
Spectral Response [%]
NOAA11
Channel 2
Wavelength [µm]

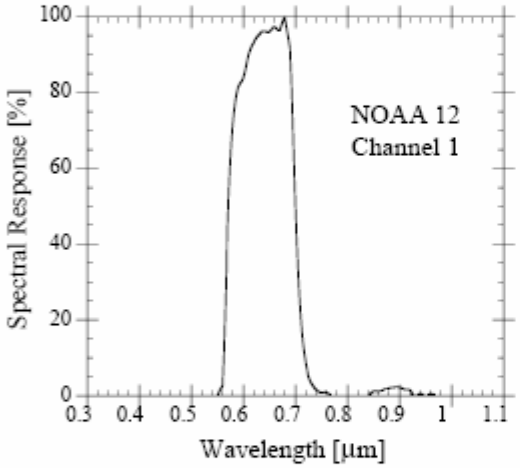
Spectral Response [%]
NOAA 12
Channel 1
Wavelength [µm]

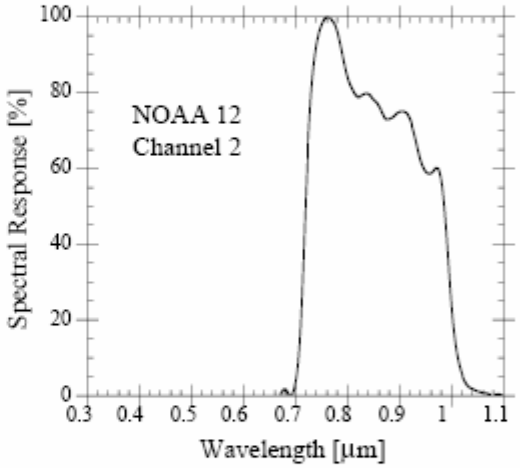
Spectral Response [%]
NOAA 12
Channel 2
Wavelength [µm]

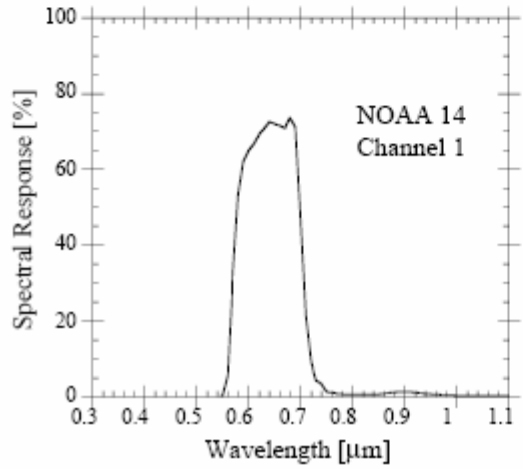
Spectral Response [%]
NOAA 14
Channel 1
Wavelength [µm]

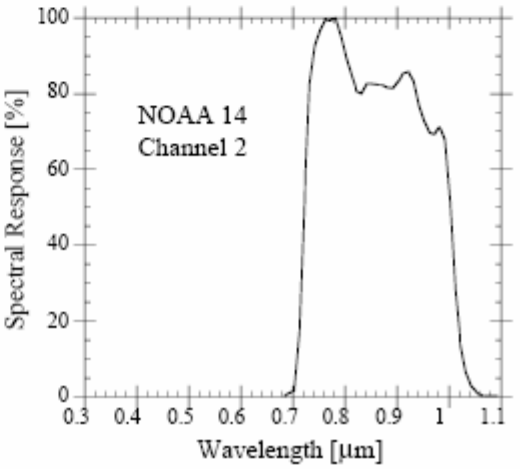
Spectral Response [%]
NOAA 14
Channel 2
Wavelength [µm]

**References**:

C.T. Due, Optical-mechanical active/passive imaging Systems - Volume II, Report number 153200-2-TIII- ERIM Infrared information and Analysis Center, P.O. BOX 8518, Ann. Arbor., MI.98107, 1982.

NOAA Polar Orbiter Data User's Guide, U.S. Dept. of Commerce, NOAA, National Environment Satellite, National Climatic Data Center, Satellite Data Service Division, World Weather Building, Room 100, Washington D.C., 202333, USA, 1985.

S.R. Schneider and D.F. McGinnis, The NOAA/AVHRR: A new satellite sensor for monitoring crop growth, *Proceedings of the Eighth International Symposium on Machine processing of remotely sensed data*, Purdue University, Indiana, 250-281, 1982.

**Links:**

http://www2.ncdc.noaa.gov/docs/klm/html/c3/sec3-1.htm

http://edc.usgs.gov/products/satellite/avhrr.html

## ***SUBROUTINE ETM***

**Function**: To read the seven (visible to thermal infrared) spectral bands and one panchromatic spectral band of Landsat ETM (Enhanced Thematic Mapper) onboard the Landsat 7 satellite (extreme wavelengths and spectral response of the filter function).

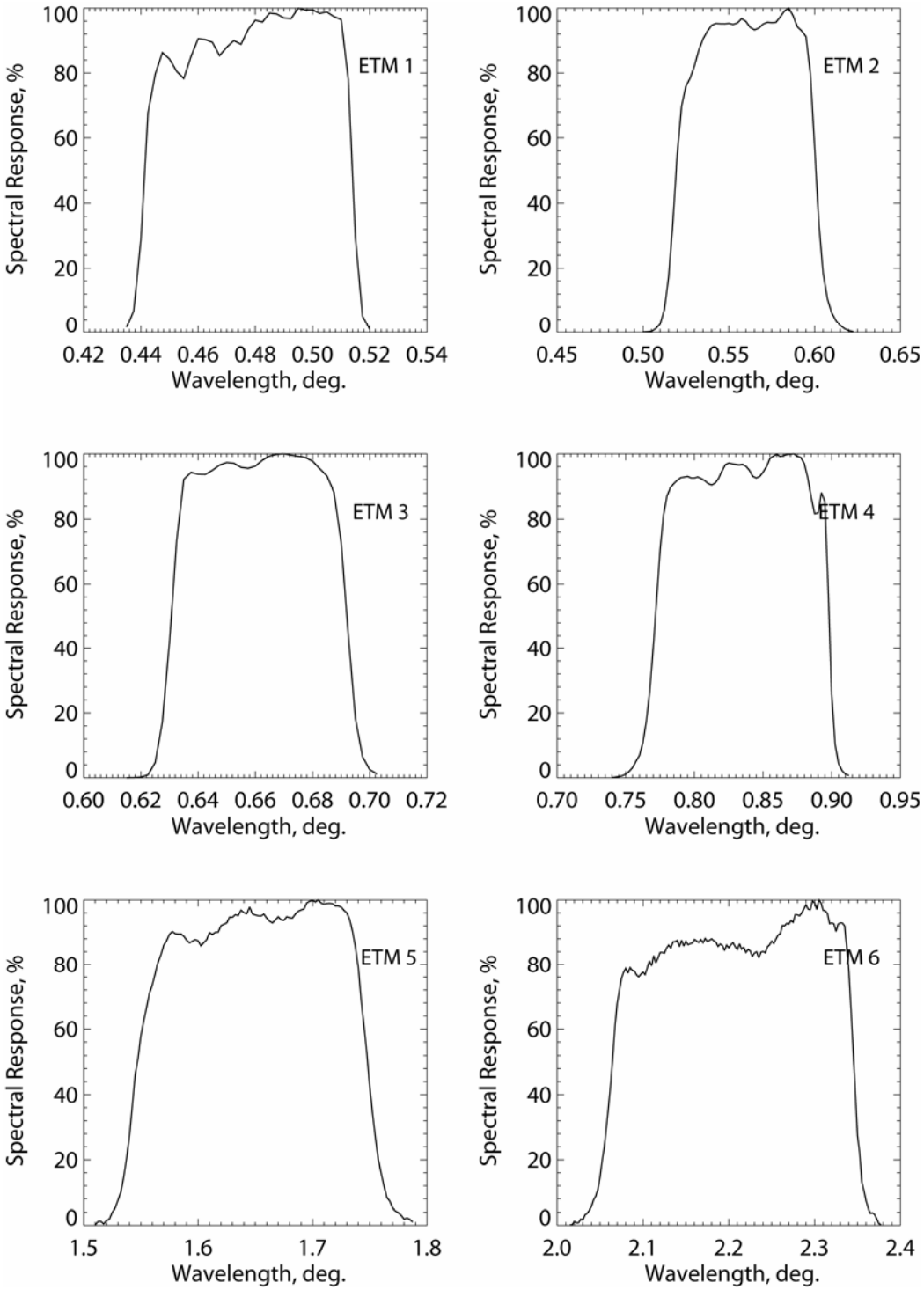

**References**:

S. Liang, H. Fang, and M. Chen, Atmospheric correction of Landsat ETM+ land surface imagery. Part I: Methods, *IEEE Transactions on Geoscience and Remote Sensing*, 39(11), 2490-2498, 2001.

S. Liang, H. Fang, J.T. Morisette, M. Chen, C.J. Shuey, C.L. Walthall, and C.S.T. Daughtry, Atmospheric correction of Landsat ETM+ land surface imagery. Part II: Validation and applications, *IEEE Transactions on Geoscience and Remote Sensing*, 40(12), 2736-2746.

**Link:**

http://edc.usgs.gov/products/satellite/landsat7.html

## ***SUBROUTINE GLI***

**Function**: To read the 30 spectral bands (23 in the visible and near infrared region, 6 in short wavelength infrared, and 1 in middle and thermal infrared) of the GLobal Imager (GLI) onboard ADEOS (extreme wavelengths and spectral response of the filter function).

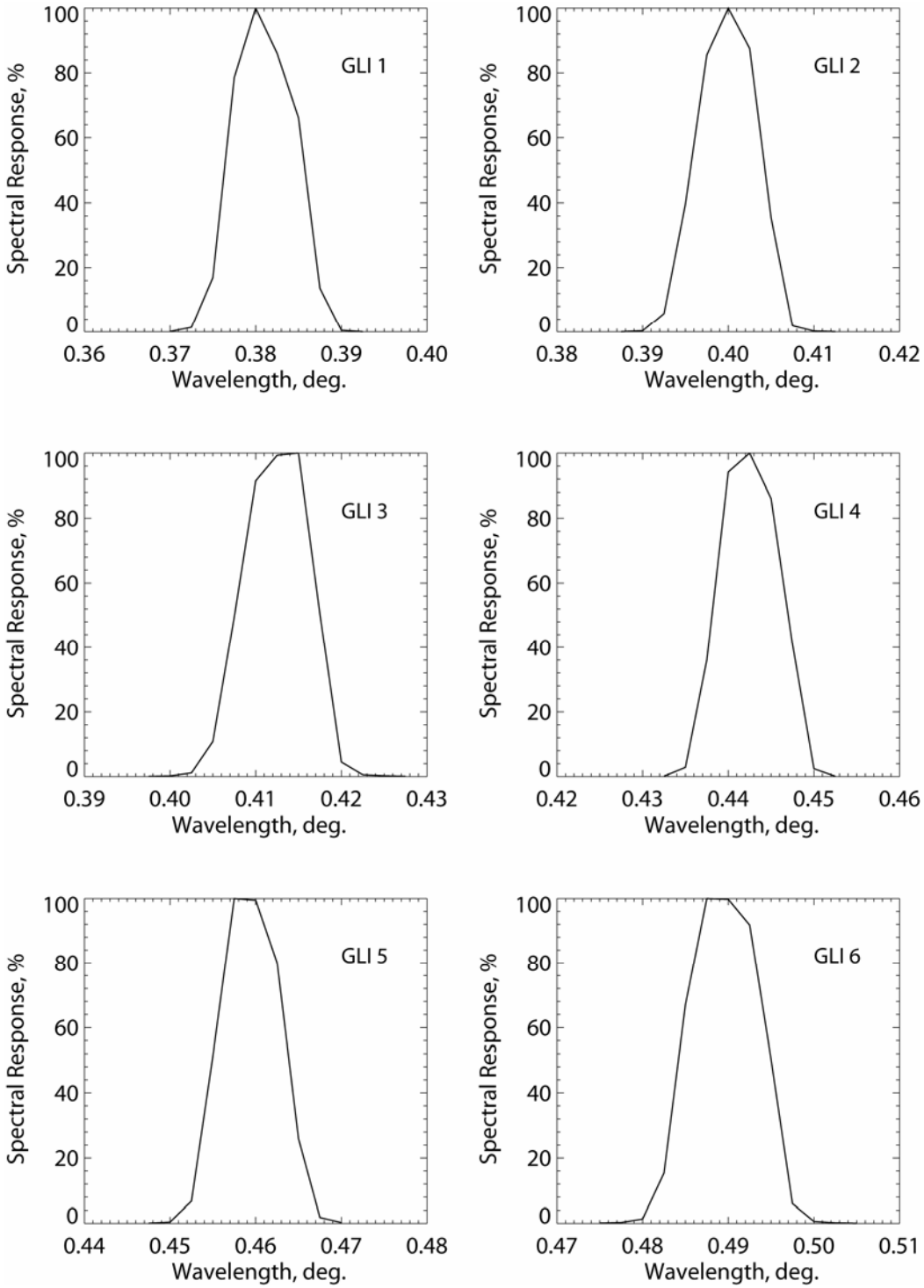

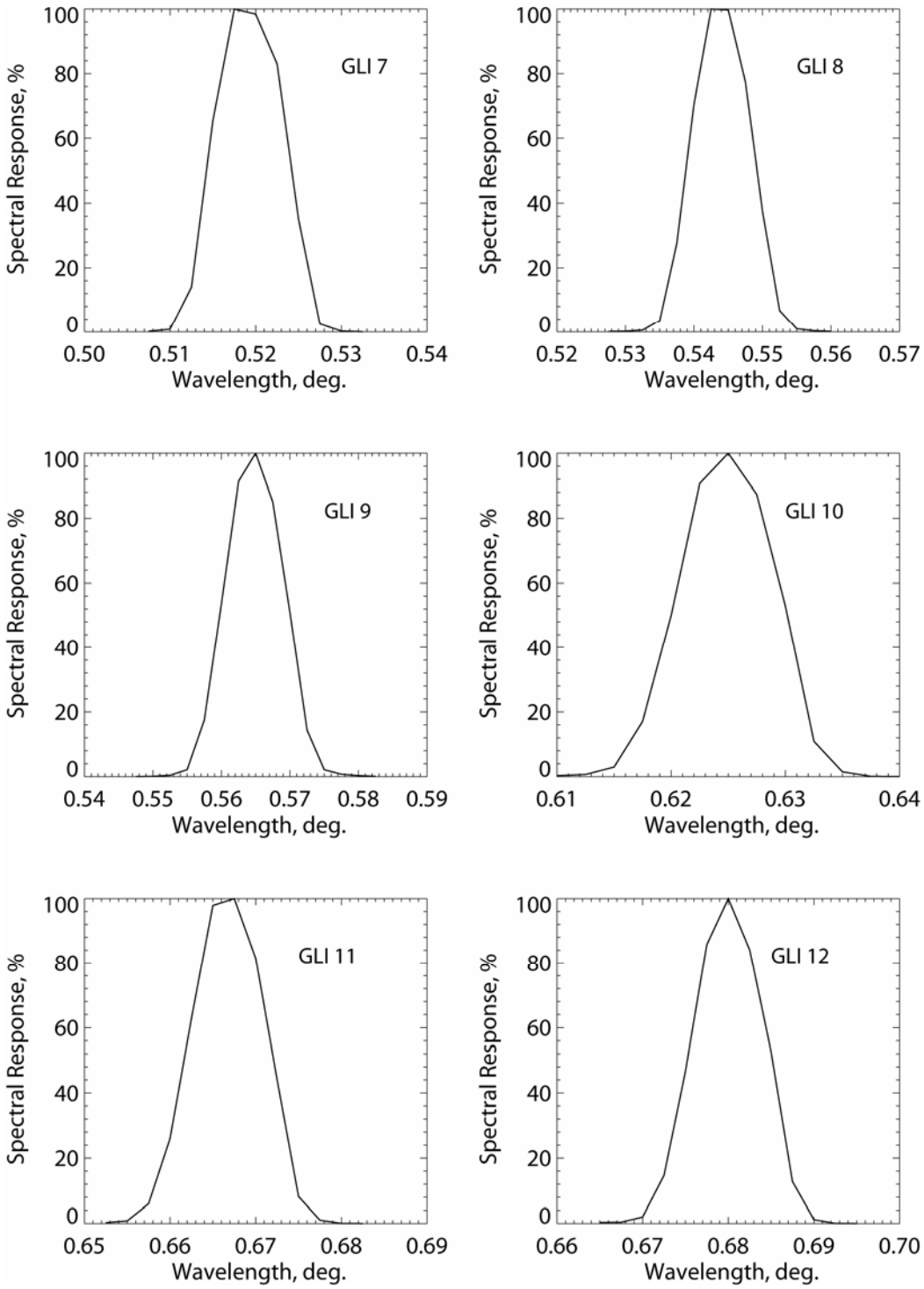
GLI 7
Spectral Response, %
Wavelength, deg.
GLI 8
Spectral Response, %
Wavelength, deg.
GLI 9
Spectral Response, %
Wavelength, deg.
GLI 10
Spectral Response, %
Wavelength, deg.
GLI 11
Spectral Response, %
Wavelength, deg.
GLI 12
Spectral Response, %
Wavelength, deg.

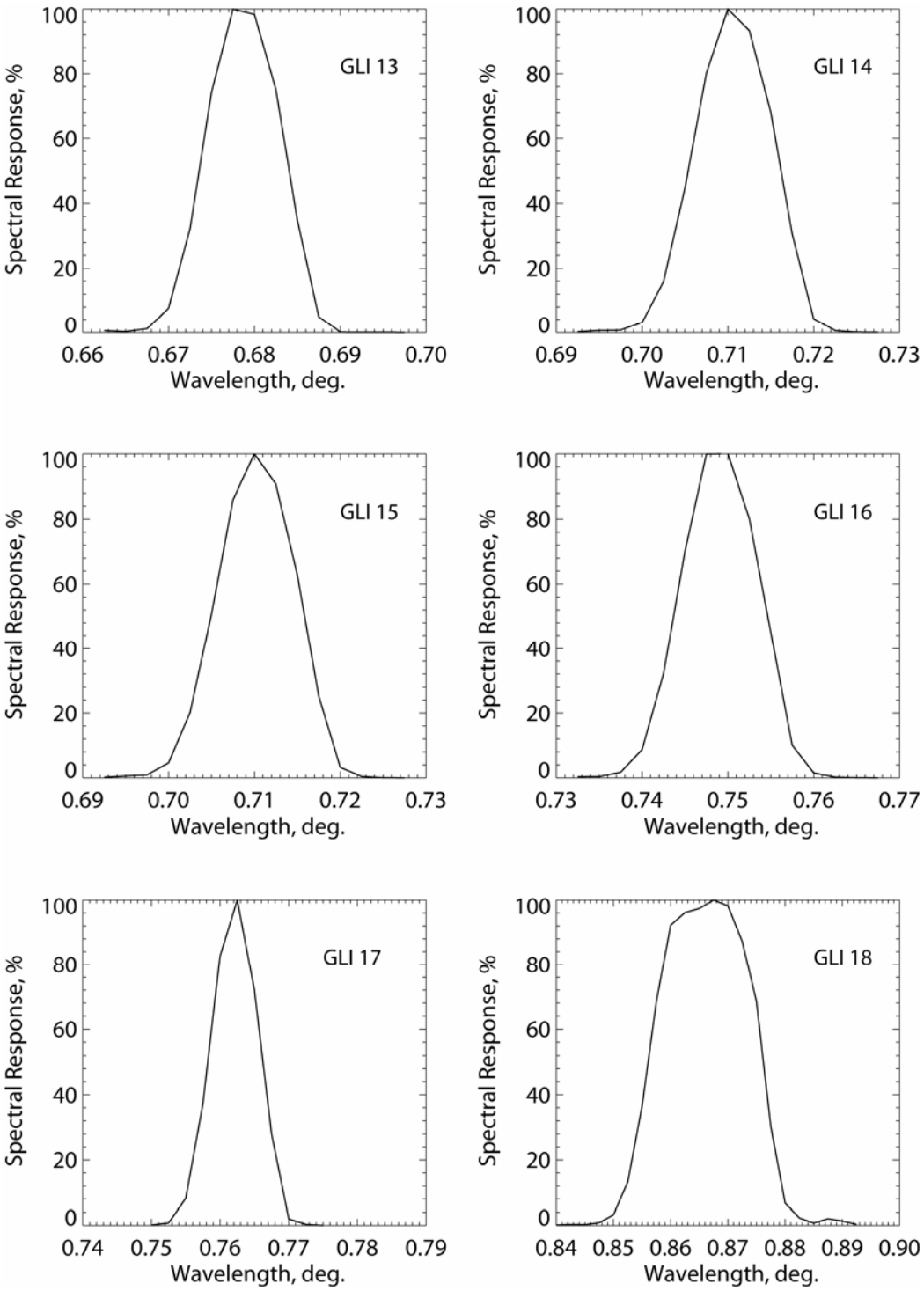
GLI 13
Spectral Response, %
Wavelength, deg.
GLI 14
GLI 15
GLI 16
GLI 17
GLI 18

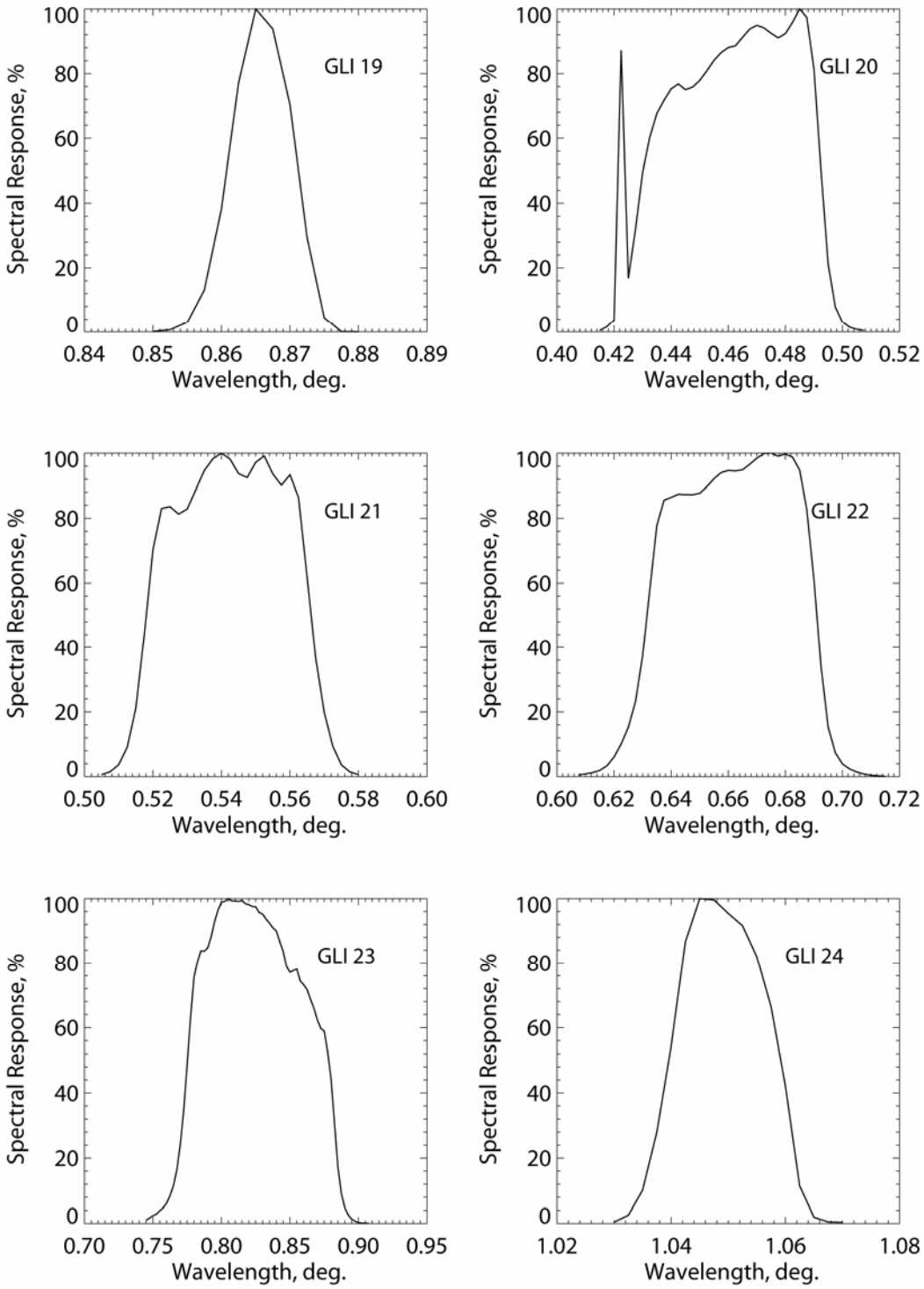
GLI 19
Spectral Response, %
Wavelength, deg.
GLI 20
Spectral Response, %
Wavelength, deg.
GLI 21
Spectral Response, %
Wavelength, deg.
GLI 22
Spectral Response, %
Wavelength, deg.
GLI 23
Spectral Response, %
Wavelength, deg.
GLI 24
Spectral Response, %
Wavelength, deg.

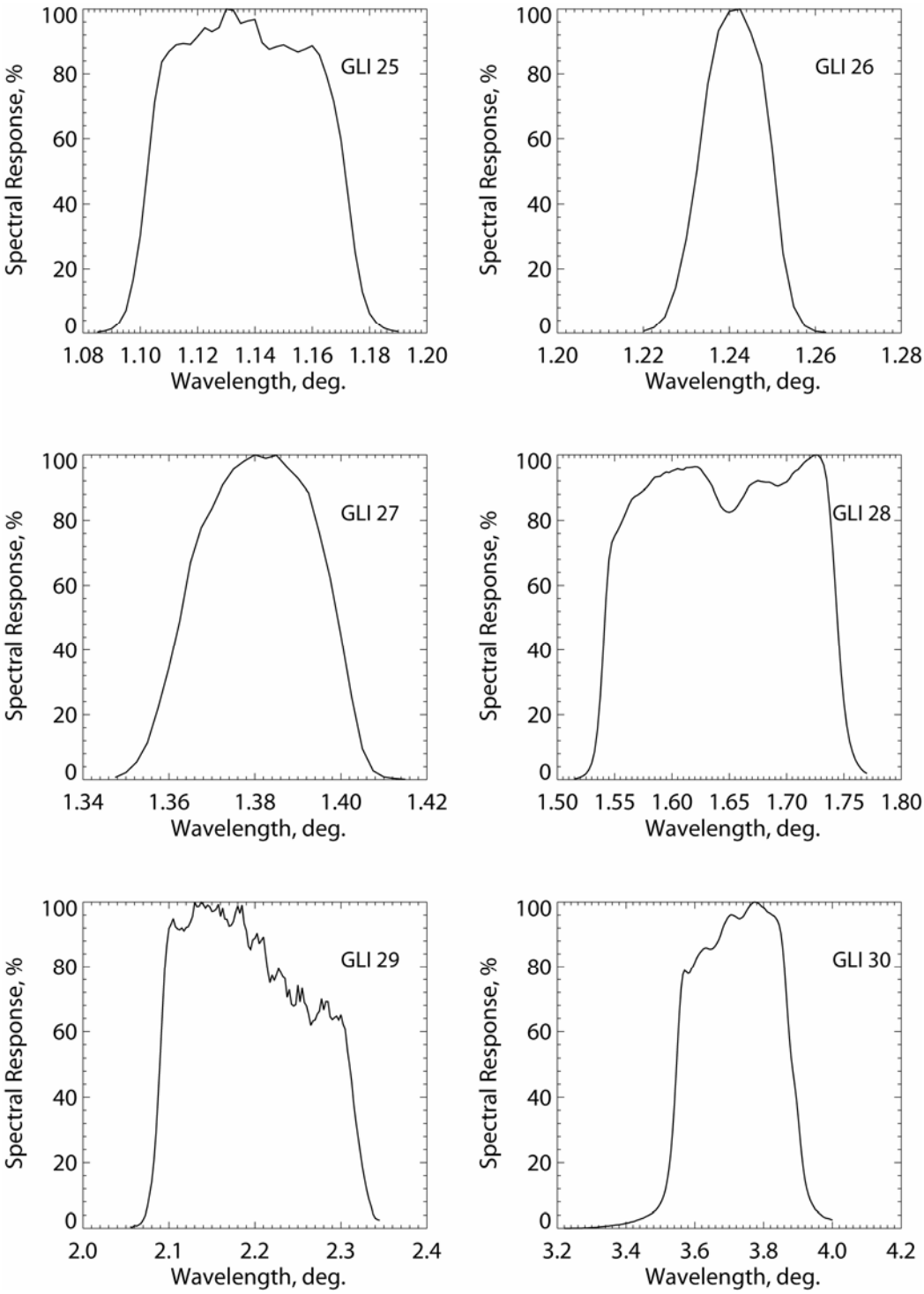
GLI 25
Spectral Response, %
Wavelength, deg.
GLI 26
GLI 27
GLI 28
GLI 29
GLI 30

**Reference:**

M. Yoshida, H. Murakami, Y. Mitomi, M. Hori, K.J. Thome, D.K. Clark, and H. Fukushima, Vicarious calibration of GLI by ground observation data, *IEEE Transactions on Geoscience and Remote Sensing*, 43(10), 2167 – 2176, 2005.

**Links**:

http://www.eoc.jaxa.jp/satellite/sendata/gli_e.html

http://suzaku.eorc.jaxa.jp/GLI/alg/alg_des.html (ATBD)

## ***SUBROUTINE GOES***

**Function**: To read the visible spectral bands of the Visible Infrared Spin-Scan Radiometer (VISSR) onboard GOES 5 (East) and GOES 4 (West) (extreme wavelengths and spectral response of the filter function).

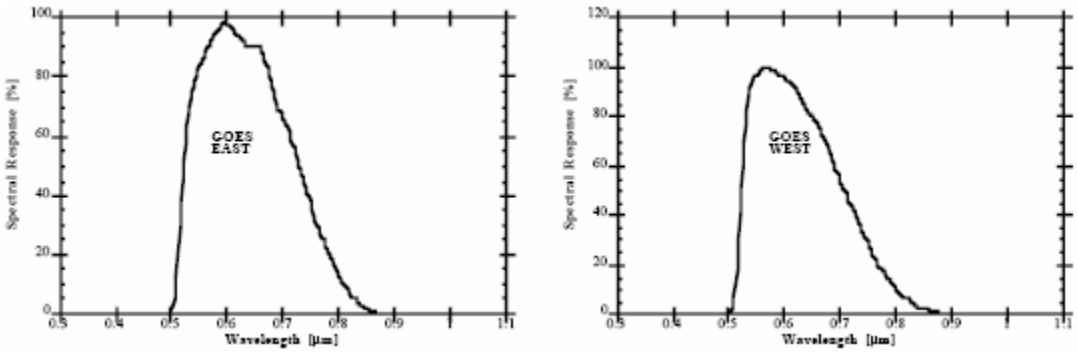


**Reference**:

R. P. Corbell, C.J. Cullahan, and W.J. Kotsch, The GOES/SMS User's Guide: U.S. Dept. of Commerce, NOAA, NESS, Washington D.C., USA, 1976.

**Links:**

http://goes.gsfc.nasa.gov/

http://www.goes.noaa.gov/

## ***SUBROUTINE HRV***

**Function**: To read the four spectral bands of the High Resolution Visible (HRV1 and 2) onboard Spot 1 (extreme wavelengths and spectral response of the filter function).

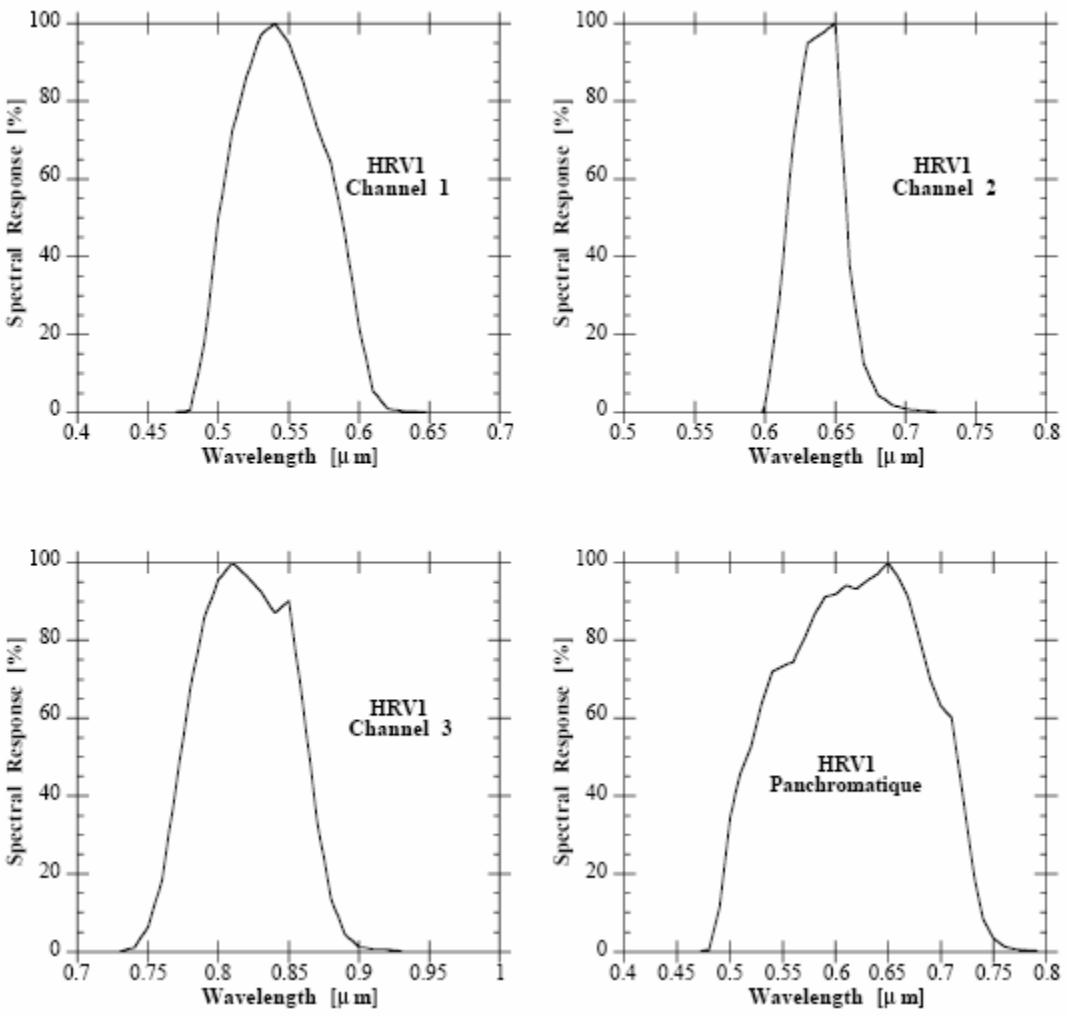

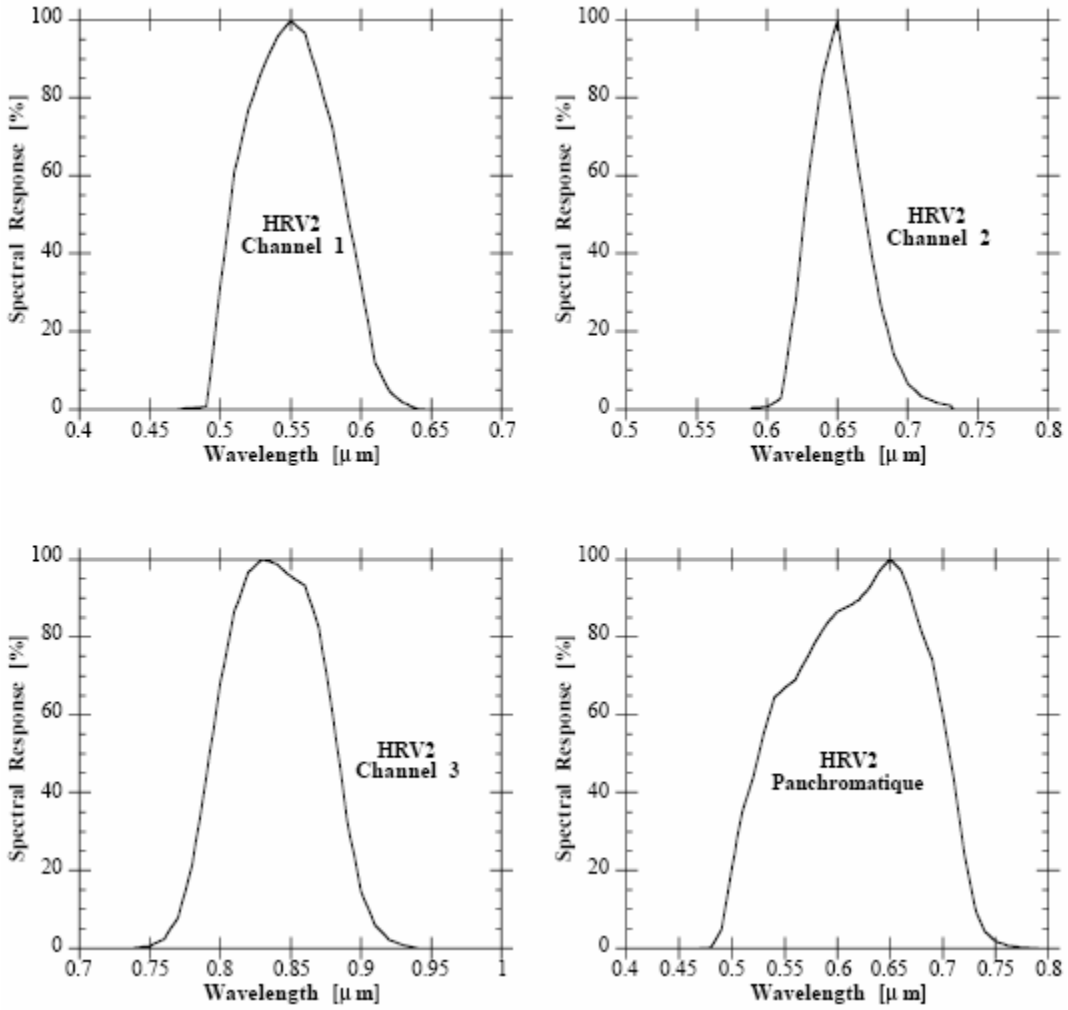


**Reference:**

M. Chevrel, M. Courtois, and G. Weill, The Spot satellite remote sensing mission, *Photogrammetric Engineering and Remote Sensing*, 47(8), 1163-1171, 1981.

**Link:**

http://earth.esa.int/object/index.cfm?fobjectid=4074

## ***SUBROUTINE HYPBLUE***

**Function**: To read the blue spectral bands of MODIS (MODerate resolution Imaging Spectrometer) onboard the Terra and Aqua satellites and of ETM (Enhanced Thematic Mapper) onboard the Landsat 7 satellite (extreme wavelengths and spectral response of the filter function).

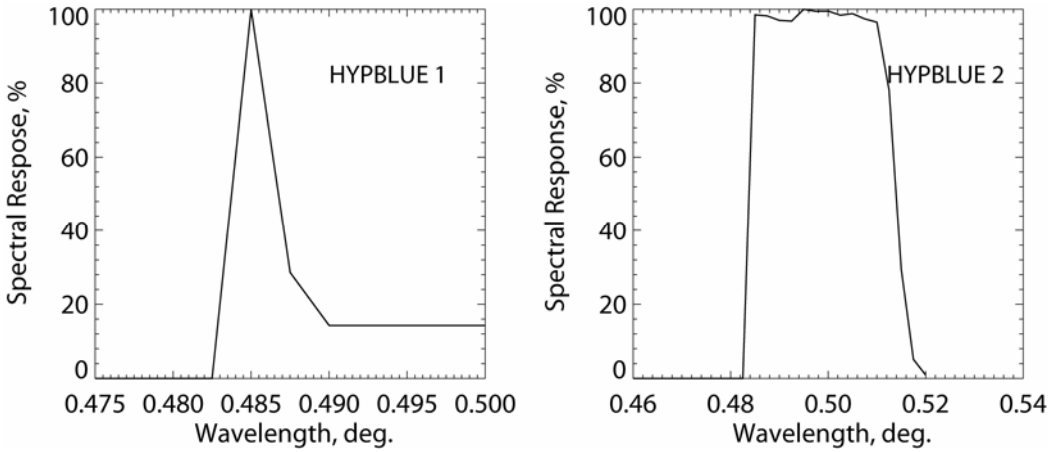


**References:**

P.E. Ardanuy, D. Han, and V. Salomonson, The Moderate Resolution Imaging Spectrometer (MODIS) science and data system requirements, *IEEE Transactions on Geoscience and Remote Sensing*, 29, 75-88, 1991.

J. Liira, K. Püssa, and U. Peterson, The radiance contrast of forest-to-clearcut edges on a medium resolution Landsat Enhanced Thematic Mapper satellite winter image, *International Journal of Remote Sensing*, 27(13), 2753-2766.

**Links:**

http://modis.gsfc.nasa.gov/

http://edc.usgs.gov/products/satellite/landsat7.html

## ***SUBROUTINE MAS***

**Function**: To read the seven spectral bands of the MODIS Airborne Simulator (MAS) (extreme wavelengths and spectral response of the filter function).

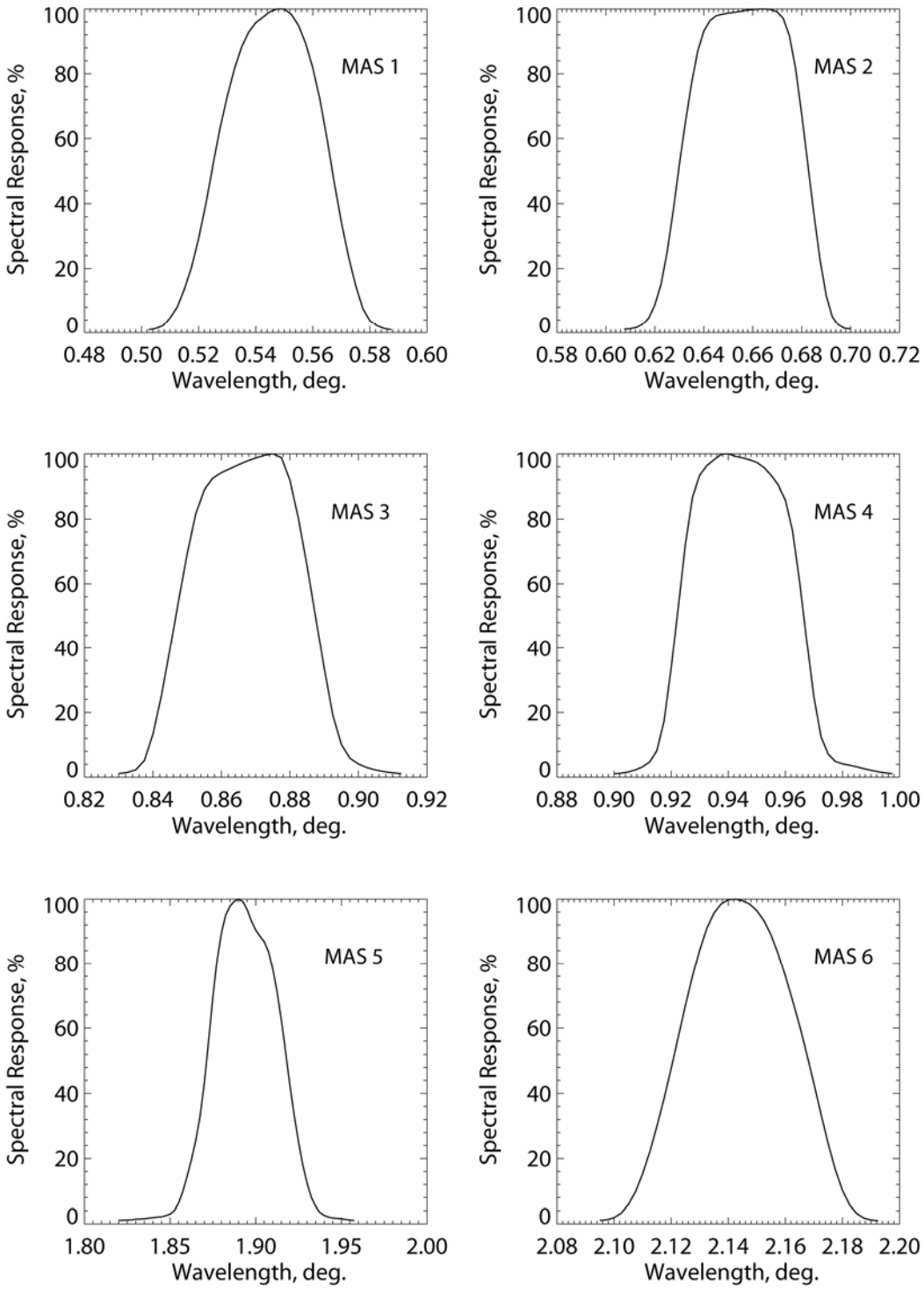

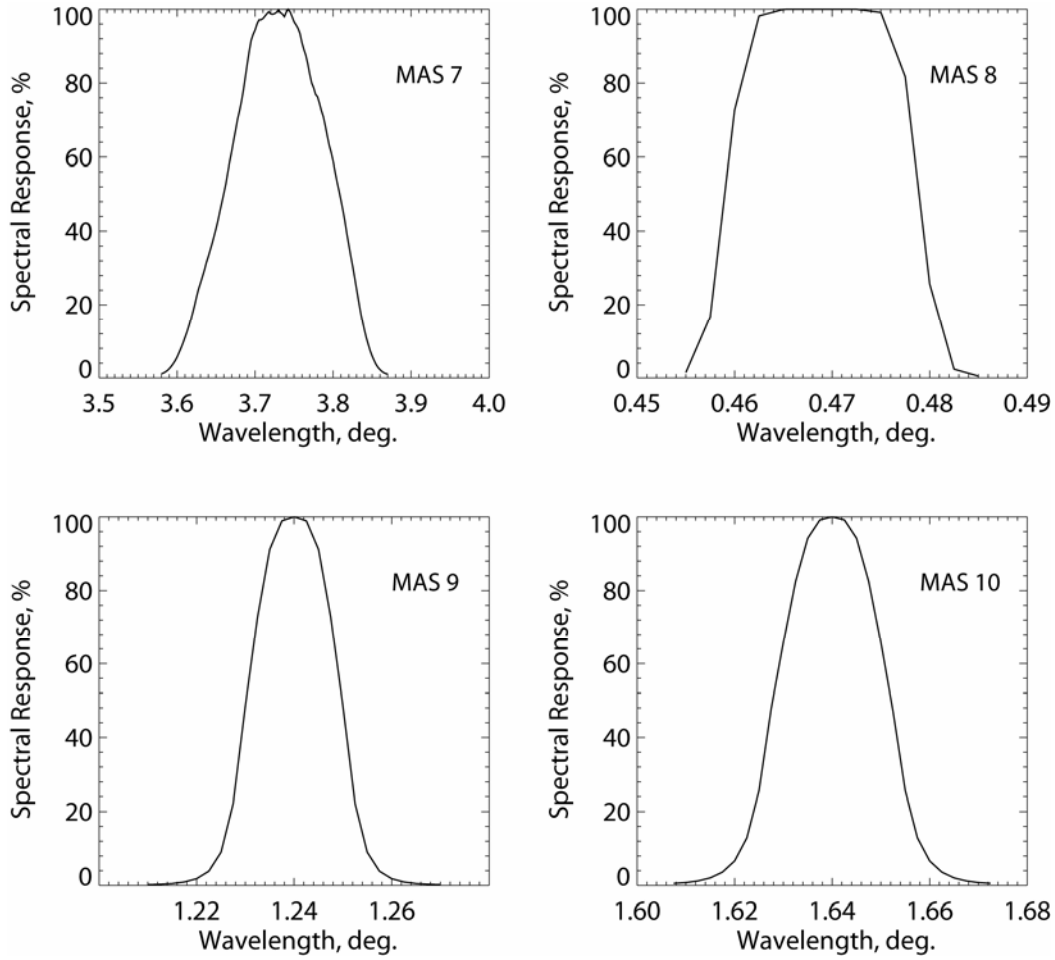


**Reference**:

M.D. King, W.P. Menzel, P.S. Grant, J.S. Myers, G.T. Arnold, S.E. Platnick, L.E. Gumley, S.C. Tsay, C.C. Moeller, M. Fitzgerald, K.S. Brown, and F.G. Osterwisch, Airborne scanning spectrometer for remote sensing of cloud, aerosol, water vapor, and surface properties, *Journal of Atmospheric and Oceanic Technology*, 13 (4), 777-794, 1996.

**Link:**

http://cimss.ssec.wisc.edu/airborne/mas/MAS.html

## ***SUBROUTINE MERIS***

**Function**: To read the 15 spectral bands (visible and near infrared) of the programmable, MEdium Resolution Imaging Spectrometer (MERIS) onboard the European Space Agency satellite ENVISAT (extreme wavelengths and spectral response of the filter function).

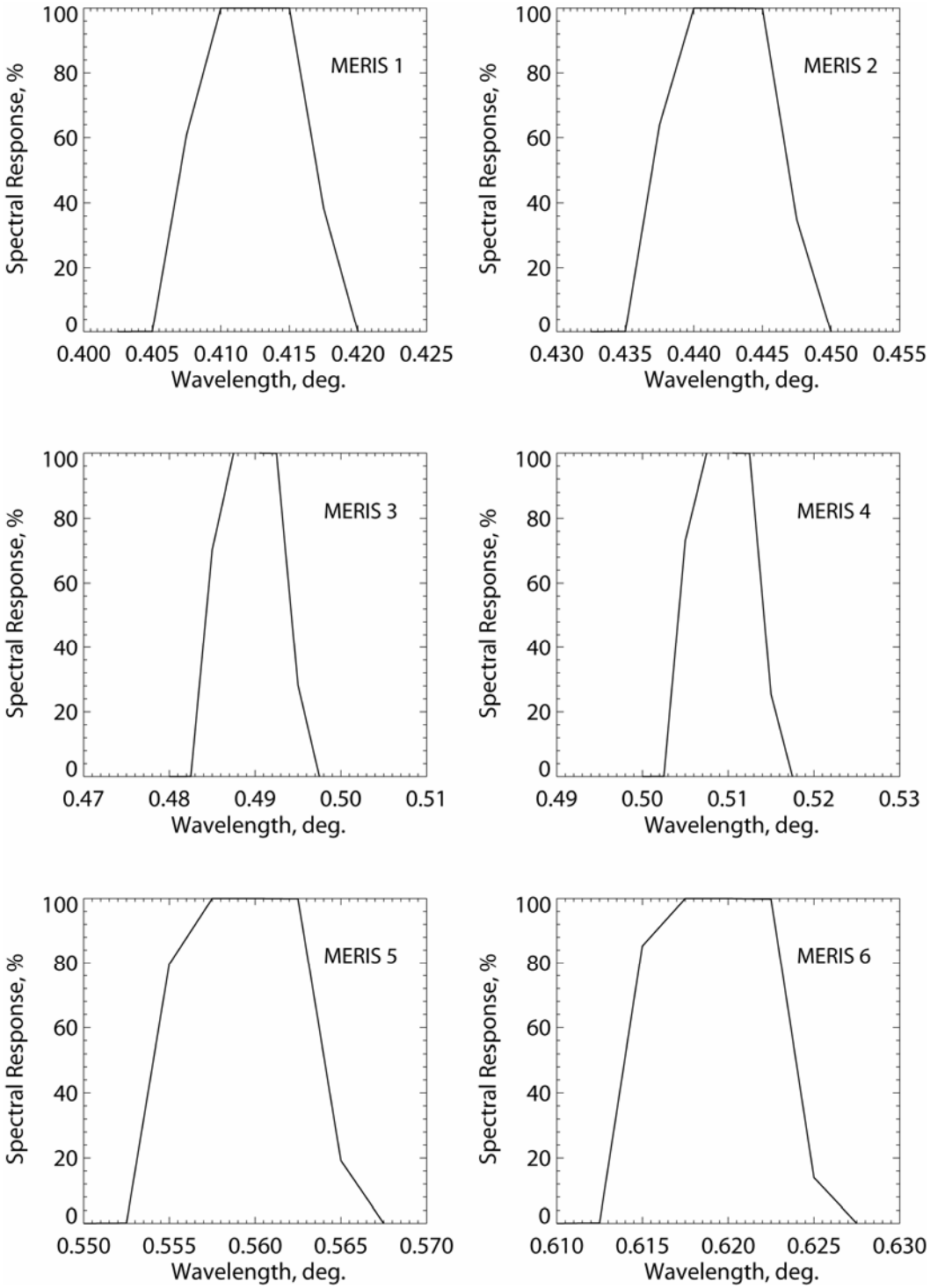

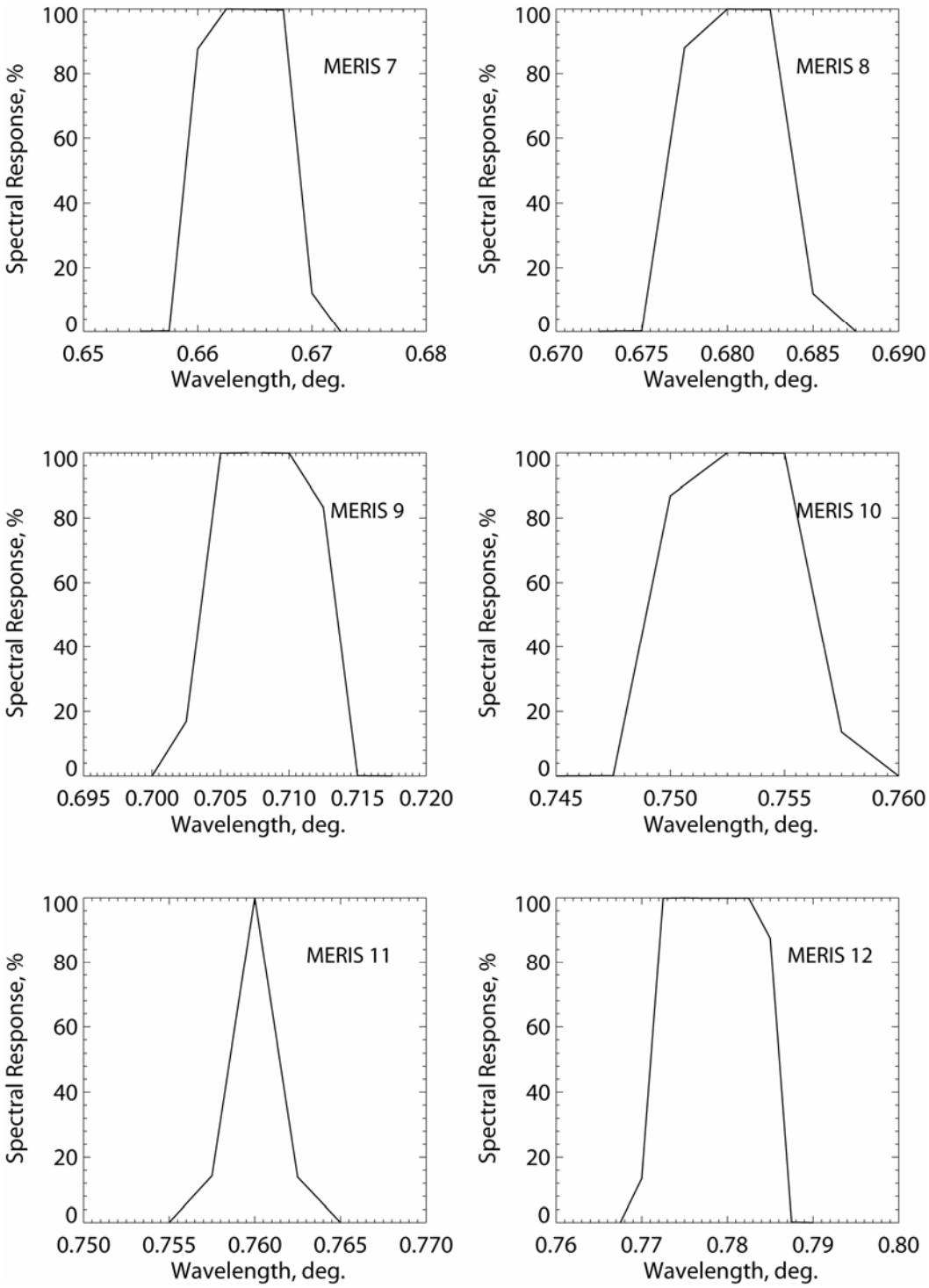
MERIS 7
Spectral Response, %
Wavelength, deg.
MERIS 8
MERIS 9
MERIS 10
MERIS 11
MERIS 12

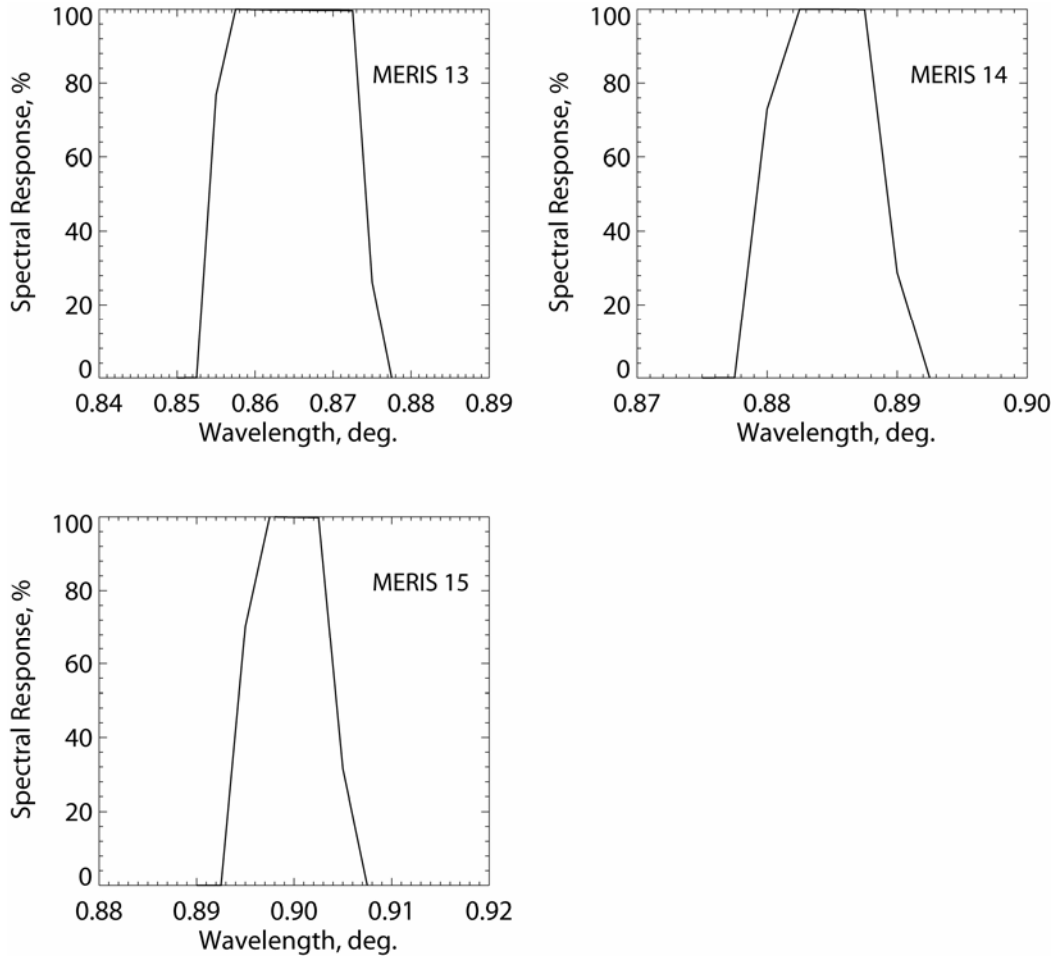


**References**:

R. Fensholt, I. Sandholt, and S. Sitzen, Evaluating MODIS, MERIS, and VEGETATION vegetation indices using in-situ measurements in a semiarid environment, *IEEE Transactions on Geoscience and Remote Sensing*, 44(7), 1774-1786, 2006.

M. Rast, J.L. Bezy, and S. Bruzzi, The ESA Medium Resolution Imaging Spectrometer MERIS a review of the instrument and its mission, *International Journal of Remote Sensing*, 20(9), 1681-1702, 1999.

**Links:**

http://envisat.esa.int/instruments/meris/

http://envisat.esa.int/dataproducts/meris/

http://envisat.esa.int/instruments/tour-index/meris/

## ***SUBROUTINE METEO***

**Function**: To read the visible spectral band of the radiometer onboard Meteosat 2 (extreme wavelengths and spectral response of the filter function).

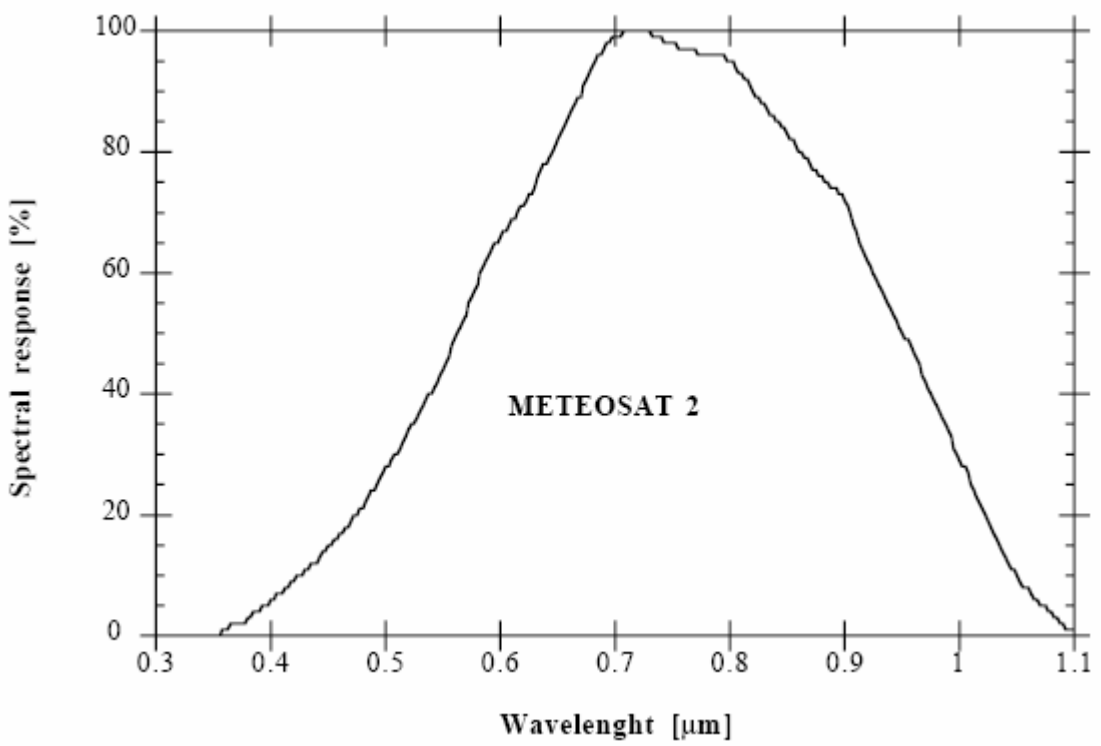


**Reference**:

J. Morgan, Introduction to the Meteosat system, ESOC, Darmstadt, R.F.A., 1981.

**Link:**

http://www.eumetsat.int/idcplg?IdcService=SS_GET_PAGE&nodeId=545&l=en

## ***SUBROUTINE MODIS***

**Function**: To read seven first visible and near-infrared spectral bands of MODIS (MODerate resolution Imaging Spectroradiometer) onboard Terra and Aqua (extreme wavelengths and spectral response of the filter function).

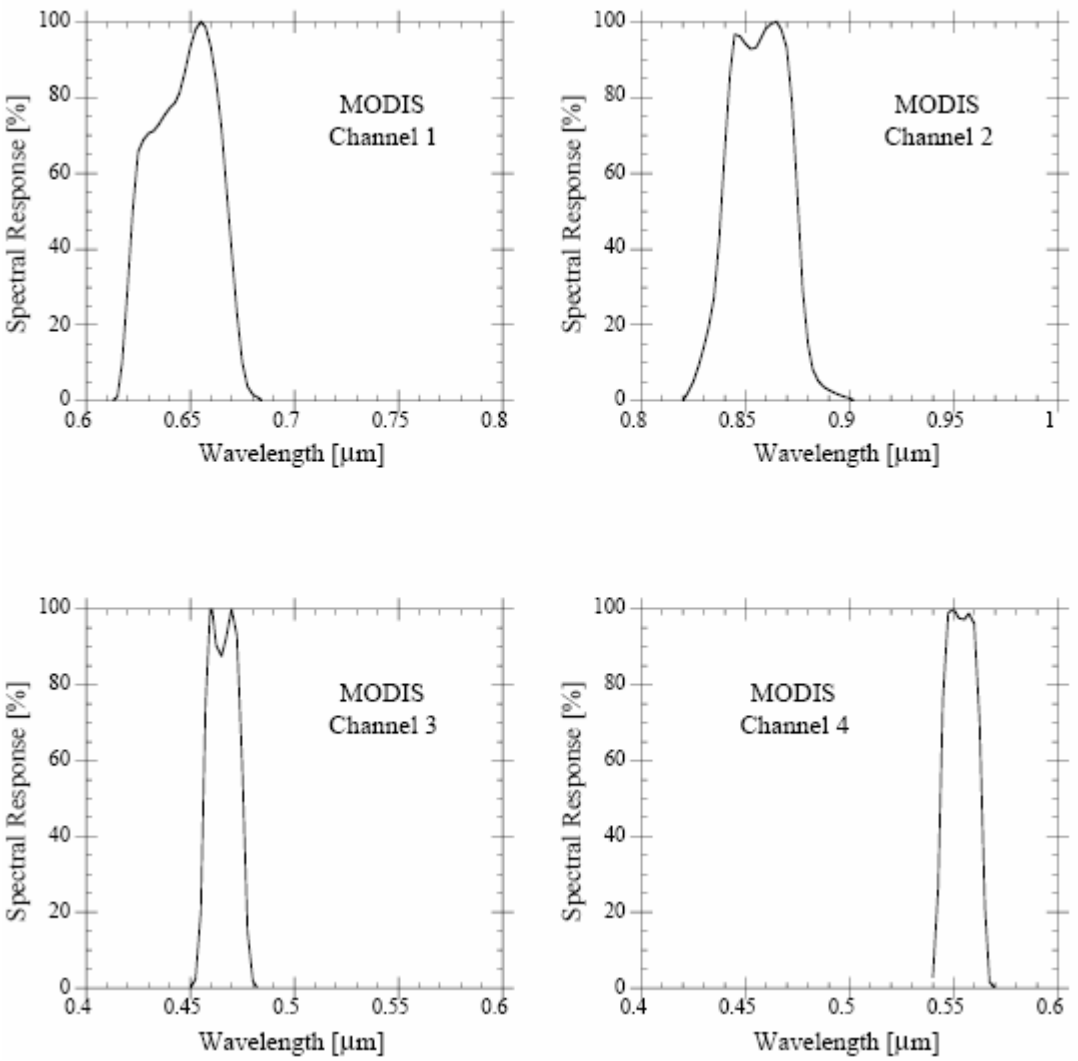

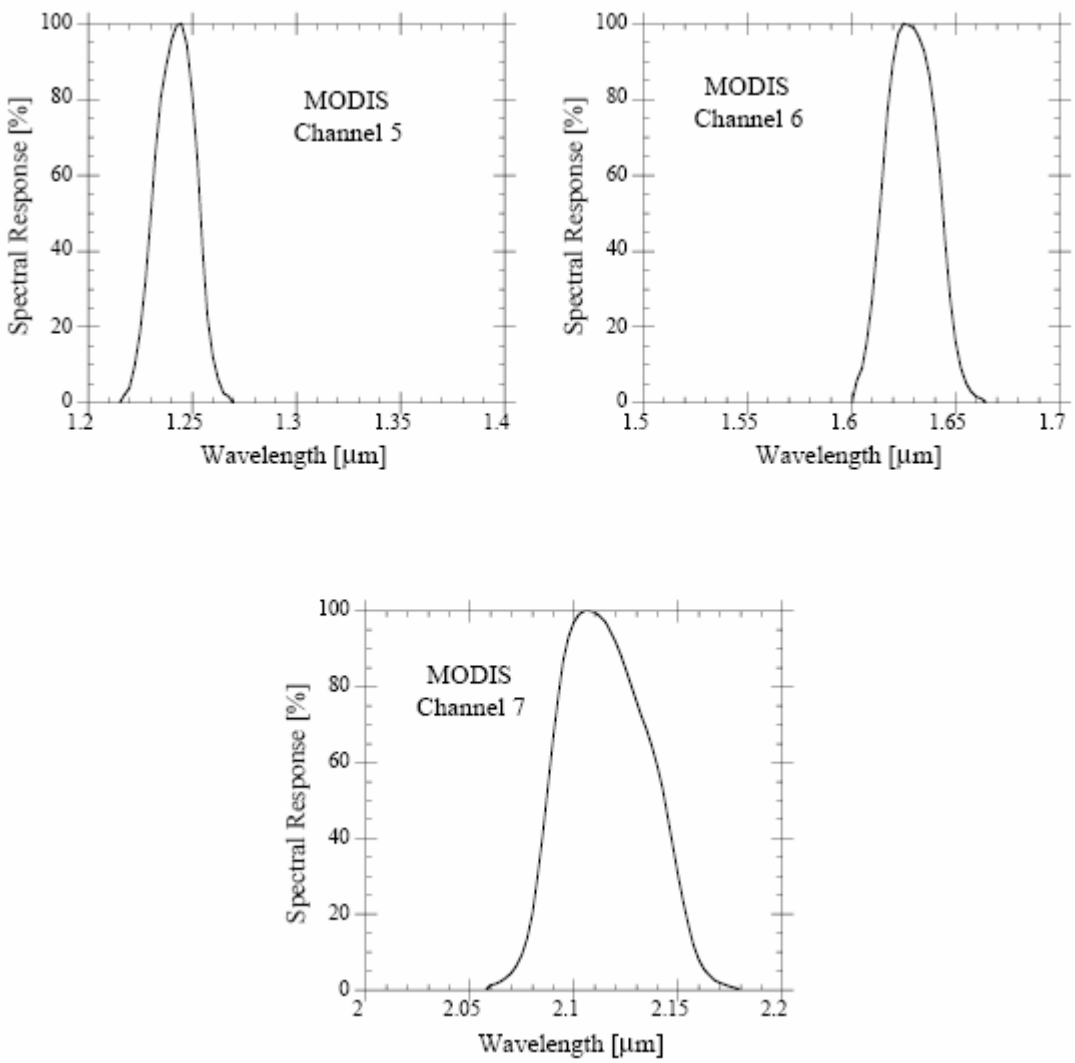


**References**:

P.E. Ardanuy, D. Han, and V.V. Salomonson, The Moderate Resolution Imaging Spectrometer (MODIS) science and data system requirements, *IEEE Transactions on Geoscience and Remote Sensing*, 29, 75-88, 1991.

W.L. Barnes, H.L. Ostrow, and V.V. Salomonson, Preliminary system concepts for MODIS: A Moderate Resolution Imaging Spectrometer for EOS, *Proceedings of the SPIE - The International Society of Optical Engineering*, 644, 86-93, 1986.

T.J. Magner and V.V. Salomonson, Moderate Resolution Imaging Spectrometer - Tilt (MODIS-T), *International Journal of Imaging Systems and Technology*, 3, 121-130, 1991.

**Link:**

http://modis.gsfc.nasa.gov

## ***SUBROUTINE MSS***

**Function**: To read the four spectral bands of the Multispectral Scanner System (MSS) onboard Landsat 5 (extreme wavelengths and spectral response of the filter function).

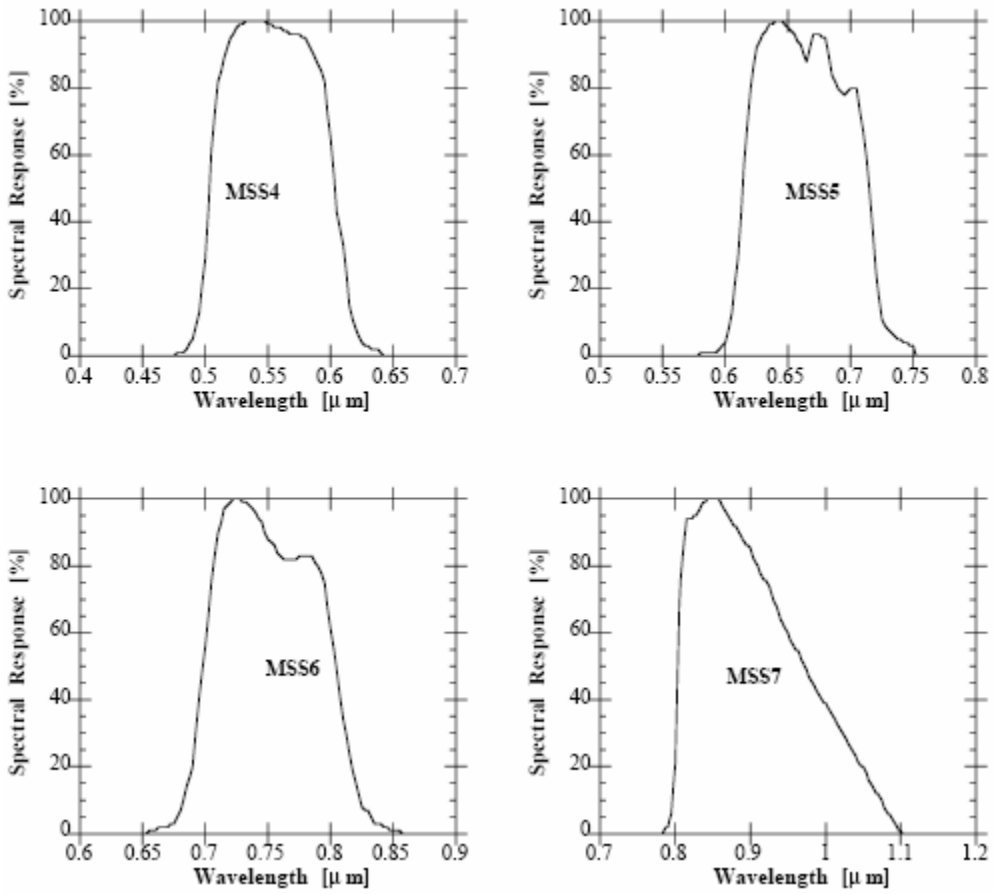


**References:**

Landsat Data User's Handbook (revised), U.S. Geol. Survey, EROS Data Center, Sioux Falls, SD 57198, 1978.

Landsat Data User's Notes, International Land Satellite programs, ibid, 1982.

**Link:**

http://eros.usgs.gov/products/satellite/mss.html

## ***SUBROUTINE POLDER***

**Function**: To read the eight visible and near-infrared spectral bands of POLDER (POLarization and Directionality of the Earth's Reflectances) on ADEOS (ADvanced Earth Observing Satellite) (extreme wavelengths and spectral response of the filter function). For the spectral bands with polarization measurements (0.443, 0.670 and 0.865 µm), only one spectral response is tabulated.

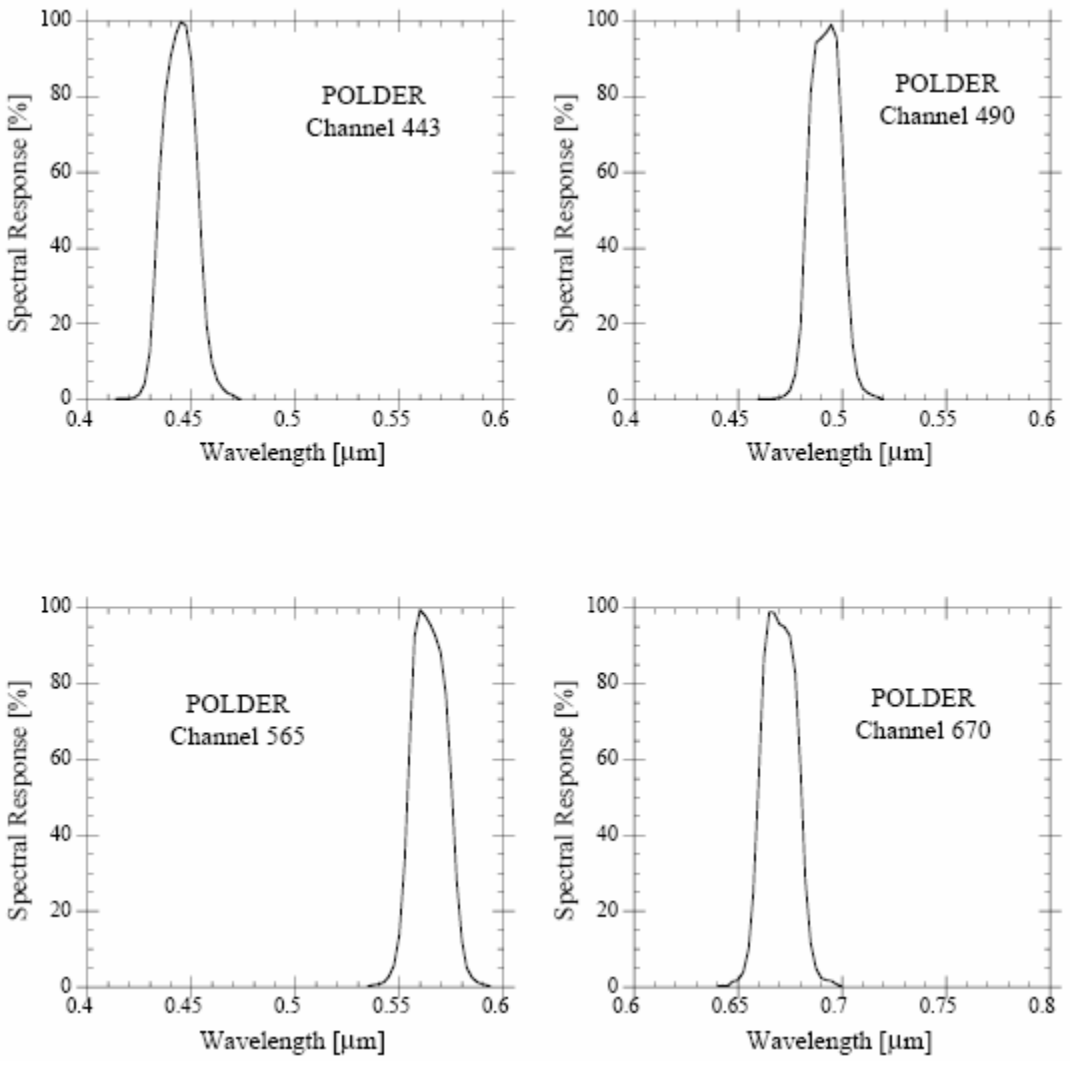

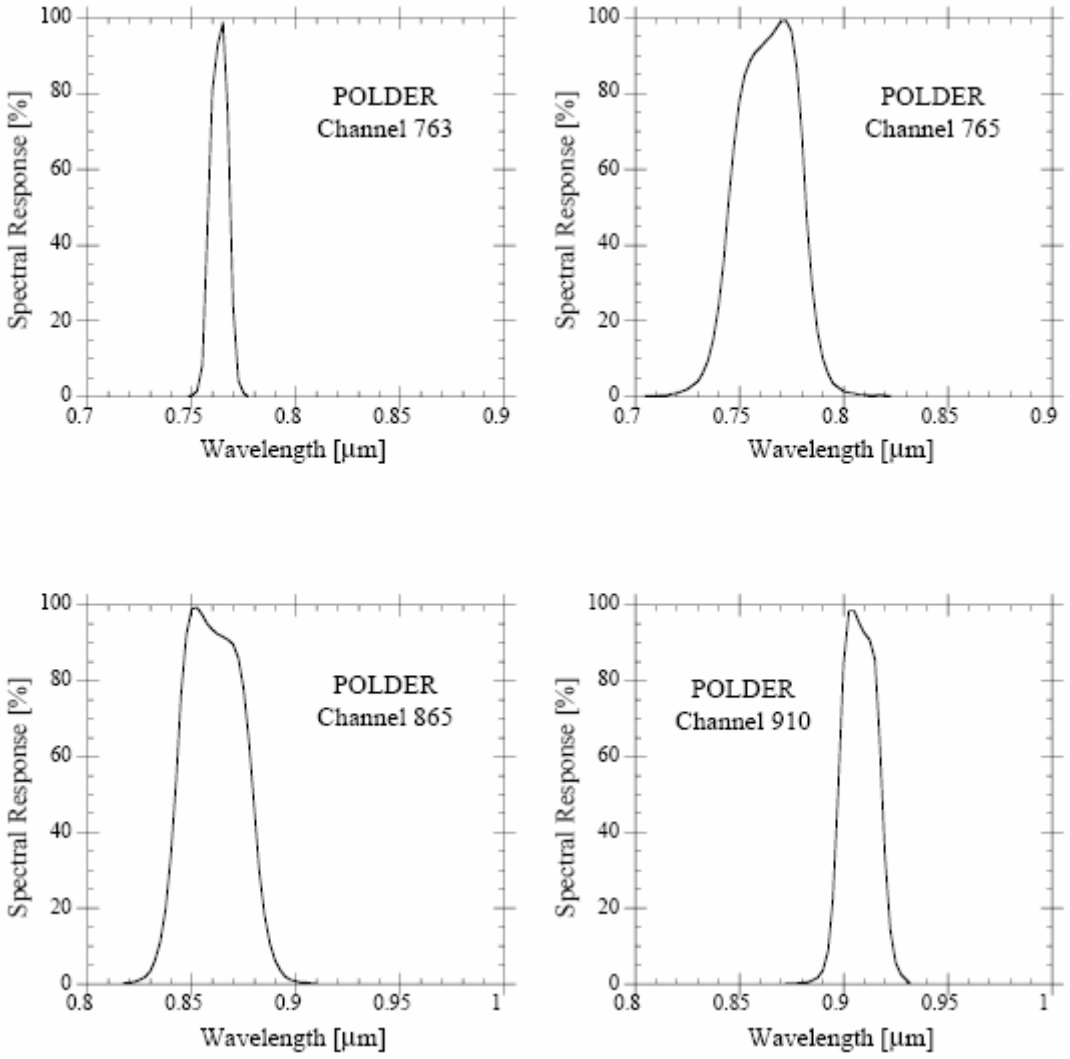


**References:**

F.-M. Breon, J.C. Buriez, P. Couvert, P.Y. Deschamps, J.L. Deuze, M. Herman, P. Goloub, M. Leroy, A. Lifermann, C. Moulin, F. Parol, G. Seze, D. Tanre, C. Vanbauce, and M. Vesperini, Scientific results from the POLarization and Directionality of the Earth's Reflectances (POLDER), *Advanced Space Research*, 30(11), 2383-2386, 2002.

P.Y. Deschamps, F.M. Breon, M. Leroy, A. Podaire, A. Bricaud, J.C. Buriez, and G. Seze, The POLDER mission: Instrument characteristics and scientific objectives, *IEEE Transactions on Geoscience and Remote Sensing*, 32, 598-615, 1994.

Leroy M. and A. Lifermann, The POLDER instrument onboard ADEOS: Scientific expectations and first results, *Advanced Space Research*, 25(5), 947-952, 2000.

**Link:** http://smsc.cnes.fr/POLDER/index.htm

## ***SUBROUTINE SEAWIFS***

**Function**: To read the eight spectral bands of the Sea-viewing Wide Field-of-view Sensor (SeaWiFS) onboard the SeaStar spacecraft (extreme wavelengths and spectral response of the filter function).

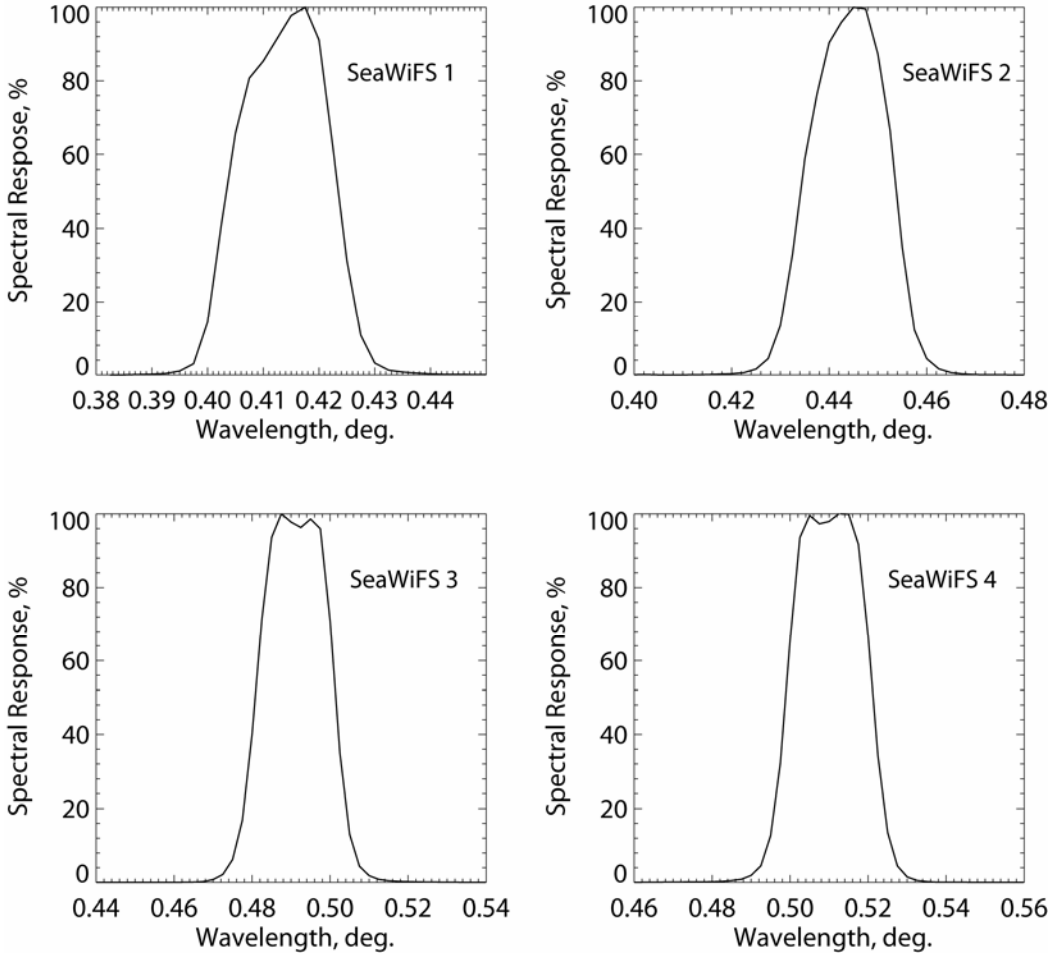

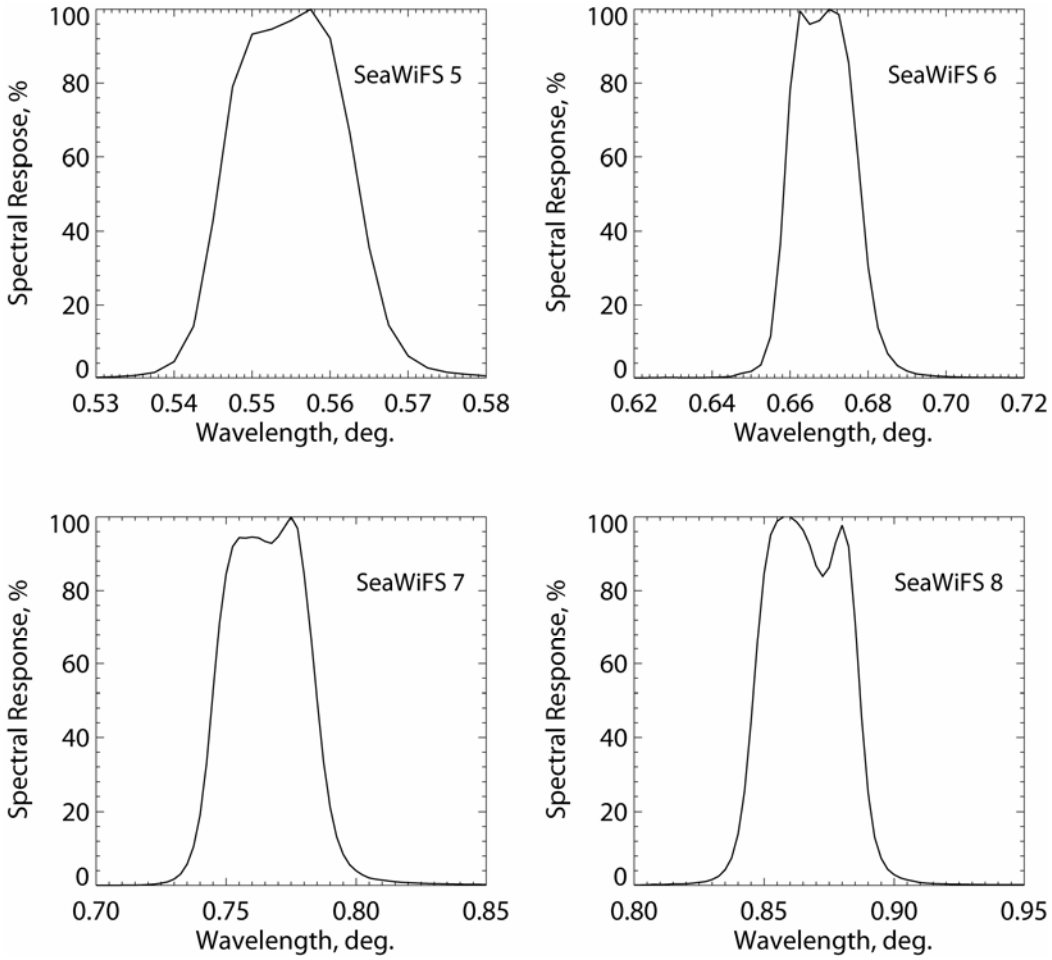


**Reference:**

B.C. Johnson, J.B. Fowler, and C.L. Cromer, The SeaWiFS transfer radiometer (SXR), NASA technical memorandum, 1998-206892, 1, S.B. Hooker and E.R. Firestone, Eds., NASA Goddard Space Flight Center, Greenbelt, Maryland, p. 58, 1998.

**Link:**

http://oceancolor.gsfc.nasa.gov/SeaWiFS/

## ***SUBROUTINE TM***

**Function**: To read the six visible spectral bands of the Thematic Mapper (TM) onboard Landsat 5 (extreme wavelengths and spectral response of the filter function).

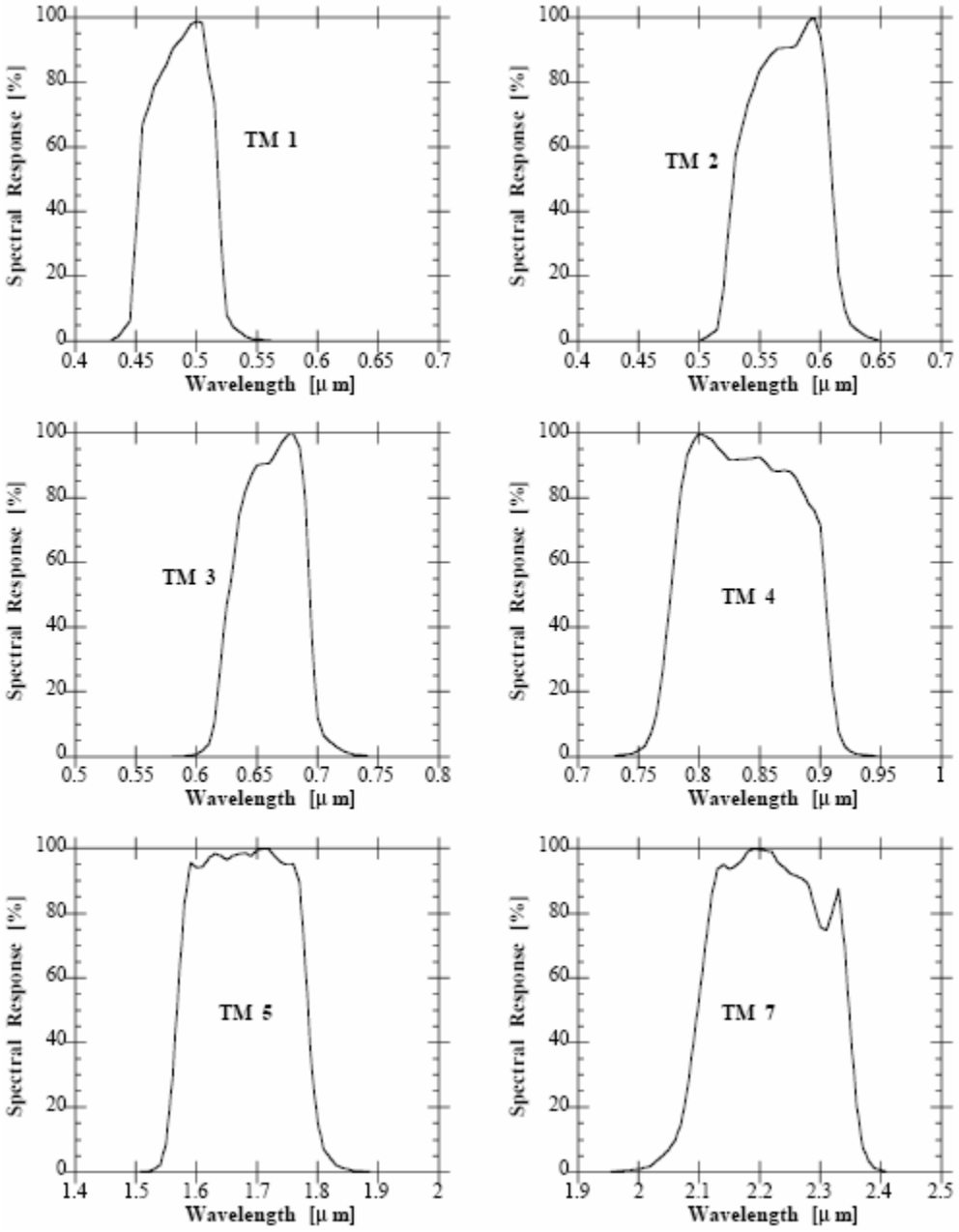

**Reference:**

B.L. Markham and J.L. Barker, Spectral characterization of the LANDSAT Thematic Mapper sensors, *International Journal of Remote Sensing*, 6, 697-716, 1985.

**Link:**

http://eros.usgs.gov/products/satellite/tm.html

## ***SUBROUTINE VGT***

**Function**: To read the four visible to short wave infrared spectral bands of VGT (VEGETATION) on the SPOT-4 satellite (extreme wavelengths and spectral response of the filter function).

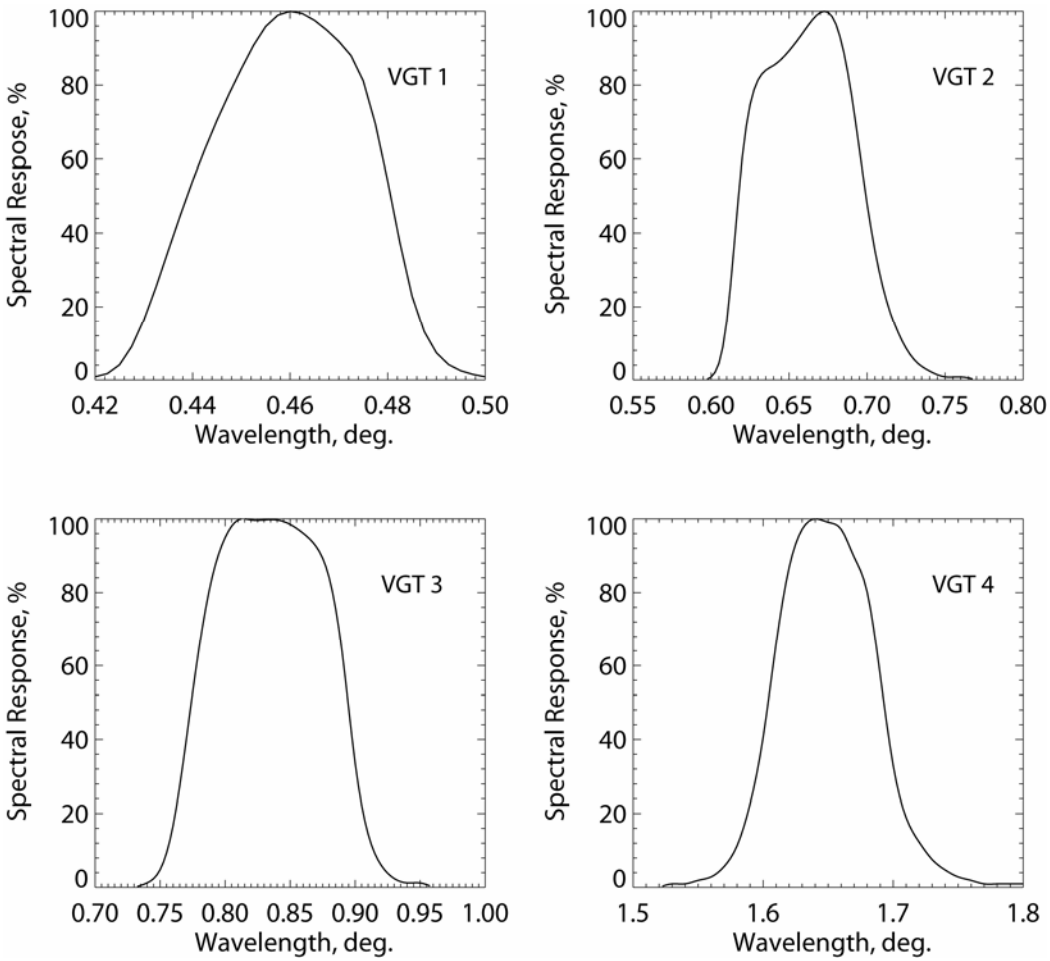


**Reference:**

R. Fensholt, I. Sandholt, and S. Sitzen, Evaluating MODIS, MERIS, and VEGETATION vegetation indices using in-situ measurements in a semiarid environment, *IEEE Transactions on Geoscience and Remote Sensing*, 44(7), 1774-1786, 2006.

**Links:**

http://www.spot-vegetation.com/

http://vegetation.cnes.fr/

## ***SUBROUTINE VIIRS***

**Function**: To read the spectral bands (red and near infrared) of the Visible/Infrared Imager/Radiometer Suite (VIIRS) onboard the NOAA satellite POES (Polar-orbiting Operational Environment Satellite) (extreme wavelengths and spectral response of the filter function).

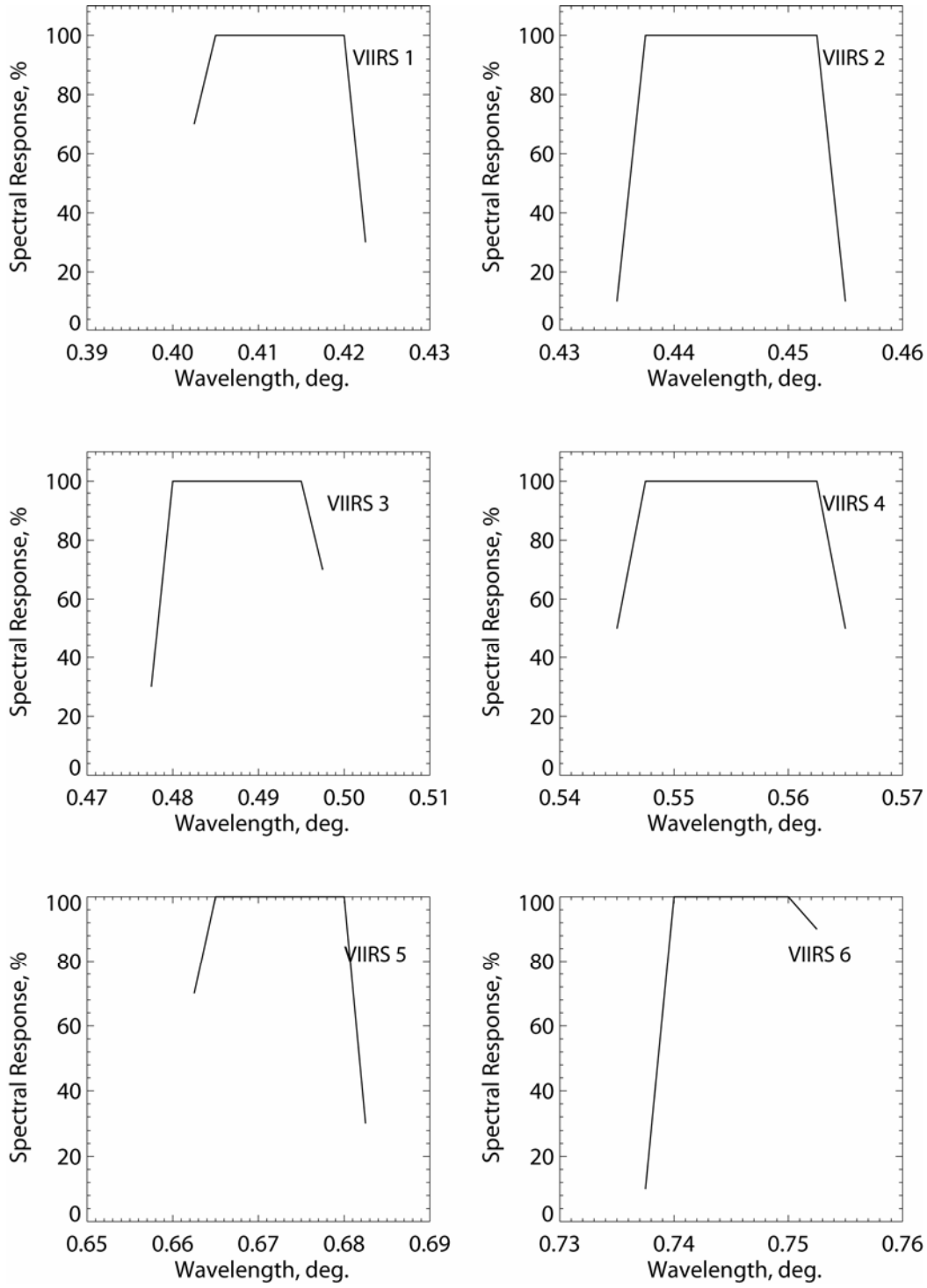

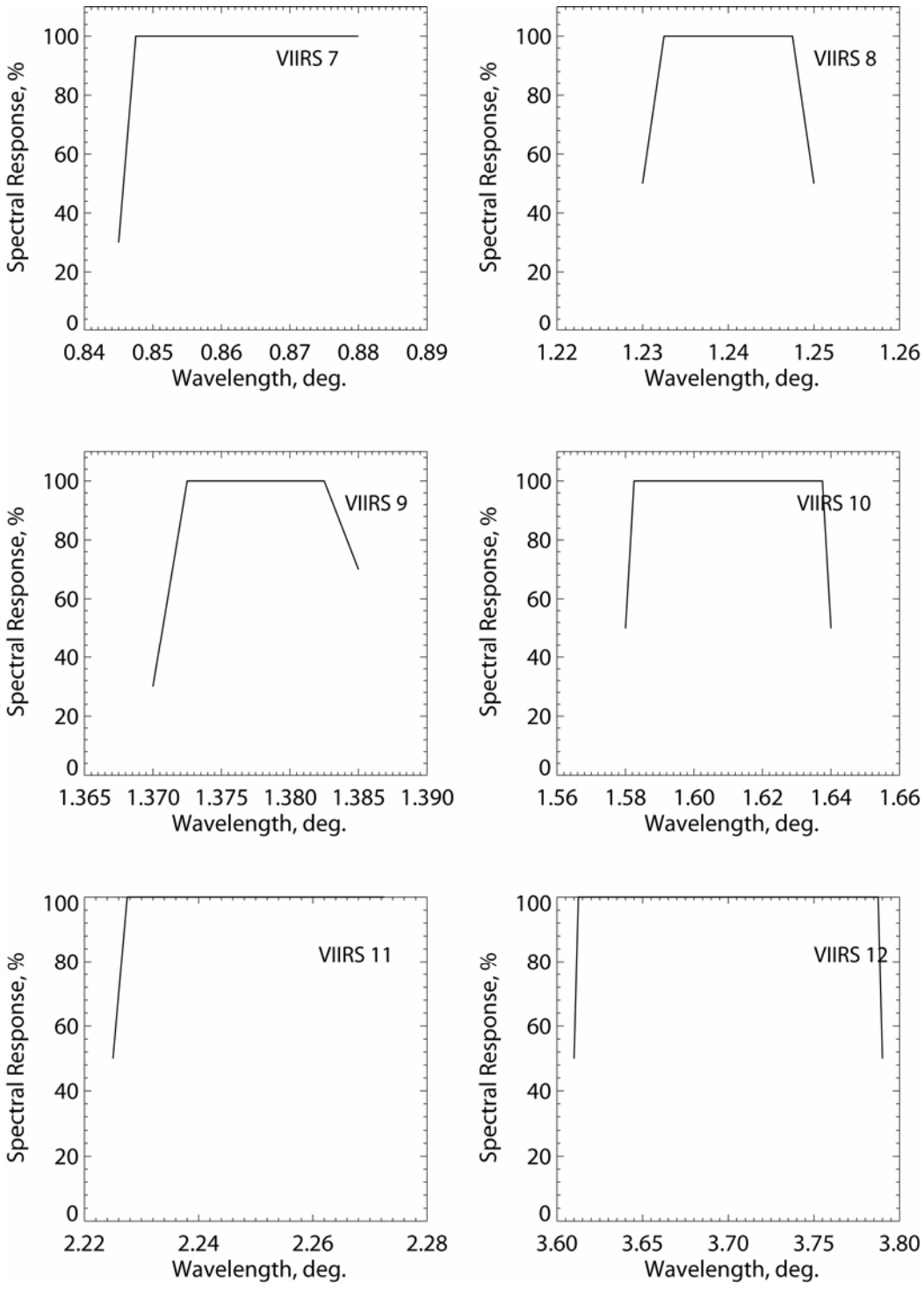
VIIRS 7
Spectral Response, %
Wavelength, deg.
0.84 0.85 0.86 0.87 0.88 0.89
VIIRS 8
1.22 1.23 1.24 1.25 1.26
VIIRS 9
1.365 1.370 1.375 1.380 1.385 1.390
VIIRS 10
1.56 1.58 1.60 1.62 1.64 1.66
VIIRS 11
2.22 2.24 2.26 2.28
VIIRS 12
3.60 3.65 3.70 3.75 3.80
0 20 40 60 80 100

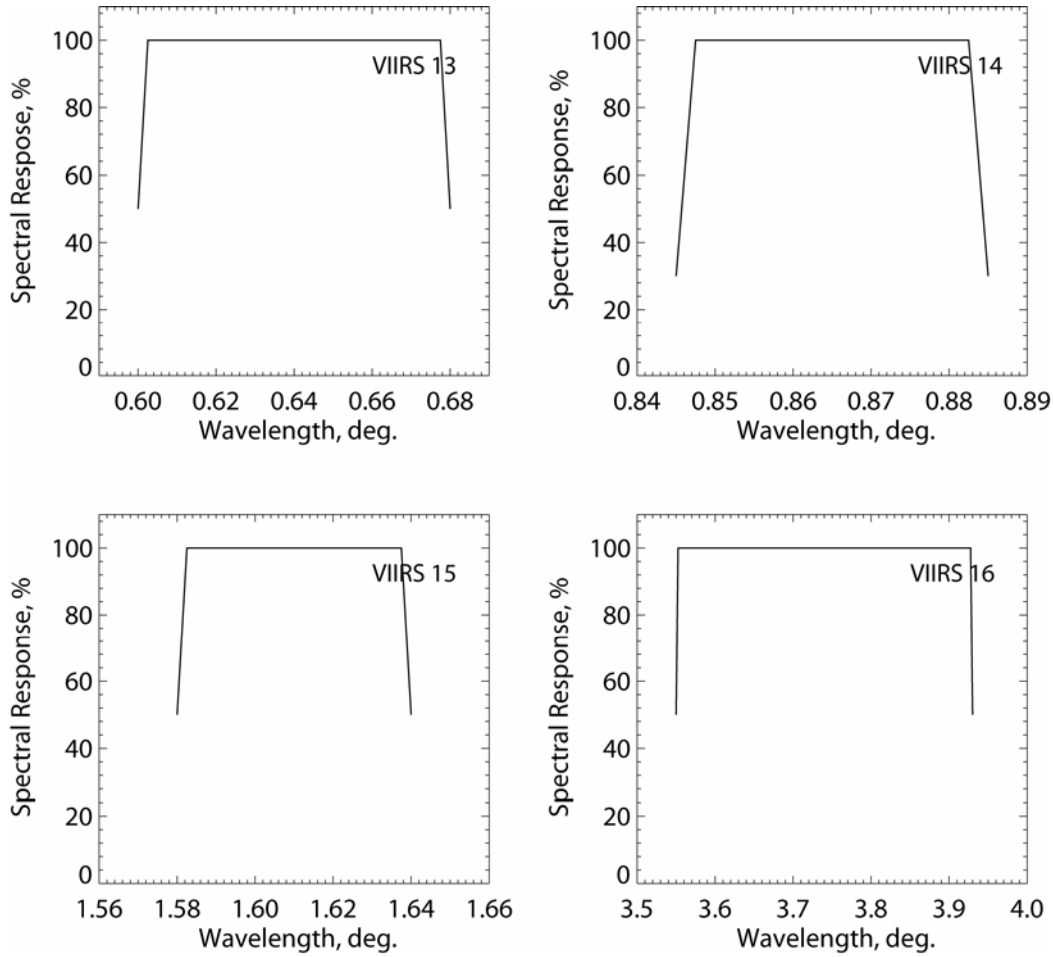


**Reference:**

T.E. Lee, S.D. Miller, F.J. Turk. C. Schueler, R. Julian, S. Deyo, P. Dills, and S. Wang, The NPOESS VIIRS day/night visible sensor, *Bulletin of the American Meteorological Society*, 87(2), 191-199, 2006.

**Link:**

http://www.ipo.noaa.gov/Technology/viirs_summary.html

## ***SUBROUTINE CLEARW***

**Function**: To read a typical spectral reflectance of clear water (sea) from 250 to 4000 nm by steps of 2.5 nm.

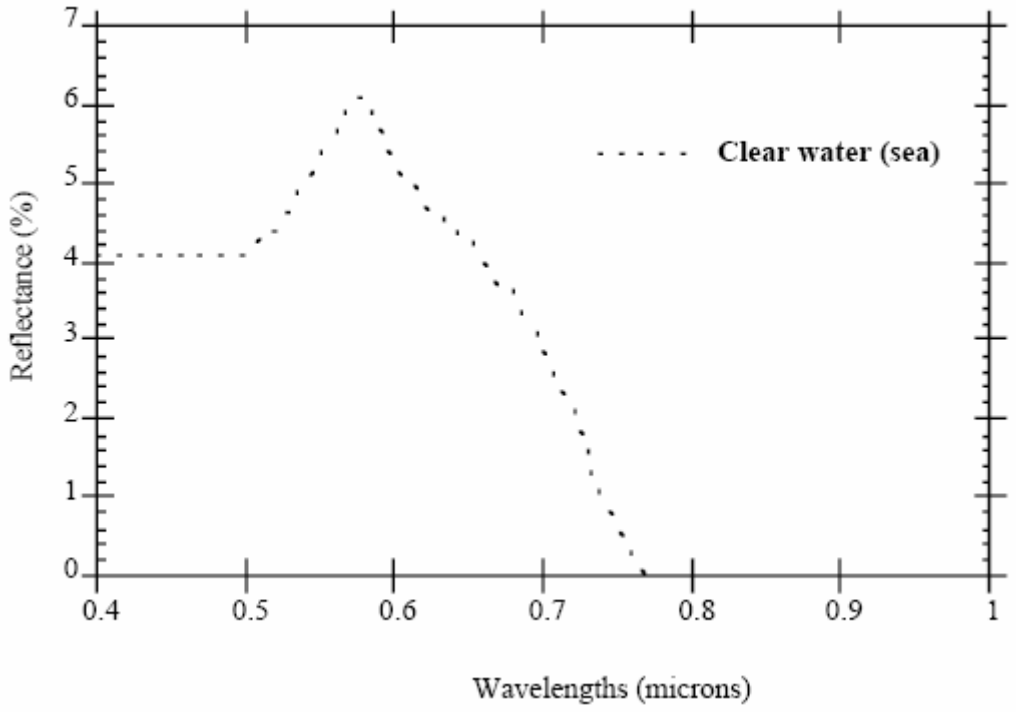


**Reference:**

M. Viollier, Télédétection des concentrations de seston et pigments chlorophylliens contenus dans l'Océan, Thèse de Doctorat d'Etat, no 503, 1980.

## ***SUBROUTINE LAKEW***

**Function**: To read a typical spectral reflectance of water (lake) from 250 to 4000 nm by steps of 2.5 nm.

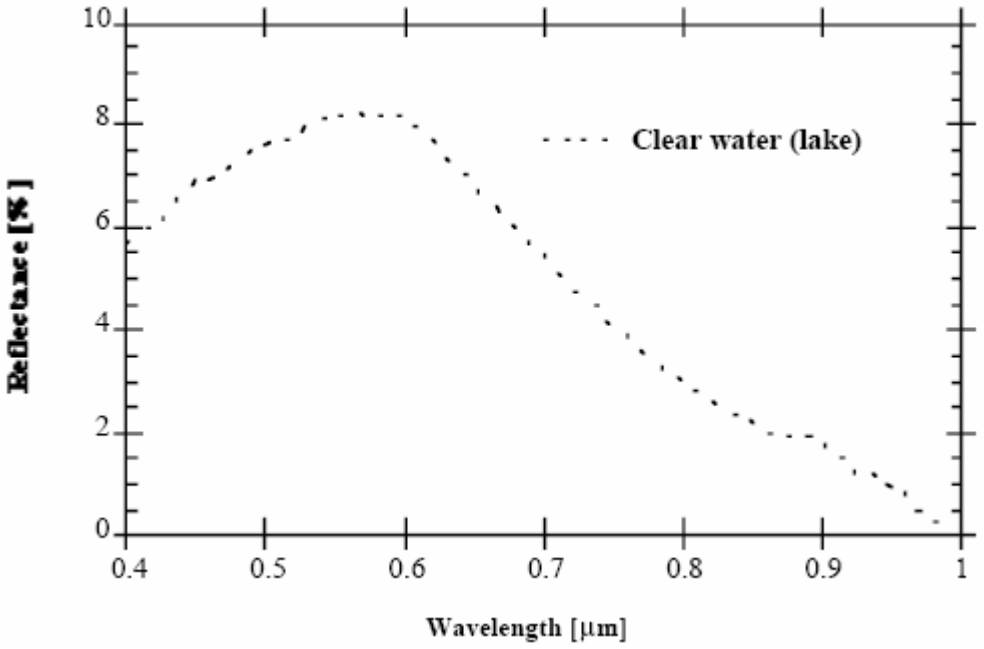


**Reference:**

K. Ya. Kondratyev, Radiation in the atmosphere, Academic Press, N.Y. 10003, USA, 1969.

## ***SUBROUTINE SAND***

**Function**: To read a typical spectral reflectance of sand from 250 to 4000 nm by steps of 2.5 nm.

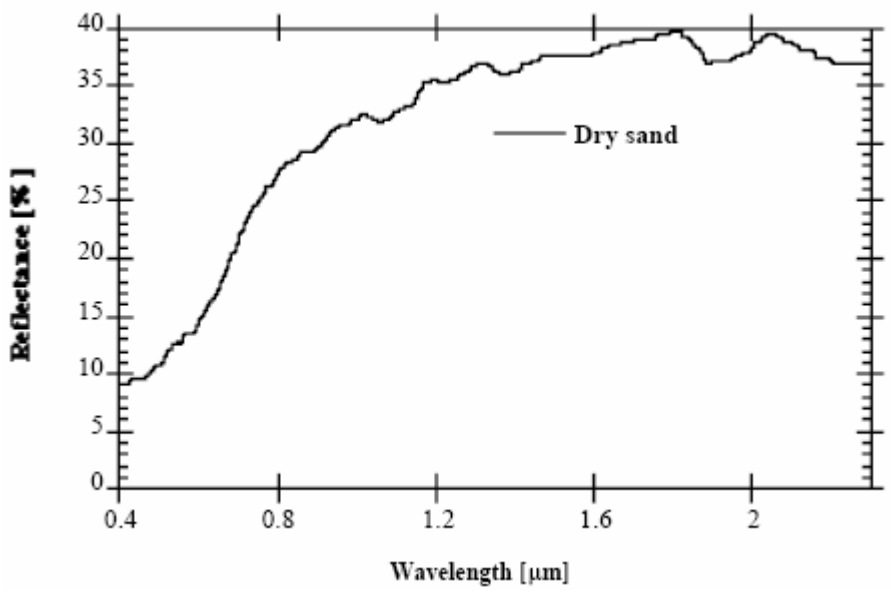


**Reference:**

R. Staetter and M. Schroeder, Spectral characteristics of natural surfaces, *Proceedings of the Tenth International Conference on Earth Observation from Space and Management of Planetary Resources*, Toulouse, France, Council of Europe, Commission of the European Communities, and European Association of Remote Sensing Laboratories, 6-11, p. 661, March 1978.

## ***SUBROUTINE VEGETA***

**Function**: To read a typical spectral reflectance of a mean green vegetation surface from 250 to 4000 nm by steps of 2.5 nm.

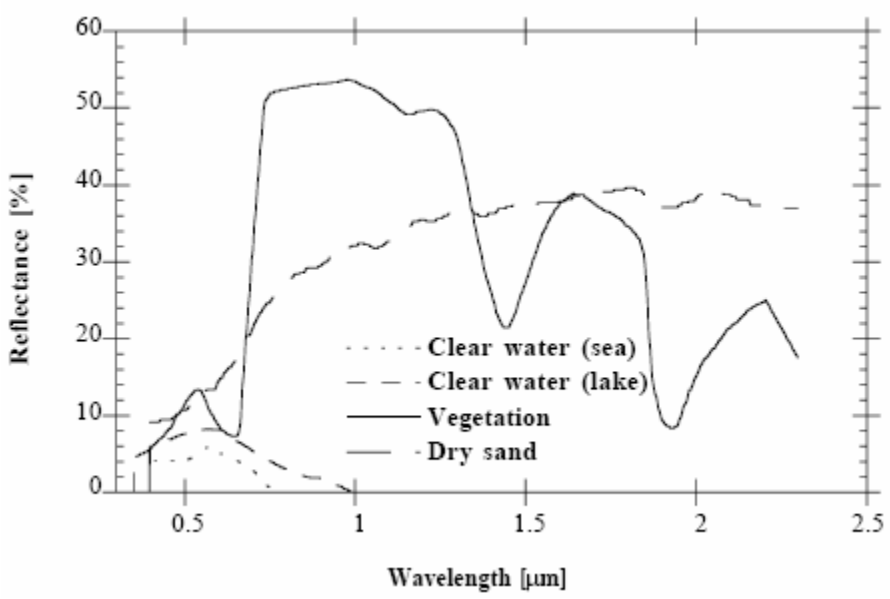


**Reference:**

Manual of Remote Sensing, Fall Church, Virginia, American Society of Photogrammetry, 1983.

## ***SUBROUTINE DICA1***

**Function**: To read the eight coefficients necessary to compute the $CO_2$ transmission according to the Malkmus model (see subroutine ABSTRA). The frequency interval is 2500-5050 $cm^{-1}$, step of 10 $cm^{-1}$.

## ***SUBROUTINE DICA2***

**Function**: Same as DICA1 but for the frequency interval 5060-7610 $cm^{-1}$.

## ***SUBROUTINE DICA3***

**Function**: Same as DICA1 but for the frequency interval 7620-10170 $cm^{-1}$.

## ***SUBROUTINE METH1***

**Function**: To read the eight coefficients necessary to compute the methane transmission according to the *Malkmus* model (see subroutine ABSTRA). The frequency interval is 2500-5050 $cm^{-1}$, step of 10 $cm^{-1}$.

## ***SUBROUTINE METH2***

**Function**: Same as METH1 but for the frequency interval 5060-7610 $cm^{-1}$.

## ***SUBROUTINE METH3***

**Function**: Same as METH1 but for the frequency interval 7620-10170 $cm^{-1}$.

## ***SUBROUTINE METH4***

**Function**: Same as METH1 but for the frequency interval 10180-12730 $cm^{-1}$.

## ***SUBROUTINE METH5***

**Function**: Same as METH1 but for the frequency interval 12740-15290 $cm^{-1}$.

## ***SUBROUTINE METH6***

**Function**: Same as METH1 but for the frequency interval 15300-17870 $cm^{-1}$.

## ***SUBROUTINE MOCA1***

**Function**: To read the eight coefficients necessary to compute the CO transmission according to the *Malkmus* model (see subroutine ABSTRA). The frequency interval is 2500-5050 $cm^{-1}$, step of 10 $cm^{-1}$.

## ***SUBROUTINE MOCA2***

**Function**: Same as MOCA1 but for the frequency interval 5060-7610 $cm^{-1}$.

## ***SUBROUTINE MOCA3***

**Function**: Same as MOCA1 but for the frequency interval 7620-10170 $cm^{-1}$.

## ***SUBROUTINE MOCA4***

**Function**: Same as MOCA1 but for the frequency interval 10180-12730 $cm^{-1}$.

## ***SUBROUTINE MOCA5***

**Function**: Same as MOCA1 but for the frequency interval 12740-15290 $cm^{-1}$.

## ***SUBROUTINE MOCA6***

**Function**: Same as MOCA1 but for the frequency interval 15300-17870 $cm^{-1}$

## ***SUBROUTINE NIOX1***

**Function**: To read the eight coefficients necessary to compute the $N_2O$ transmission according to the *Malkmus* model (see subroutine ABSTRA). The frequency interval is 2500-5050 $cm^{-1}$, step of 10 $cm^{-1}$.

## ***SUBROUTINE NIOX2***

**Function**: Same as NIOX1 but for the frequency interval 5060-7610 $cm^{-1}$.

## ***SUBROUTINE NIOX3***

**Function**: Same as NIOX1 but for the frequency interval 7620-10170 $cm^{-1}$.

## ***SUBROUTINE NIOX4***

**Function**: Same as NIOX1 but for the frequency interval 10180-12730 $cm^{-1}$.

## ***SUBROUTINE NIOX5***

**Function**: Same as NIOX1 but for the frequency interval 12740-15290 $cm^{-1}$.

## ***SUBROUTINE NIOX6***

**Function**: Same as NIOX1 but for the frequency interval 15300-17870 $cm^{-1}$.

## ***SUBROUTINE OXYG3***

**Function**: To read the eight coefficients necessary to compute the $O_2$ transmission according to the *Malkmus* model (see subroutine ABSTRA). The frequency interval is 2500-5050 $cm^{-1}$, step of 10 $cm^{-1}$.

## ***SUBROUTINE OXYG4***

**Function**: Same as OXYG3 but for the frequency interval 10180-12730 $cm^{-1}$.

## ***SUBROUTINE OXYG5***

**Function**: Same as OXYG3 but for the frequency interval 12740-15290 $cm^{-1}$.

## ***SUBROUTINE OXYG6***

**Function**: Same as OXYG3 but for the frequency interval 15300-17870 $cm^{-1}$.

## ***SUBROUTINE OZON1***

**Function**: To read the eight coefficients necessary to compute the $O_3$ transmission according to the *Malkmus* model (see subroutine ABSTRA). The frequency interval is 2500-5050 $cm^{-1}$, steps of 10 $cm^{-1}$.

## ***SUBROUTINE WAVA1***

**Function**: To read the eight coefficients necessary to compute the $H_2O$ transmission according to the *Goody* model (see subroutine ABSTRA). The frequency interval is 2500-5050 $cm^{-1}$, steps of 10 $cm^{-1}$.

## ***SUBROUTINE WAVA2***

**Function**: Same as WAVA1 but for the frequency interval 5060-7610 $cm^{-1}$.

## ***SUBROUTINE WAVA3***

**Function**: Same as WAVA1 but for the frequency interval 7620-10170 $cm^{-1}$.

## ***SUBROUTINE WAVA4***

**Function**: Same as WAVA1 but for the frequency interval 10180-12730 $cm^{-1}$.

## ***SUBROUTINE WAVA5***

**Function**: Same as WAVA1 but for the frequency interval 12740-15290 $cm^{-1.}$

## ***SUBROUTINE WAVA6***

**Function**: Same as WAVA1 but for the frequency interval 15300-17860 $cm^{-1}$.

## ***SUBROUTINE DUST***

**Function**: To read the scattering phase function for the dust-like component. Computations have been performed for 83 angles (80 Gaussian angles and 0°, 90° and 180°) and 20 wavelengths (0.350, 0.400, 0.412, 0.443, 0.470, 0.488, 0.515, 0.550, 0.590, 0.633, 0.670, 0.694, 0.760, 0.860, 1.240, 1.536, 1.650, 1.950, 2.250, and 3.750 nm).

## ***SUBROUTINE OCEA***

**Function**: Same as DUST but for the oceanic component.

## ***SUBROUTINE SOOT***

**Function**: Same as DUST but for the soot component.

## ***SUBROUTINE WATE***

**Function**: Same as DUST but for the water-soluble component.

**Reference:**

J. Lenoble, ed., Radiative transfer in scattering and absorbing atmospheres: standard computational procedures, A. DEEPAK Publishing, Hampton, Virginia, USA, 1985.

## ***SUBROUTINE BBM***

**Function**: Same as DUST but for the biomass burning model.

**Reference:** O. Dubovik, B. Holben, T. F. Eck, A. Smirnov, Y. J. Kaufman, M. D. King, D. Tanré, and I. Slutsker, Variability of absorption and optical properties of key aerosol types observed in worldwide locations, *Journal of the Atmospheric Sciences*, 59, 590-608, 2002.

## ***SUBROUTINE BDM***

**Function**: Same as DUST but for the background desert model.

**Reference:** G. A. d'Almeida, P. Koepke, and E. P. Shettle, Atmospheric aerosols: global climatology and radiative characteristics, A. DEEPAK Publishing, Hampton, Virginia, USA, 1991, p. 48, 80 and 120.

## ***SUBROUTINE STM***

**Function**: Same as DUST but for the stratospheric model.

**Reference:** P.B. Russel, J.M. Livingston, R.F. Pueschel; J.J. Bauman, J.B. Pollac, S.L. Brooks, P. Hamill, L.W. Thomason, L.L. Stowe, T. Deshler, E.G. Dutton, and R.W. Bergstrom, Global to microscale evolution of the Pinatubo volcanic aerosol derived from diverse measurements and analyses, *Journal of Geophysical Research*, 101(D13), 18745-18763, 1996.

## ***SUBROUTINE MIDSUM***

**Function**: To read the midlatitude summer atmosphere model, i.e., pressure (mb), temperature (K), and water vapor and ozone concentrations ($g/m^3$) as functions of altitude (34 levels).

- $\Delta Z = 1$ km for $0 < Z < 25$ km;
- $\Delta Z = 5$ km for $25 < Z < 50$ km;
- $\Delta Z = 70$, 100 km and $\infty$ ($p = 0$).

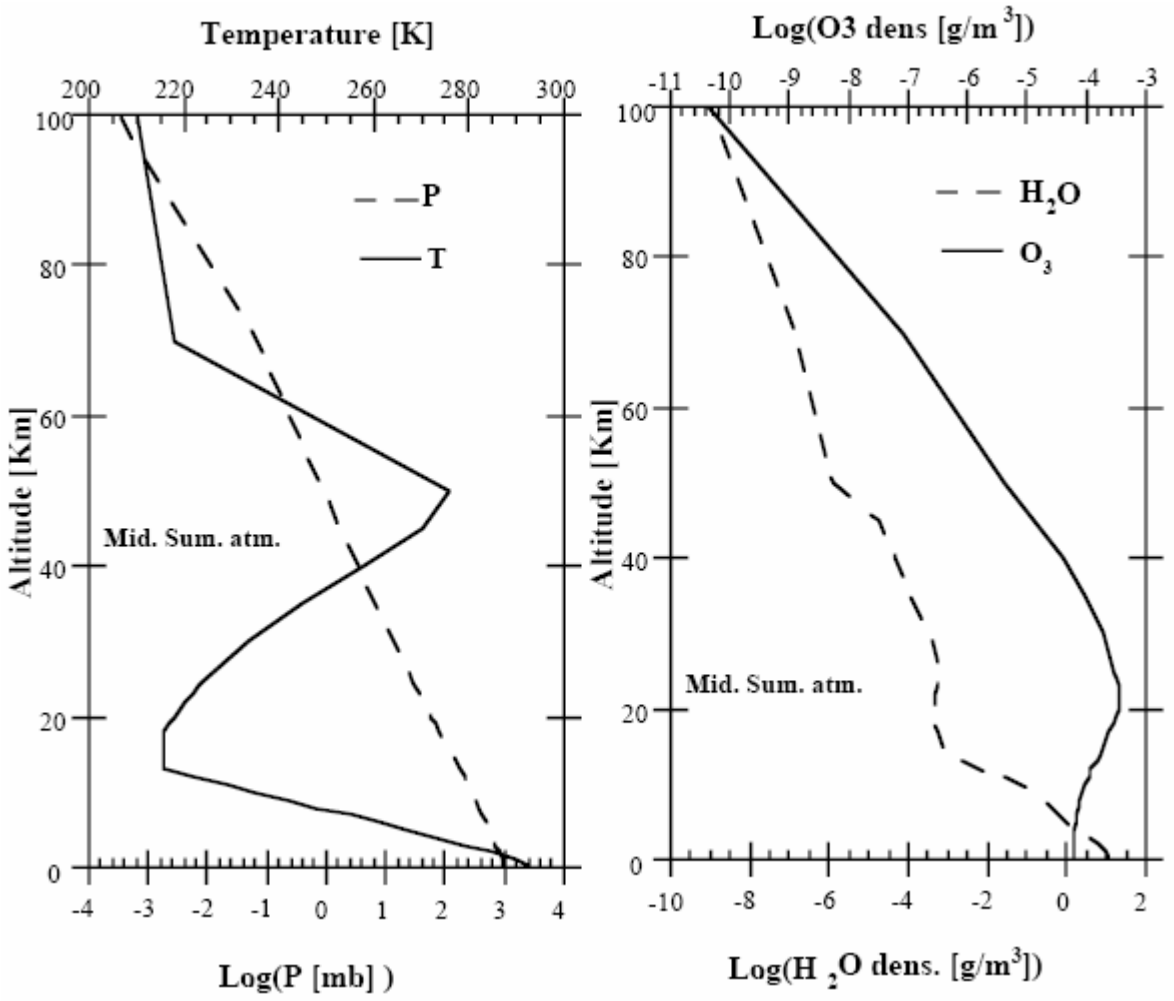


**Reference**:

R.A. Mc Clatchey, R.W. Fenn, J.E.A. Selby, F.E. Volz, and J.S. Garing, Optical properties of the Atmosphere, AFCRL-TR-71-0279, *Environment Research papers*, No 354, L.G. Hancom Fiel Bedford, Mass. USA, 1971.

## ***SUBROUTINE MIDWIN***

**Function**: To read the midlatitude winter atmosphere model, i.e., pressure (mb), temperature (K), water vapor and ozone concentrations ($g/m^3$) as functions of altitude (34 levels).

- $\Delta Z = 1$ km for $0 < Z < 25$ km;
- $\Delta Z = 5$ km for $25 < Z < 50$ km;
- $Z = 70$, 100 km and $\infty$ ($p = 0$).

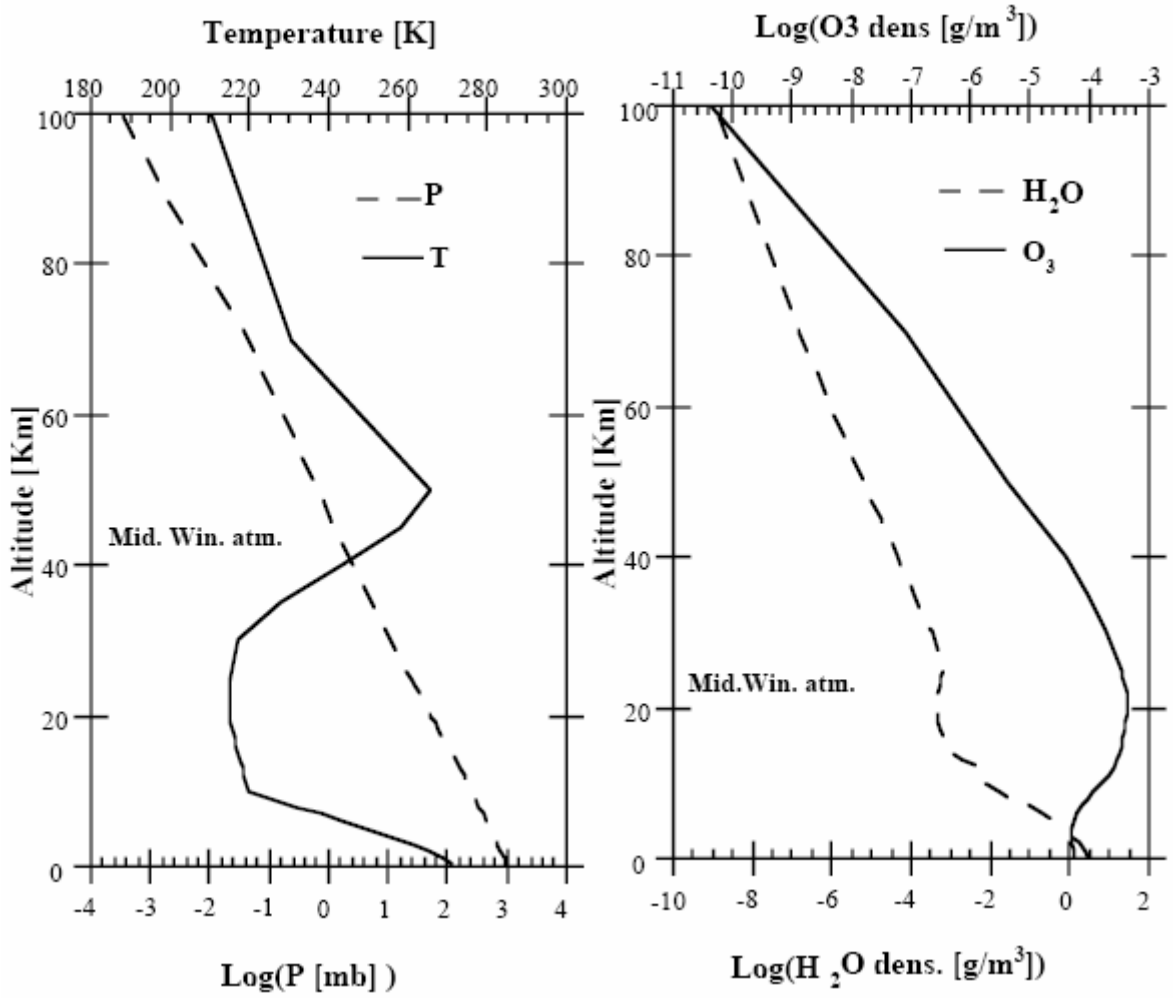


**Reference**:

R.A. Mc Clatchey, R.W. Fenn, J.E.A. Selby, F.E. Volz, and J.S. Garing, Optical properties of the Atmosphere, AFCRL-TR-71-0279, *Environment Research papers*, No 354, L.G. Hancom Fiel Bedford, Mass. USA, 1971.

## ***SUBROUTINE SUBSUM***

**Function**: To read the subarctic summer atmosphere model, i.e., pressure (mb), temperature (K), water vapor and ozone concentrations ($g/m^3$) as functions of altitude (34 levels).

- $\Delta Z = 1$ km for $0 < Z < 25$ km;
- $\Delta Z = 5$ km for $25 < Z < 50$ km;
- $Z = 70$, 100 km and $\infty$ ($p = 0$).

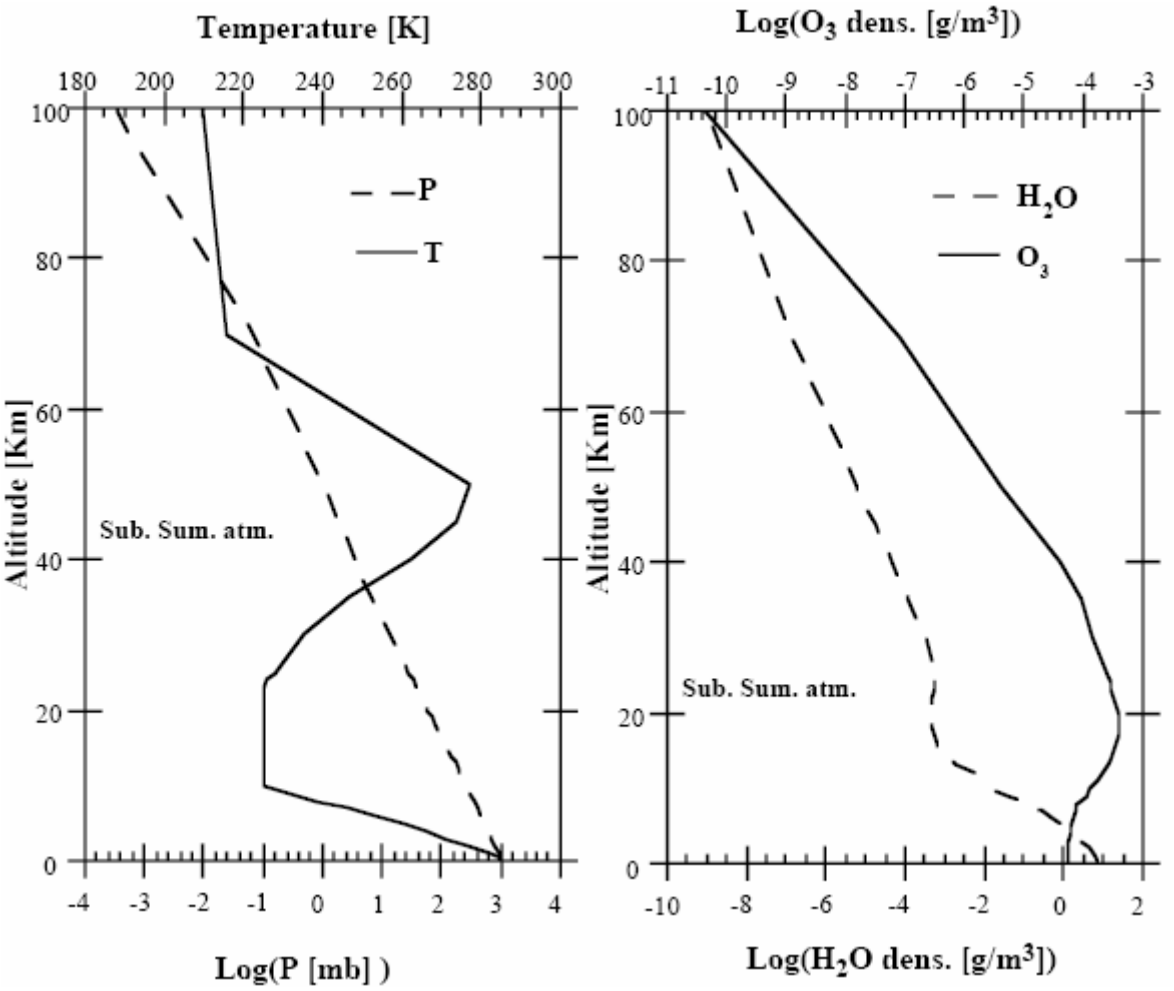


**Reference**:

R.A. Mc Clatchey, R.W. Fenn, J.E.A. Selby, F.E. Volz, and J.S. Garing, Optical properties of the Atmosphere, AFCRL-TR-71-0279, *Environment Research papers*, No 354, L.G. Hancom Fiel Bedford, Mass. USA, 1971.

## ***SUBROUTINE SUBWIN***

**Function**: To read the subarctic atmosphere model, i.e., pressure (mb), temperature (K), water vapor and ozone concentrations ($g/m^3$) as functions of altitude (34 levels).

- $\Delta Z = 1$ km for $0 < Z < 25$ km;
- $\Delta Z = 5$ km for $25 < Z < 50$ km;
- $Z = 70$, 100 km and $\infty$ ($p = 0$).

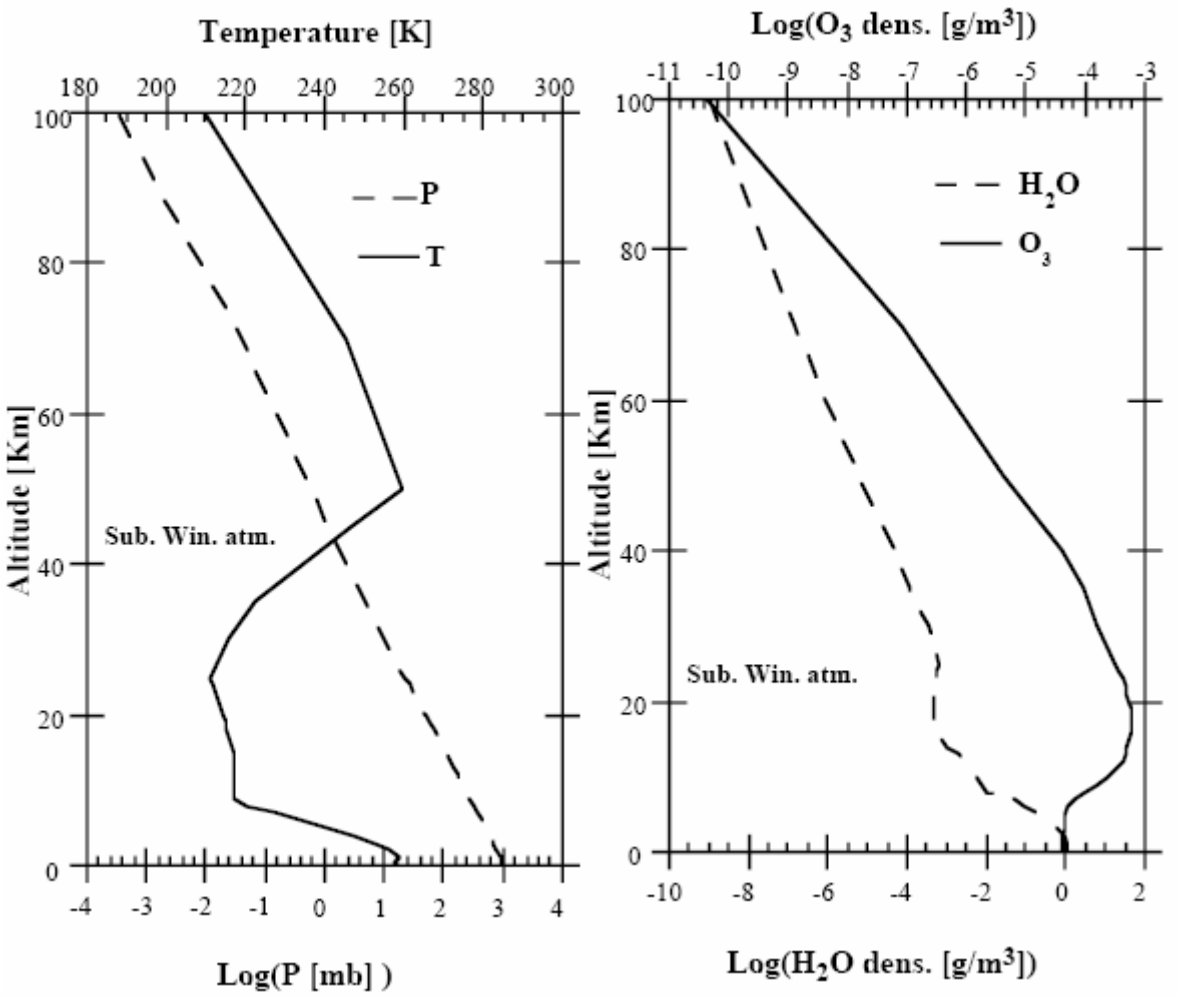


**Reference**:

R.A. Mc Clatchey, R.W. Fenn, J.E.A. Selby, F.E. Volz, and J.S. Garing, Optical properties of the Atmosphere, AFCRL-TR-71-0279, *Environment Research papers*, No 354, L.G. Hancom Fiel Bedford, Mass. USA, 1971.

## ***SUBROUTINE TROPIC***

**Function**: To read the tropical atmosphere model, i.e., pressure (mb), temperature (K), water vapor and ozone concentrations ($g/m^3$) as functions of altitude (34 levels).

- $\Delta Z = 1$ km for $0 < Z < 25$ km;
- $\Delta Z = 5$ km for $25 < Z < 50$ km;
- $Z = 70$, 100 km and $\infty$ ($p = 0$).

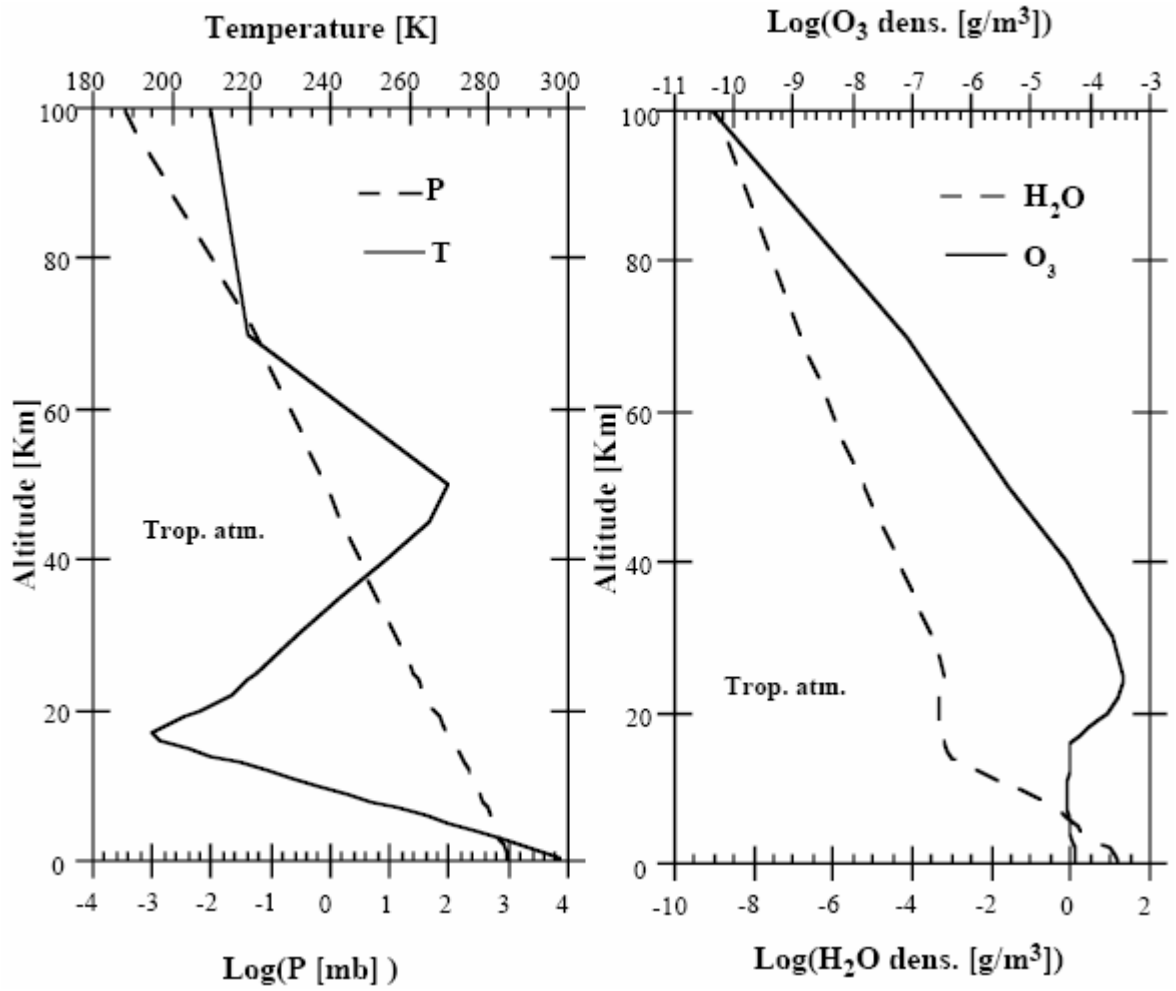


**Reference**:

R.A. Mc Clatchey, R.W. Fenn, J.E.A. Selby, F.E. Volz, and J.S. Garing, Optical properties of the Atmosphere, AFCRL-TR-71-0279, *Environment Research papers*, No 354, L.G. Hancom Fiel Bedford, Mass. USA, 1971.

## ***SUBROUTINE US62***

**Function**: To read the U.S. Standard Atmosphere, i.e., pressure (mb), temperature (K), water vapor and ozone concentrations ($g/m^3$) as functions of altitude (34 levels).

- $\Delta Z = 1$ km for $0 < Z < 25$ km;
- $\Delta Z = 5$ km for $25 < Z < 50$ km;
- $Z = 70$, 100 km and $\infty$ ($p = 0$).

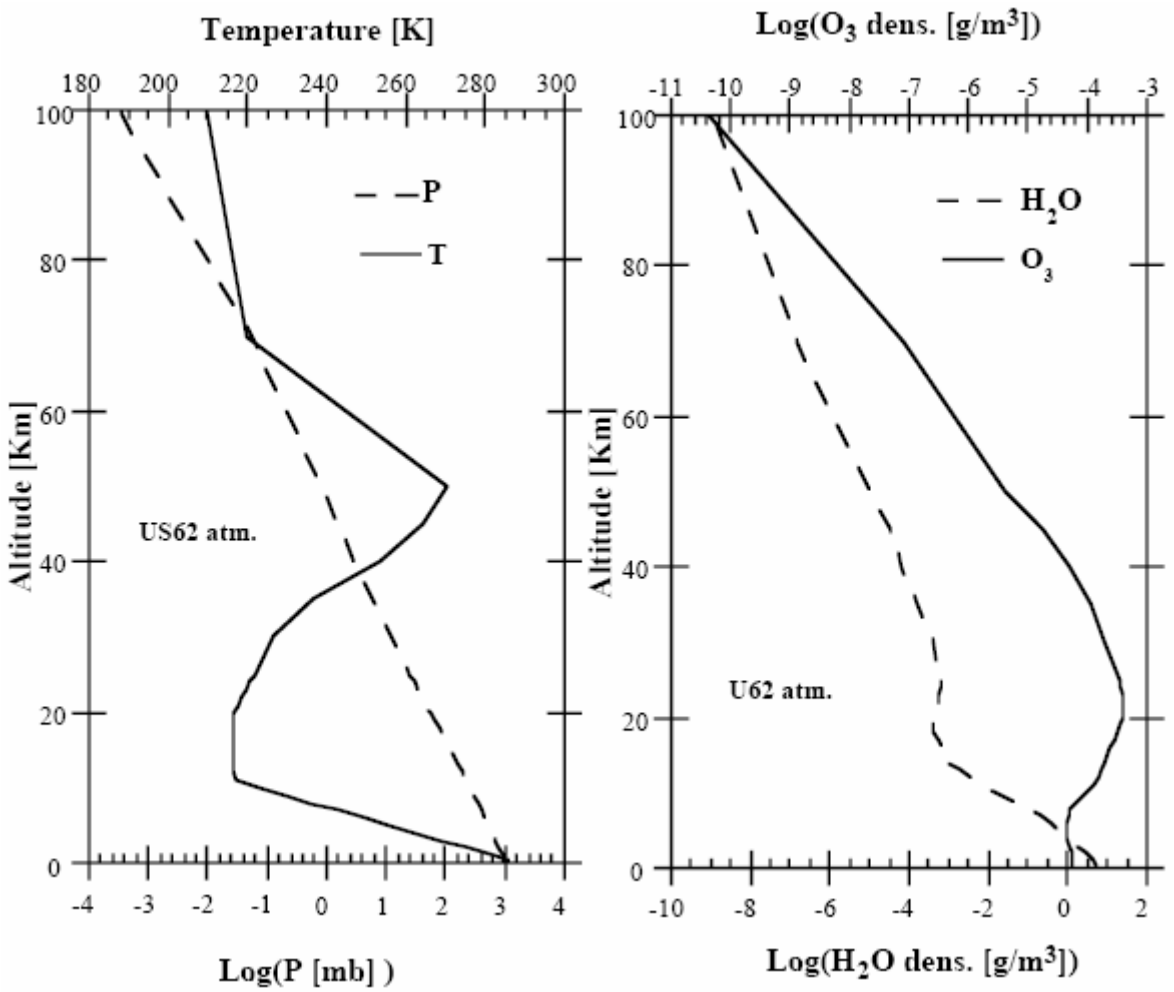


**Reference**:

R.A. Mc Clatchey, R.W. Fenn, J.E.A. Selby, F.E. Volz, and J.S. Garing, Optical properties of the Atmosphere, AFCRL-TR-71-0279, *Environment Research papers*, No 354, L.G. Hancom Fiel Bedford, Mass. USA, 1971.

# ***MISCELLANEOUS***

## ***SUBROUTINE EQUIVWL***

**Function**: To compute the equivalent wavelength needed for the calculation of the downward radiation field used in the computation of the non-Lambertian target contribution (file main.f).

**Description**: The input is the spectral response of the selected sensor as well as the solar irradiance spectrum. The output is the equivalent wavelength which is computed by averaging the spectral response of the sensor over the solar irradiance using an increment of 2.5 nm.

## ***SUBROUTINE PRINT_ERROR***

**Function**: To provide centralized error handling for the code and specific output error messages.

## ***SUBROUTINE SPECINTERP***

**Function**: To compute atmospheric properties at the equivalent wavelength (see subroutine EQUIVWL) needed for the calculation of the downward radiation field used in the computation of the non-Lambertian target contribution (file main.f).

**Description:** The input is the equivalent wavelength for which the coupling between the BRDF and the atmosphere is to be computed. Using the actual aerosol model, the outputs are the atmospheric properties at this wavelength, that is the aerosol optical thickness, single scattering albedo and phase function. In addition, this routine modifies the thickness and single scattering albedo of the aerosol layer below an aircraft.

## ***SUBROUTINE SPlIE2, SPLIN2, SPLINE, SPLINT***

**Function:** To perform interpolation of a furnished BDRF discrete dataset (BRDFGRID, option 1 of the BRDF model) to compute the albedo and BRDF value at the Gaussian quadrature points.